



**HAL**  
open science

# Finite temperature phases of two-dimensional spin-orbit-coupled bosons

Eiji Kawasaki

► **To cite this version:**

Eiji Kawasaki. Finite temperature phases of two-dimensional spin-orbit-coupled bosons. Quantum Physics [quant-ph]. Université Grenoble Alpes, 2017. English. NNT: 2017GREAY073. tel-01759245

**HAL Id: tel-01759245**

**<https://theses.hal.science/tel-01759245>**

Submitted on 5 Apr 2018

**HAL** is a multi-disciplinary open access archive for the deposit and dissemination of scientific research documents, whether they are published or not. The documents may come from teaching and research institutions in France or abroad, or from public or private research centers.

L'archive ouverte pluridisciplinaire **HAL**, est destinée au dépôt et à la diffusion de documents scientifiques de niveau recherche, publiés ou non, émanant des établissements d'enseignement et de recherche français ou étrangers, des laboratoires publics ou privés.

## THÈSE

Pour obtenir le grade de

### **DOCTEUR DE LA COMMUNAUTE UNIVERSITE GRENOBLE ALPES**

Spécialité : **Physique théorique**

Arrêté ministériel : 25 mai 2016

Présentée par

**Eiji KAWASAKI**

Thèse dirigée par **Markus HOLZMANN**, Directeur de Recherche  
au Laboratoire de Physique et de Modélisation des Milieux  
Condensés

préparée au sein du **Laboratoire de Physique et de  
Modélisation des Milieux Condensés**  
dans l'**École Doctorale de Physique**

## **Etablissement du diagramme de phase de bosons bidimensionnels avec couplage spin-orbite**

## **Finite temperature phases of two- dimensional spin-orbit-coupled bosons**

Thèse soutenue publiquement le **20 octobre 2017**,  
devant le jury composé de :

**Monsieur Simone FRATINI**

Directeur de recherche, Institut Néel – CNRS, Président du Jury

**Madame Patrizia VIGNOLO**

Professeur des Universités, Institut de Physique de Nice, Rapporteur

**Monsieur Jordi BORONAT**

Professeur, Universitat Politècnica de Catalunya, Rapporteur

**Monsieur Stefano GIORGINI**

Professeur, INO-CNR BEC Center, Università di Trento, Examineur

**Monsieur Tommaso ROSCILDE**

Maître de Conférences, ENS de Lyon, Examineur.





[...]  
*Regardez-les ! Avant d'atteindre sa chimère,  
Plus d'un, l'aile rompue et du sang plein les yeux,  
Mourra. Ces pauvres gens ont aussi femme et mère,  
Et savent les aimer aussi bien que vous, mieux.*

*Pour choyer cette femme et nourrir cette mère,  
Ils pouvaient devenir volaille comme vous.  
Mais ils sont avant tout les fils de la chimère,  
Des assoiffés d'azur, des poètes, des fous.*  
[...]

*Les oiseaux de passage  
La chanson des gueux (1876) de Jean Richepin  
Poème interprété par Georges Brassens*



# Acknowledgments

The very first person I wish to thank is the director of this thesis, Markus Holzmann. I feel very lucky as I had the privilege of working alongside him, grasping every answer he gave to my too often naive questions. Markus truly is a remarkable supervisor, inside and outside the office, and I hope that he will continue to share his knowledge in his pleasant, passionate and easy way.

I would also like to thank all the members of the jury, for their expertise, time and kindness. My very last PhD physics discussion, during the defense, will be a lasting memory that I will enjoy remembering thanks to each member of the jury.

I thank the president of the jury Simone Fratini for his perfect french accent among many others things, as a representative of my university the Communauté Université Grenoble Alpes. I would like also to deeply thank the two rapporteurs Jordi Boronat and Patrizia Vignolo for their time and work. Their comments were especially important to me. Indeed, while writing the manuscript a PhD student needs to focus on all its defects aiming on how to improve the thesis. Their constructive and positive feedbacks were then very precious to me. I would like to thank the two examiners Stefano Giorgini and Tommaso Roscilde with whom I already had very interesting discussions on the topic of this thesis.

My gratitude goes also to my former internship supervisor Anna Minguzzi who is the current director of the laboratory LPMMC as she introduced me both to the laboratory and to Markus. The very first director of the laboratory that I met was Frank Hekking who was also my teacher, I would particularly like to thank him.

Lastly I wish to thank the University UGA for giving me the opportunity of doing my PhD at the LPMMC. I wish here to thank all the members of this University that were very helpful from my very first year in Grenoble, in particular Arnaud Ralko and Thierry Klein.

Je voudrais également remercier toute l'équipe pédagogique d'informatique de l'UPMF (puis UGA) qui m'a permis d'enseigner durant ces trois années de thèse. Ce fût une expérience très enrichissante, remplie de belles rencontres comme Nathalie Denos et Dominique Vaufreydaz.

Je voudrais ensuite chaleureusement remercier l'ensemble de mes collègues de laboratoire enseignants, gestionnaires, chercheurs, ingénieurs de recherche, informaticiens, stagiaires, post-docs ou doctorants, en particulier Malo, Aleksandr, Guillaume, Van-Duy, Jose Maria, Natalia, Ivan, Katarina, Antton, Steven, Li-Jing, Florian et Davide. Merci pour nos belles discussions et pour m'avoir accompagné tout au long de ces années.

Questa tesi deve anche molto ai "vecchi" membri del laboratorio che sono oggi grandi amici. Auguro un bel in bocca al lupo a Daniel e Maria che ringrazio per la loro amicizia. Grazie anche al mitico trio degli italiani Angelo, Marco e Francesco. Il filosofo Marco e lo spericolato Francesco mi hanno trasmesso innumerevoli consigli già utili per il seguito della tesi.

Merci aussi à la nouvelle génération de doctorants Evrard-Ouicem, Etienne et Nicolas avec qui j'ai partagé la dernière partie de ma thèse. Je vous souhaite le meilleur pour la suite et que tous vos projets se réalisent. Enfin j'ai été accompagné durant ces années par les gestionnaires du laboratoire Habiba et Claudine que je tiens à remercier. Merci Habiba pour ces longues discussions et rires, durant lesquelles ta gentillesse et ta spontanéité m'ont permis de rester moi-même.

Je remercie mes parents pour leurs encouragements et leur foi en moi, j'ai été très heureux et ému de partager ce moment symbolique avec vous, au nez et à la barbe des tumultes de la vie. En parlant de famille, un grand merci à mon frère de pensée et ami philosophe Benjamin Le Roux à qui je souhaite tout ce qu'il y a de meilleur pour la suite.

Océane, tu es présente et m'accompagnes à chaque page de cette thèse et il m'est impossible de résumer ma gratitude envers toi. Je me contenterai de te remercier pour le sourire que tu me donnes chaque jour.

En conclusion, je remercie mon pays et ses habitants pour l'université qui m'a été offerte, le CROUS qui m'a accompagné de mille façons et la CAF qui m'a permis d'avoir un logement durant mes études pour ne citer que quelques exemples. Enfin, je voudrais terminer ces remerciements en exprimant ma reconnaissance envers toutes celles et tous ceux sans qui je n'aurais jamais pu vivre cette aventure. Merci pour tout et à très bientôt.

---





# Table of Contents

	<b>Page</b>
<b>0 Overview</b>	<b>1</b>
<b>1 Introduction</b>	<b>7</b>
1.1 Spin-orbit coupling (SOC) in ultra-cold atoms . . . . .	7
1.1.1 Artificial gauge fields . . . . .	9
1.1.2 Rashba-Dresselhaus spin-orbit coupling . . . . .	13
1.2 Non interacting SOCed Bose gases . . . . .	14
1.2.1 Diagonal form . . . . .	14
1.2.2 Energy spectrum . . . . .	16
1.2.3 Ideal Bose gas in 3D . . . . .	16
1.2.4 Ideal Bose gas in 2D . . . . .	20
1.3 Interacting Bose gas: Mean Field Approximation . . . . .	22
1.3.1 High temperature Mean Field Hartree approximation . . . . .	23
1.3.2 Mean Field ground states: Plane-Wave & Stripe phase . . . . .	25
1.4 Fluctuations & Open questions . . . . .	29
1.5 Outline of the thesis . . . . .	31
1.6 <i>Résumé</i> . . . . .	32
<b>2 Methods</b>	<b>35</b>
2.1 Introduction . . . . .	35
2.2 Classical field approximation . . . . .	38
2.3 Markov Chain Monte Carlo . . . . .	41
2.3.1 Effective action S . . . . .	41
2.3.2 Monte Carlo algorithms: Metropolis, Heat bath and Fourier moves	43
2.3.3 Partition function . . . . .	49
2.4 Density matching . . . . .	50

2.4.1	Procedure . . . . .	50
2.4.2	Lattice expressions for ideal and mean-field classical fields . . .	50
2.4.3	Convergence and scale of energy . . . . .	55
2.5	<i>Résumé</i> . . . . .	56
<b>3</b>	<b>Interacting Bosons with SOC in 2D: Phase Diagram</b>	<b>59</b>
3.1	Introduction . . . . .	59
3.2	Bose gas without SOC: Berezinskii, Kosterlitz and Thouless phase transition . . . . .	61
3.3	Bose gas with SOC: condensate fraction . . . . .	62
3.4	Superfluidity . . . . .	69
3.5	Conclusion and phase diagram . . . . .	70
3.6	<i>Résumé</i> . . . . .	71
<b>4</b>	<b>Low temperature states: Plane Wave and Stripe Phase</b>	<b>73</b>
4.1	Introduction and motivations . . . . .	73
4.2	Reduced single body density matrix . . . . .	75
4.3	Local Spin Density . . . . .	80
4.4	Spin density correlation functions . . . . .	84
4.5	Isotropic interaction: Fragmented condensate . . . . .	84
4.6	Low temperature wave-function . . . . .	86
4.6.1	Bosons pairs . . . . .	88
4.7	<i>Résumé</i> . . . . .	90
<b>5</b>	<b>Conclusion and Perspectives</b>	<b>93</b>
<b>6</b>	<b>Appendix</b>	<b>99</b>
6.1	Fluctuations of the density at low temperature . . . . .	99





## Overview

**S**<sup>PIN-ORBIT</sup> coupling links a particle's velocity to its quantum-mechanical spin, and it is essential in numerous condensed matter phenomena. Recently, in ultracold atomic systems [1], highly tunable synthetic spin-orbit couplings have been engineered enabling unique features and new physical phenomena. Spin-orbit coupled Bose gases present a notable example raising fundamentally new questions [2, 3, 4, 5]. For instance, a pioneering experiment at NIST achieved a spin-orbit coupled Bose gas and Bose-Einstein condensation [2]. Indeed realization of a pseudo-spin one-half Bose gas was achieved by selecting two internal states of the atoms and by coupling them through Raman processes.

At the mean-field level, spin-orbit coupling (SOC) introduces degenerate ground states expected to enhance fluctuation effects and giving rise to new, exotic quantum phases. However, the occurrence and nature of finite temperature transitions in bosonic systems have not yet been fully established [6, 7, 8, 9, 10].

**In this thesis, we determine the finite-temperature phase diagram of a two-dimensional interacting Bose gas with two hyperfine (pseudospin) states coupled via a Rashba-Dresselhaus spin-orbit interaction using classical field Monte Carlo calculations.**

First, we review the results of mean-field calculations [8, 9, 10, 11, 12] that indicate a Bose condensed ground state strongly dependent on the anisotropy of the interparticle interactions. At zero temperature, we expect exotic ground states formed by either a single plane wave with non-vanishing momentum or a linear superposition of two plane waves with opposite momenta, called plane wave state (PW) and stripe phase (SP), respectively. For spin-independent interaction between

atoms, PW and SP remain degenerate at the mean-field level.

We then explore the phase diagram using classical field Monte Carlo calculations, and present the main results of the thesis. Classical field Monte Carlo simulations provide a numerical method to accurately describe continuous phase transitions of Bose gases at finite temperatures. We have adapted this method to perform simulations of interacting Bose gases with SOC. In two spatial dimensions, we show that for anisotropic SOC, the systems undergoes a Kosterlitz-Thouless phase transition from a normal to superfluid state. In the superfluid state, the single particle density matrix decays algebraically and directly reflects the PW/SP character of the mean-field ground state. In the limit of isotropic interparticle interaction, the PW/SP degeneracy is unaffected by the transition and fragmentation of the condensate occurs [13].

In the case of isotropic SOC, we show that the transition temperature decreases with increasing system size due to the increasing number of degenerate mean-field ground states and eventually vanishes in the thermodynamic limit. Our simulations show that the circular degeneracy of the single-particle ground state destroys the algebraic ordered phase. No superfluid transition is then expected in the thermodynamic limit.

We start with a brief introduction to artificial gauge fields in ultracold atomic gases, motivating our theoretical study. Then, we provide a description of the classical field Monte Carlo methods, used to obtain the main, new results of the thesis, presented in chapter three and four. Our conclusions together with perspectives for future work are summarized in chapter five.

## *Introduction et Résumé*

LE COUPLAGE spin-orbite, essentiel dans de nombreux phénomènes en matière condensée, fait interagir la vitesse d'une particule avec son propre spin. Récemment dans le domaine des atomes froids [1], un couplage spin-orbite finement réglable a été conçu. Il a depuis ouvert la voie à des dispositifs uniques et à la découverte de nouveaux phénomènes physiques. Les gaz de Bose avec couplage spin-orbite sont un exemple majeur de ces nouvelles pistes qui soulèvent des questions inédites [2, 3, 4, 5]. Par exemple, une expérience pionnière au laboratoire NIST a permis d'obtenir un gaz de Bose avec couplage spin-orbit ainsi qu'une condensation de Bose-Einstein dans ce système [2]. Le gaz de bosons avec des pseudo spins  $1/2$  a été réalisé en sélectionnant deux états internes propre à chaque atome et en les couplant à travers un processus Raman.

Selon l'approximation champ moyen, le couplage spin-orbite introduirait une forte dégénérescence de l'état fondamental qui donnerait lieu à des phases quantiques exotiques et qui permettrait également d'envisager un rôle prépondérant des effets des fluctuations. Pourtant, l'apparition, l'existence et la nature de transitions à température finie dans un système de bosons avec couplage spin-orbite ne sont pas encore réellement établies [6, 7, 8, 9, 10].

**L'objectif de cette thèse est de déterminer le diagramme de phase à température finie d'un gaz de Bose bidimensionnels interagissant avec deux états hyperfins (pseudospins) couplés à travers une interaction spin-orbite Rashba-Dresselhaus en utilisant des calculs Monte Carlo type champs classiques.**

Tout d'abord, nous examinons les résultats des calculs type champ moyen [8, 9, 10, 11, 12] qui indiquent un état fondamental, du gaz de Bose condensé, fortement déterminé par l'anisotropie des interactions interparticules. A température nulle, des phases exotiques sont attendues formant soit un état type onde plane avec une impulsion non-nulle soit une superposition linéaire de deux ondes planes avec deux impulsions opposées, chacune appelée respectivement onde plane (PW) et état de bande (SP). Pour des interactions indépendantes du spin de chaque atome, les états PW et SP restent dégénérés dans le cadre de la théorie champ moyen.

Nous explorons alors le diagramme de phase en utilisant les calculs Monte Carlo basés sur champs classiques pour ensuite présenter les résultats principaux de cette thèse. Les simulations Monte Carlo avec champs classiques fournissent une méthode décrivant précisément les transitions de phases continues dans les gaz

de Bose à températures finies. Nous avons adapté cette méthode afin d'effectuer des simulations d'un gaz de Bose interagissant avec couplage spin-orbite. En deux dimensions spatiales, nous montrons que, pour un couplage spin-orbite anisotrope, le système subit une transition de phase type Kosterlitz-Thouless qui sépare une phase dite normale d'une phase superfluide. Dans la phase superfluide, la matrice densité à un corps décroît algébriquement et reflète directement le caractère type PW/SP en écho avec les prédictions d'état fondamental provenant de la théorie champ moyen. Dans la limite d'interactions interparticules totalement isotropes, la dégénérescence entre les états PW et SP n'est pas affectée par la transition. Une fragmentation du quasi-condensat s'opère dans ce cas [13].

Dans le cas d'un couplage spin-orbite isotrope, nous montrons que la température de transition diminue avec la taille du système à cause du nombre croissant d'états fondamentaux décrivant le minimum dégénéré d'énergie champ moyen. Cette température tend alors vers zéro à la limite thermodynamique. Nos simulations montrent que la dégénérescence circulaire de la courbe de dispersion de l'énergie de chaque particule détruit l'ordre algébrique et donc la phase ordonnée. Aucune transition vers une phase superfluide n'est attendue dans ce cas à température finie à la limite thermodynamique.

Nous commençons ce manuscrit avec une brève introduction aux champs de jauge artificiels dans les atomes froids qui appuient notre étude théorique. Nous fournissons ensuite une description des méthodes Monte Carlo basées sur champs classiques utilisées pour obtenir les résultats nouveaux et principaux de cette thèse qui seront présentés durant les Chapitre III et IV. Nos conclusions ainsi que des perspectives pour de prochaines études sont résumées Chapitre V.





# Chapter 1

## Introduction

### Contents

---

<b>1.1 Spin-orbit coupling (SOC) in ultra-cold atoms . . . . .</b>	<b>7</b>
1.1.1 Artificial gauge fields . . . . .	9
1.1.2 Rashba-Dresselhaus spin-orbit coupling . . . . .	13
<b>1.2 Non interacting SOCed Bose gases . . . . .</b>	<b>14</b>
1.2.1 Diagonal form . . . . .	14
1.2.2 Energy spectrum . . . . .	16
1.2.3 Ideal Bose gas in 3D . . . . .	16
1.2.4 Ideal Bose gas in 2D . . . . .	20
<b>1.3 Interacting Bose gas: Mean Field Approximation . . . . .</b>	<b>22</b>
1.3.1 High temperature Mean Field Hartree approximation . . . . .	23
1.3.2 Mean Field ground states: Plane-Wave & Stripe phase . . . . .	25
<b>1.4 Fluctuations &amp; Open questions . . . . .</b>	<b>29</b>
<b>1.5 Outline of the thesis . . . . .</b>	<b>31</b>
<b>1.6 <i>Résumé</i> . . . . .</b>	<b>32</b>

---

### 1.1 Spin-orbit coupling (SOC) in ultra-cold atoms

"The achievement of Bose Einstein condensation (BEC) (Anderson et al. 1995; Bradley et al. 1995; Davis et al. 1995) and of Fermi degeneracy (DeMarco and Jin, 1999; Schreck et al., 2001; Truscott et al. 2001) in ultra-cold dilute gases has opened a

new chapter in atomic and molecular physics, in which particle statistics and their interactions, rather than the study of single atoms or photons, are at center stage." *Extracted from [14].*

### **Why simulate gauge fields in ultra-cold atoms ?**

Trapped cold atoms usually have a neutral charge. However, magnetic phenomena are of a particular interest in quantum mechanics. They appear for example in spin Hall effects [15, 16], spin-orbit coupling[17, 18], Aharonov-Bohm effect, Hofstadter butterfly physics and topological insulators [19, 20, 21] when a charged particle interacts with a magnetic field. In order to better understand these effects in situations where particle statistics and interactions are important, various propositions to enable such physics in ultra-cold gases were explored. Very recently new ways of creating artificially synthetic magnetic couplings have been found [22]. This thesis focuses on the interplay between collective behavior and single particle magnetic phenomena in ultra-cold gases. In particular, we study the effect of a spin-orbit coupling in a homogeneous Bose gas with repulsive hardcore two-body interaction.

In the following we will first sketch how magnetic phenomena and artificial gauge fields can be created in single atoms, then we will describe the collective behavior of homogeneous bosonic gases in the presence of this new coupling. In the next chapters we will then focus on the interplay between the two-body interaction and the single particle spin-orbit coupling (SOC) spectrum.

### 1.1.1 Artificial gauge fields

A free non-relativistic particle of mass  $m$  with a charge  $q$  coupled to a magnetic field  $\mathbf{B} = \nabla \times \mathbf{A}$  with  $\mathbf{A}$  being the vector potential, is described by the Hamiltonian,

$$\mathcal{H} = \frac{1}{2m} \left( \mathbf{p} - \frac{q}{c} \mathbf{A} \right)^2 \quad (1.1)$$

where  $c$  is the speed of light and  $\mathbf{p}$  is the canonical momentum operator. In most experimental systems, trapped ultra-cold atoms are neutral ( $q = 0$ ) and do not naturally couple to electromagnetic fields. In the next section we will very briefly introduce how to create artificial gauge fields that mimics the effect of electromagnetic fields on neutral atoms.

#### Rotating gas

Artificial gauge fields were studied very early in trapped gases [23]. A standard way of creating strong artificial magnetic field is by rotating a neutral particle system which is equivalent to placing them in a magnetic field proportional to the rotation vector  $\Omega$  with the appearance of additional terms.

$$\frac{\mathbf{p}^2}{2m} - \Omega(\mathbf{r} \times \mathbf{p}) = \frac{(\mathbf{p} - m\Omega \times \mathbf{r})^2}{2m} - \frac{1}{2}m(\Omega \times \mathbf{r})^2 \quad (1.2)$$

The artificial magnetic field produced through rotation is necessarily uniform. This idea has shown to be very effective to study the creation of vortex lattices in BECs [14].

#### Raman induced gauge field

Here we consider a toy model of a three-level atom coupled to two lasers in order to give a little insight on how induced transitions can simulate artificial gauge fields. This toy model is presented from the reference [1], which contains a more accurate and detailed description of artificial gauge field in ultracold atoms. As in the rotational gas case we will aim to cast the Hamiltonian in a form like Eq. (1.1), we will however not give an accurate explanation of the experimental realization itself.

Figure 1.1 shows the induced transitions of a schematic three-level atom placed in two counter propagating laser beams. A Raman transition corresponds to the absorption of a single photon from one laser beam and its stimulated re-emission into the second. The momentum carried by each of these photons can be quite large compared to the typical ultra-cold atom setup. It is possible to coherently couple the state and the momentum of the cold atoms as we will see in the next

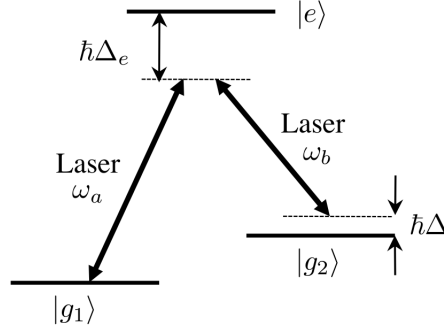


Figure 1.1: Figure extracted from [1]. Representation of a Raman transition in an atom with two low energies states and one high energy excited state. The states  $|g_1\rangle$  and  $|g_2\rangle$  are usually hyperfine states and they will later be labeled as  $|\uparrow\rangle$  and  $|\downarrow\rangle$ .

section. The transfer of momentum can be realized with no change in energy for  $\omega_a = \omega_b$ , such that the two ground states of energies  $E_1$  and  $E_2$  can be equally populated and considered degenerate,  $E_1 = E_2$ , as it will be the case in the rest of this thesis.

In the rotating frame we can extract an effective Hamiltonian that does not depend on the excited state but only on  $|g_1\rangle$  and  $|g_2\rangle$ . Raman transitions do not necessary populate the excited state (for large detuning  $\Delta_e$ ) which is very convenient in cold atoms experiments. The reduced Hamiltonian for this effective two-level system is then a  $2 \times 2$  matrix and writes in this basis,

$$\mathcal{H} = \frac{\hbar}{2} \begin{pmatrix} \Delta & \kappa^* \\ \kappa & -\Delta \end{pmatrix} \quad (1.3)$$

The effective Rabi frequency and the Raman mismatch write

$$\kappa = \frac{\kappa_a \kappa_b^*}{2\Delta_e} \quad \Delta = \hbar(\omega_a - \omega_b) - (E_2 - E_1) \quad (1.4)$$

with  $\kappa_a$  and  $\kappa_b$  the Rabi frequencies corresponding to the two lasers of frequencies  $\omega_a$  and  $\omega_b$ . The light intensity is proportional to  $|\kappa|^2$ . In order to extract the gauge field term appearing in the Hamiltonian, we write Eq. (1.3) in the a general form

$$\mathcal{H} = \frac{\hbar}{2} \begin{pmatrix} \cos(\theta) & e^{-i\phi} \sin(\theta) \\ e^{i\phi} \sin(\theta) & -\cos(\theta) \end{pmatrix} \quad (1.5)$$

with the generalized Rabi frequency  $\Omega = (\Delta^2 + |\kappa|^2)^{1/2}$ , the mixing angle  $\tan(\theta) = |\kappa|/\Delta$  and the phase  $\phi$  from  $\kappa = |\kappa|e^{i\phi}$ . In the basis defined by the eigenvalues  $|\psi_{\pm}\rangle$

and  $|\psi_{\pm}\rangle$ , the two energies write  $E_{\pm} = \pm \frac{\hbar\Omega}{2}$ .

$$|\psi_{-}\rangle = \begin{pmatrix} \sin(\theta/2) \\ -e^{-i\phi} \sin(\theta/2) \end{pmatrix} \quad |\psi_{+}\rangle = \begin{pmatrix} \cos(\theta/2) \\ e^{i\phi} \sin(\theta/2) \end{pmatrix} \quad (1.6)$$

Up to now Eq. (1.3) only described the internal degree of freedom of an atom. In order to describe the spatial degree of freedom of the whole atom we treat the internal (electronic) state in the adiabatic approximation.

In the adiabatic approximation  $\Psi(\mathbf{r}, t) = \phi_{-}(\mathbf{r}, t) |\psi_{-}(\mathbf{r})\rangle$  the equation of evolution for an atom in its internal ground state  $E_{-}$  can be written in the form like Eq. (1.1)

$$i\hbar \frac{\partial \phi_{-}}{\partial t} = \left[ \frac{(\mathbf{p} - \mathbf{A}_{-}(\mathbf{r}))^2}{2M} + E_{-}(\mathbf{r}) + v_{-}(\mathbf{r}) \right] \phi_{-}(\mathbf{r}, t) \quad (1.7)$$

Where  $v_{-}(\mathbf{r}) = \frac{\hbar^2}{8M} [(\Delta\theta)^2 + \sin^2\theta(\Delta\phi)^2]$  and the vector potential is defined by

$$\mathbf{A}_{-}(\mathbf{r}) = i\hbar \langle \psi_{-} | \nabla | \psi_{-} \rangle \quad (1.8)$$

Creating an artificial magnetic field, this causes a shearing of the atomic cloud and allows the entry of vortices into the BEC as presented in figure 1.2.

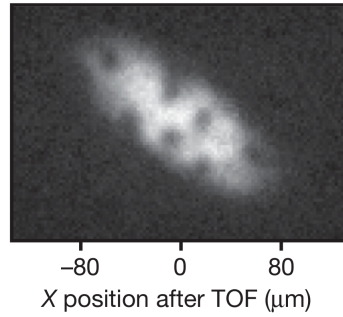


Figure 1.2: Figure extracted from [22]. Vortices created in a BEC of  $^{87}\text{Rb}$  coupled to an artificial magnetic field.

In contrast to the case of a rotational gas which was equivalent to a uniform magnetic field, the coupling  $\kappa$  in Eq. (1.3) may depend on the position of the atom and on the shape of the laser beam. The two plane waves created by the two lasers can be each tuned independently described as  $\kappa_{a/b}(\mathbf{r}) = \kappa_0 e^{i2\mathbf{k}_{a/b} \cdot \mathbf{r}}$  where  $2\mathbf{k}_{a/b}$  is the momentum transferred to the atom. During a Raman process, the single atom then acquires in total the difference of the two momenta carried from the two photons.

### Raman induced SOC

"Thus, as first put forward by Higbie and Stamper-Kurn [24], Raman transitions can provide the required velocity-dependent link between the spin [the internal state of the atom] and momentum: because the Raman lasers resonantly couple the spin states together when an atom is moving, its Doppler shift effectively tunes the lasers away from resonance, altering the coupling in a velocity-dependent way."

*Extracted from [4]*

It is then possible to simulate different shapes of the vector potential  $\mathbf{A}$  and tune each component differently. When the vector potential components  $\mathbf{A} = (\mathbf{A}_x, \mathbf{A}_y, \mathbf{A}_z)$  do not commute, the gauge potential is called non-abelian. One particular example of non commuting components are Pauli matrices which give rise to SOC terms. Generating non-abelian gauge potential is of a higher level of difficulty and it relies on multipod configuration (multiple low energy states).

In summary, it is possible to generate a vector potential  $\mathbf{A}$  such that,

$$\mathcal{H} = \frac{(\mathbf{p} - \mathbf{A})^2}{2M} \quad (1.9)$$

where the components of  $\mathbf{A}$  do not necessary commute. In particular, in this thesis, we will study the case  $\mathbf{A} \propto (\sigma_x, \sigma_y, 0)^T$  where  $\sigma_x$  and  $\sigma_y$  are the  $x$  and  $y$  Pauli spin matrices acting on a two level atom (figure 1.1) [3].

Ultra-cold SOCed systems have been of a great interest recently from both experimental and theoretical point of view [3, 22, 25]. Indeed extremely tunable SOC are a good playground for new accessible questions to arise. Some examples of phenomena that do not exist in standard condensed matter systems are listed here below.

- What is the collective behavior of SOCed bosons?
- How does SOC change when the spin is  $S > 1/2$ ?
- What is the interplay between interactions and SOC for bosons?

After a more precise definition of our SOC Hamiltonian, we will study the single particle spectrum of SOCed atoms and then ask again the questions arising from these new features.

## 1.1.2 Rashba-Dresselhaus spin-orbit coupling

### Spin-orbit coupling in condensed matter

For electrons in atoms or solid, the spin-orbit coupling is naturally present due to relativistic corrections. When a charged particle is moving in an electric field, the particle in its reference frame sees a magnetic field which couples to the internal magnetic moment (spin).

Different physical realizations produce different types of SOC with different symmetries. In two dimensions they are generally regrouped in two classes called Rashba [17] and Dresselhaus [18] SOC. These couplings were originally studied in the context of two dimensional semiconductors.

In the context of ultra-cold gases, the SOC is not a relativistic correction to the electronic energy levels but arises as an effective description for the hyperfine states of the atom and its coupling to the laser fields via the atomic momentum. The form and the strength of the SOC are experimentally tunable and therefore their study is distinct and often far from the SOC studies based on electrons in standard condensed matter. We quickly define below the terminology used in the context of ultra-cold atoms where different types of SOC are experimentally achievable [3, 26].

### Rashba and Dresselhaus couplings

The general Rashba-Dresselhaus coupling is defined as

$$\mathcal{H}_{\text{RD}} = \frac{\hbar^2 \kappa}{m} p_x \sigma_x + \eta_{\text{soc}} \frac{\hbar^2 \kappa}{m} p_y \sigma_y$$

where  $\kappa$  corresponds to the strength of the SOC. The real scalar  $\eta_{\text{soc}}$  characterizes the anisotropy/isotropy of the SOC in the  $x$ - $y$  plane which can be experimentally controlled by coupling lasers with different amplitudes in the  $x$ - $y$  plane. As a definition, the pure Rashba case corresponds to an isotropic SOC with  $\eta_{\text{soc}} = 1$ . Otherwise for  $0 \leq \eta_{\text{soc}} < 1$  the anisotropic coupling is called Rashba-Dresselhaus. In the next section we will draw the energy spectrum of the free particle Hamiltonian including the general SOC and discuss its dependency on the parameter  $\eta_{\text{soc}}$ .

## 1.2 Non interacting SOCed Bose gases

Before discussing the implications of including SOC in the Hamiltonian for interacting many body systems, let us first study the single particle spectrum of the ideal (non interacting) SOCed atoms. We introduce in this section the eigenbasis of the non interacting Hamiltonian given by a linear superposition of spin up and down states.

### 1.2.1 Diagonal form

In this thesis we will consider bosons with two internal degrees of freedom coupled by a Rashba-Dresselhaus SOC in a homogeneous system. In the second quantization basis the field creator operator writes

$$\hat{\Psi}^\dagger(\mathbf{r}) = \frac{1}{V} \sum_{\mathbf{k}} e^{i\mathbf{k}\cdot\mathbf{r}} \hat{\Psi}_{\mathbf{k}}^\dagger \quad (1.10)$$

We define  $\hat{u}_{\mathbf{k}}^\dagger$  and  $\hat{d}_{\mathbf{k}}^\dagger$  as creation operator of a spin up and down particle of momentum  $\mathbf{k}$ .

$$\hat{\Psi}_{\mathbf{k}}^\dagger = \left( \hat{u}_{\mathbf{k}}^\dagger, \hat{d}_{\mathbf{k}}^\dagger \right) \quad (1.11)$$

In a homogeneous system and in presence of a SOC, the Hamiltonian takes the form

$$\hat{\mathcal{H}}_0 = \sum_{\mathbf{k}} \hat{\Psi}_{\mathbf{k}}^\dagger \left[ \left( \frac{\hbar^2 k^2 + \hbar^2 \kappa^2}{2m} \right) I_2 + \frac{\hbar^2 \kappa}{m} k_x \sigma_x + \eta_{soc} \frac{\hbar^2 \kappa}{m} k_y \sigma_y \right] \hat{\Psi}_{\mathbf{k}} \quad (1.12)$$

with  $I_2$  the  $2 \times 2$  identity matrix. The constant term  $\frac{\hbar^2 \kappa^2}{2m}$  is added for convenience in order to set the absolute minimum of the energy to zero. The following results are of course completely independent of it. In matrix form, the Hamiltonian  $\hat{\mathcal{H}}_0$  writes

$$\hat{\mathcal{H}}_0 = \frac{1}{V} \sum_{\mathbf{k}} \int d\mathbf{r} \hat{\Psi}_{\mathbf{k}}^\dagger M(\mathbf{k}) \hat{\Psi}_{\mathbf{k}} \quad (1.13)$$

For simplicity we set  $\hbar = m = 1$  in the following. The matrix  $M(\mathbf{k})$  writes

$$M(\mathbf{k}) = \begin{pmatrix} k^2/2 + \kappa^2/2 & \kappa(k_x - i\eta_{soc}k_y) \\ \kappa(k_x + i\eta_{soc}k_y) & k^2/2 + \kappa^2/2 \end{pmatrix} = \begin{pmatrix} k^2/2 + \kappa^2/2 & \kappa k_{\perp} e^{-i\theta_{\mathbf{k}}} \\ \kappa k_{\perp} e^{i\theta_{\mathbf{k}}} & k^2/2 + \kappa^2/2 \end{pmatrix} \quad (1.14)$$

where we have written the off-diagonal terms as

$$\kappa(k_x \pm i\eta_{soc}k_y) = \kappa k_{\perp} e^{\pm i\theta_{\mathbf{k}}} \quad (1.15)$$

or

$$e^{\pm i\theta_{\mathbf{k}}} = \frac{k_x \pm i\eta_{soc}k_y}{k_{\perp}} \quad k_{\perp} = \sqrt{k_x^2 + \eta_{soc}^2 k_y^2} \quad (1.16)$$

Diagonalizing  $M(\mathbf{k})$ , we obtain

$$\hat{\mathcal{H}}_0 = \sum_{\mathbf{k}, \sigma=+,-} \epsilon_{\sigma}(\mathbf{k}) \hat{\Phi}_{\mathbf{k}}^{\sigma \dagger} \hat{\Phi}_{\mathbf{k}}^{\sigma} \quad (1.17)$$

where the energies of the two branches write

$$\epsilon_{\pm}(\mathbf{k}) = k^2/2 + \kappa^2/2 \pm |\kappa k_{\perp}| = \frac{(k_{\perp} \pm \kappa)^2 + (1 - \eta_{soc}^2) k_y^2 + k_z^2}{2} \quad (1.18)$$

The new field operators write

$$\hat{\Phi}_{\mathbf{k}}^{\pm} = \frac{\hat{u}_{\mathbf{k}} \pm e^{i\theta_{\mathbf{k}}} \hat{d}_{\mathbf{k}}}{\sqrt{2}} \quad (1.19)$$

The energy eigenfunctions is composed out of the two spin states of the corresponding momentum with equal amplitude but momentum dependent phase. Figure 1.3 shows the single particle energy spectrum of the ideal gas for two different values of  $\eta_{soc}$ .

### 1.2.2 Energy spectrum

These last years in the context of ultra-cold atoms [4, 8], both fermionic and bosonic systems were studied in presence of these energy spectra.

In the case of bosons, at low temperature a large fraction of particles occupy the lowest energy state and can give rise to the phase transition known as Bose Einstein condensation (BEC). The absolute minimum of the energy is the key feature for the physics of bosons at low temperature which is strongly affected by the presence of a SOC term. For the pure Rashba gauge potential  $\eta_{soc} = 1$  the dispersion curve minimum is a constant nonzero radius in the momentum space as shown in the left figure 1.3. This corresponds to a massive degeneracy of the single-particle ground level. In this particular case, as we will see, Bose-Einstein condensation does not necessary occur and a highly correlated ground state may be expected in the presence of a contact interaction.

The existence of this degeneracy determines strongly the behavior of such bosonic systems. The simplest way to break explicitly this symmetry is to change the intensity of the two Raman lasers e.g. changing the amplitude of their plane-waves in the x-y plane leading to  $\eta_{soc} \neq 1$ , as shown in the right figure 1.3.

*What happens to the BEC scenario in presence of a SOC?*

### 1.2.3 Ideal Bose gas in 3D

In three dimensions the degeneracy of the single particle ground state critically changes the BEC scenario. We study, in this section, the effect of SOC term in a homogeneous three dimensional Bose gas. The impact of a SOC on a BEC was already pointed out in recent theoretical studies [7, 28].

#### **Ideal Bosons in absence of SOC : $\kappa = 0$**

We briefly recall the standard BEC phase transition in a three dimensional homogeneous system without any coupling or interaction. The number of particles at temperature  $T = (k_B \beta)^{-1}$  and chemical potential  $\mu \leq 0$  in the energy eigenstate  $\epsilon(\mathbf{k})$  is simply given by the Bose distribution,  $N_{\mathbf{k}} = (\exp(\beta[\epsilon_{\mathbf{k}} - \mu]) - 1)^{-1}$ , and the density of the excited states writes

$$n_{\text{ex}} \equiv \frac{1}{V} \sum_{\mathbf{k} \neq \vec{0}} N_{\mathbf{k}} = \frac{g_{\frac{3}{2}}(e^{\beta\mu})}{\lambda_T^3} \quad (1.20)$$

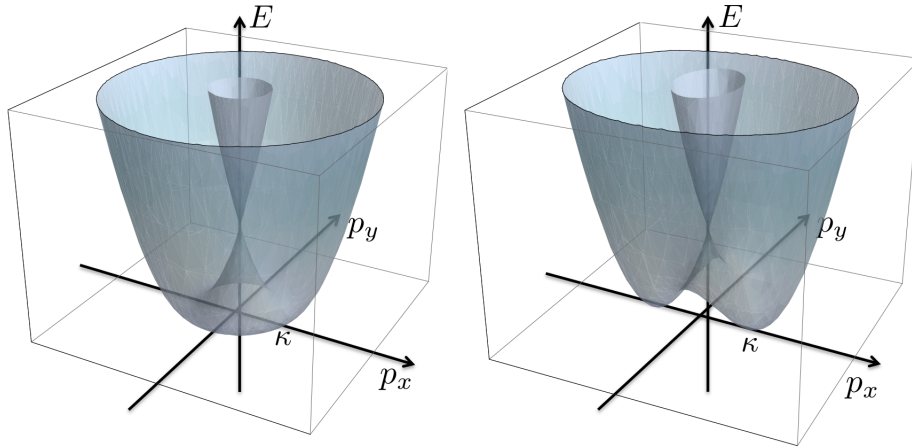


Figure 1.3: Figures extracted from [27]. Two dimensional dispersion of a homogeneous SOCed system. The two branches  $\epsilon_{\pm}$  touch at the origin. The left graph corresponds to the pure Rashba term whereas the right graph is plotted for  $\eta_{soc} = 0.7$ . We see in this last case that only two minima appear in  $p_x = \pm\kappa$ .

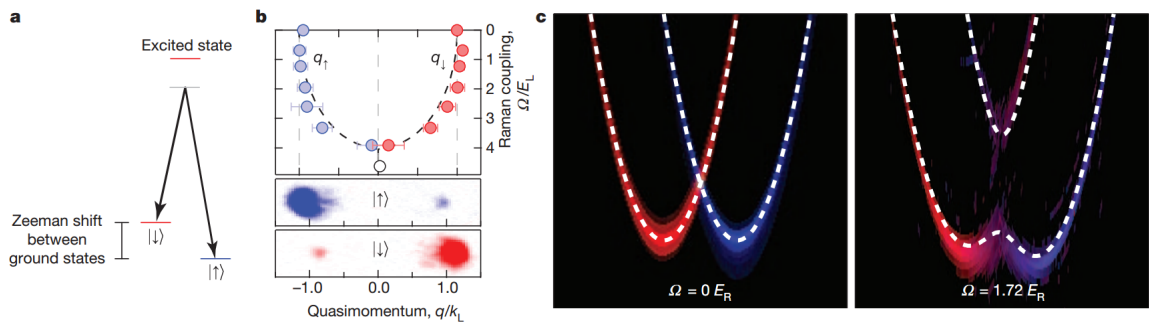


Figure 1.4: Figure extracted from [4] a) Typical level diagram. b) Minima location. Measured location of energy minimum or minima, where as a function of laser intensity the characteristic double minima of SOC dispersion move together and finally merge. c) Dispersion measured in  ${}^6\text{Li}$ .

where  $g_\alpha(z) = \sum_{l=1}^{\infty} \frac{z^l}{l^\alpha}$  is the Riemann Zeta function and

$$\lambda_T = \sqrt{\frac{2\pi\hbar^2}{mk_B T}} \quad (1.21)$$

is the thermal de Broglie wavelength. The BEC phase transition occurs at  $\mu = 0$  corresponding to a critical temperature  $T_C$  where the density of particles in the excited state, Eq.(1.20) saturates and the number of particles in the ground state,  $N_0$ , becomes extensive. The condensed fraction  $N_0/N$  remains non-zero even in the thermodynamic limit. In this case the system has formed a Bose-Einstein condensate in the zero momentum mode  $k = 0$ .

### Impact of SOC : $\kappa \neq 0$

We now consider a bosonic gas with two internal degrees of freedom. As we have seen in the previous section, in presence of the SOC the dispersion relation  $\epsilon_{\pm}(\mathbf{k})$  is not minimal at  $k = 0$  any more. In the basis of energy eigenstates, the total number of particles is given by the sum over both energy branches. The excited state density now writes

$$n_{\text{ex}} = \int \frac{d^3 k}{(2\pi)^3} \left( \frac{1}{e^{\beta(\epsilon_+(\mathbf{k})-\mu)} - 1} + \frac{1}{e^{\beta(\epsilon_-(\mathbf{k})-\mu)} - 1} \right) \quad (1.22)$$

Depending on the value of  $\eta_{\text{soc}}$ , two very different effects occur.

**Rashba-Dresselhaus term  $\eta_{\text{soc}} = 0$**  In this case, the two energy branches simply correspond to a shift of the energy dispersion in the  $k_x$  direction

$$\begin{aligned} (2\pi)^3 n_{\text{ex}} &= \int_{-\infty}^{\infty} dk_z \int_{-\infty}^{\infty} dk_y \int_{-\infty}^{\infty} dk_x \left( e^{\beta \left( \frac{(k_x+\kappa)^2 + k_y^2 + k_z^2}{2m} - \mu \right)} - 1 \right)^{-1} \\ &+ \int_{-\infty}^{\infty} dk_z \int_{-\infty}^{\infty} dk_y \int_{-\infty}^{\infty} dk_x \left( e^{\beta \left( \frac{(k_x-\kappa)^2 + k_y^2 + k_z^2}{2m} - \mu \right)} - 1 \right)^{-1} \end{aligned} \quad (1.23)$$

Shifting the integration variable, we recover the ideal gas expression for the density of excited particles in each energy branch. Below the transition at  $\mu = 0$ , both eigenstates with  $k_x = \pm\kappa$  become occupied. The condensate is therefore built out of two exactly degenerate modes.

**Pure Rashba**  $\eta_{soc} = 1$  Whereas  $\eta_{soc} < 1$  is qualitatively similar to the scenario with  $\eta_{soc} = 0$  leading to a two-fold degeneracy of the condensate, fully isotropic SOC,  $\eta_{soc} = 1$ , is essentially different. It was experimentally achieved and explored [2, 3]. For  $\eta_{soc} = 1$  the minimum of the single particle energies is infinitely degenerate.

$$(2\pi)^2 n_{ex} = \int_{-\infty}^{\infty} dk_z \int_0^{\infty} k_{\perp} dk_{\perp} \left( e^{\beta \left( \frac{(k_{\perp} + \kappa)^2 + k_z^2}{2m} - \mu \right)} - 1 \right)^{-1} + \int_{-\infty}^{\infty} dk_z \int_0^{\infty} k_{\perp} dk_{\perp} \left( e^{\beta \left( \frac{(k_{\perp} - \kappa)^2 + k_z^2}{2m} - \mu \right)} - 1 \right)^{-1} \quad (1.24)$$

This expression does not simplify as in the pure Rashba case, but can be written as

$$n_{ex} = n_+ + n_- = 2 \frac{g_{\frac{3}{2}}(e^{\beta\mu - \frac{\beta\kappa^2}{2m}})}{\lambda_T^3} + \frac{\kappa}{\lambda_T^2} \sum_{n=1}^{\infty} \frac{e^{n\beta\mu}}{n} \operatorname{erf} \left( \sqrt{\frac{\beta n}{2m}} \kappa \right) \quad (1.25)$$

where  $\operatorname{erf}(x) = \frac{1}{\sqrt{\pi}} \int_{-x}^x e^{-t^2} dt$  is the error function. The last term in this expression prevents the occurrence of BEC since it diverges in the limit of vanishing chemical potential. Any arbitrary high density is therefore accessible without the need of macroscopically occupying any single particle state. In contrast to  $\eta_{soc} < 1$ , the ideal Bose gas with isotropic SOC does not have a BEC phase transition at finite temperature.

As pointed out by reference [27], the absence of a BEC at finite temperature can be explained by the infinite degeneracy of the single particle ground state in the pure Rashba case ( $\eta_{soc} = 1$ ). At very low energies the density of states is constant like for non-interacting particles in two dimensions

$$n(E) = \int \frac{d^3 k}{(2\pi)^3} \delta(E - \epsilon_-(\mathbf{p})) \sim \frac{\kappa}{2\pi} \quad (1.26)$$

Therefore, at low temperatures, our system behaves similar to a two dimensional Bose gas without SOC where Bose condensation is suppressed by the higher density of states.

### 1.2.4 Ideal Bose gas in 2D

In two spatial dimensions, a Kosterlitz-Thouless phase transition occurs for an interacting homogeneous Bose gas without SOC, so that we expect also the SOCed Bose gas to be particularly affected by presence of interactions. These systems are also of great interest for experimental groups [5]. Before focusing on the interacting system in the next chapters, we study quantitatively in this section the impact of the SOC on a two dimensional non interacting gas.

#### Ideal Bose gas without SOC: $\kappa = 0$

Similar to Eq.(1.22), we calculate the density of non-condensed particles

$$n = \frac{\pi}{4\pi^2} \frac{2mT}{\hbar^2} \int_0^\infty dx \frac{e^{-x+\beta\mu}}{1 - e^{-x+\beta\mu}} \quad (1.27)$$

$$= -\frac{mT}{2\pi\hbar^2} \log[1 - e^{\beta\mu}] \quad (1.28)$$

Using the thermal wave length defined in Eq.(1.21) the density writes

$$n\lambda_T^2 = -\log[1 - e^{\beta\mu}] \quad (1.29)$$

As anticipated, Bose-Einstein condensation is absent, since the density diverges for vanishing chemical potential. Nevertheless, the number of bosons in the ground state,  $N_0$ , becomes large at low temperatures,

$$N_0 \simeq \frac{T}{|\mu|} \simeq e^{n\lambda^2} \quad (1.30)$$

though never macroscopic at any finite temperature,  $N_0/V = 0$  in the thermodynamic limit.

**Isotropic (pure Rashba) SOC**

Since we have seen that no BEC occurs in two dimensions, we limit ourself to study the impact of a pure Rashba SOC,  $\eta_{soc} = 1$ , where the single particle ground state is infinitely degenerate. In the two dimensional system, we get for the density

$$2\pi n = \int_0^\infty k_\perp dk_\perp \left( e^{\beta \left( \frac{(k_\perp + \kappa)^2}{2m} - \mu \right)} - 1 \right)^{-1} \quad (1.31)$$

$$+ \int_0^\infty k_\perp dk_\perp \left( e^{\beta \left( \frac{(k_\perp - \kappa)^2}{2m} - \mu \right)} - 1 \right)^{-1} \quad (1.32)$$

which can be simplified by changing the integration variables

$$2\pi n = 2 \int_0^\infty r dr \left( e^{\beta \left( \frac{r^2}{2m} - \mu \right)} - 1 \right)^{-1} + 2\kappa \int_0^\kappa dr \left( e^{\beta \left( \frac{r^2}{2m} - \mu \right)} - 1 \right)^{-1} \quad (1.33)$$

$$(1.34)$$

or

$$n\lambda^2 = -\log[1 - e^{\beta\mu}] + \frac{2\kappa}{mT} \int_0^\kappa dr \frac{1}{e^{\beta \left( \frac{r^2}{2m} - \mu \right)} - 1} \quad (1.35)$$

The additional term on the density due to SOC is always positive, so that the density of particles per spin at constant chemical potential is higher than without SOC.

Although BEC does not occur for  $\eta_{soc} = 1$  in two and three dimensions at finite temperatures for ideal Bosons, this does not exclude the occurrence of a phase transition in the interacting case. Therefore we investigate the effect of interparticle interactions within the mean field approximation in the next section.

*What is the effect of the interactions ?*

### 1.3 Interacting Bose gas: Mean Field Approximation

In a dilute system, interactions between the particles are dominated by two-body collisions. At low energies, the two-body interaction can be effectively described by a single parameter, the s-wave scattering length  $a$ , independently of the details of the two body potential. In the following, we will use a contact pseudo-potential  $g\delta(\mathbf{r})$  for the interaction where the interaction strength  $g$  is related to the scattering length  $a$  through  $g = 4\pi\hbar^2 a/m$  [29]. In the case of a Bose gas with two internal (spin) states, three coupling parameter are in general needed,  $g_{\sigma'\sigma}$  proportional to the scattering amplitudes between different the various hyperfine states as  $\sigma$  and  $\sigma'$ . In second quantization, the interaction part of the Hamiltonian is then given by

$$\hat{\mathcal{H}}_{\text{int}} = \int d\mathbf{x} \sum_{\sigma, \sigma'=\uparrow, \downarrow} g_{\sigma'\sigma} \hat{\Psi}_{\sigma'}^\dagger(\mathbf{x}) \hat{\Psi}_\sigma^\dagger(\mathbf{x}) \hat{\Psi}_{\sigma'}(\mathbf{x}) \hat{\Psi}_\sigma(\mathbf{x}) \quad (1.36)$$

with  $g_{\uparrow\downarrow} = g_{\downarrow\uparrow}$ . Together with the single particle Hamiltonian, Eq.(1.17), the total Hamiltonian then writes

$$\hat{\mathcal{H}} = \hat{\mathcal{H}}_0(\mu, \kappa, \eta_{soc}) + \hat{\mathcal{H}}_{\text{int}}(g_{\uparrow\uparrow}, g_{\downarrow\downarrow}, g_{\uparrow\downarrow}) \quad (1.37)$$

At high density and low temperature the energy is dominated by interactions proportional to the density squared, Eq. (1.36). We may expect fluctuations of the density to be strongly suppressed. Replacing the density operator by its expectation value, we obtain a mean-field description neglecting fluctuation effects.

As we will show, within mean-field, the low temperature phases are selected by the single combination

$$g = 2g_{\uparrow\downarrow} - g_{\uparrow\uparrow} - g_{\downarrow\downarrow} \quad (1.38)$$

In the other limit of high temperatures and low densities, the interparticle interaction can be considered as a perturbation to the non-interacting kinetic energy. This regime is again correctly described in leading order by a mean field theory. In the next section we will study the two mean field prediction at high and low temperature.

### 1.3.1 High temperature Mean Field Hartree approximation

In this section to review the derivation of the high temperature mean field approximation following closely the reference of J-P Blaizot and G.Ripka, Quantum theory of finite systems [30] where the interaction leads to a simple shift of the effective chemical potential. For simplicity, we only consider an averaged interaction strength with  $g_{\uparrow\uparrow} = g_{\downarrow\downarrow} = g_{\uparrow\downarrow}$ , or  $g = 0$ . Corrections due to an anisotropy  $g \neq 0$  of the couplings  $g_{\uparrow\uparrow}, g_{\downarrow\downarrow}, g_{\uparrow\downarrow}$  can be included without difficulty, but are negligible for all coupling parameters considered in this thesis.

The free energy of the system is defined as,

$$F = E - TS - \mu N = -k_B T \log(Z) \quad (1.39)$$

where  $Z = \text{Tr}[\exp(-\beta(H - \mu N))]$  is the grand canonical partition function.

The mean field approximation is based on the following inequality

$$F \leq \frac{1}{\beta} \langle \log \rho_0 \rangle_0 + \langle \hat{\mathcal{H}} \rangle_0 \quad (1.40)$$

where  $\rho_0 = \exp[-H_0]/Z_0$  is any trial density matrix corresponding to a Hamiltonian  $H_0$  and  $Z_0$  is the corresponding partition function,  $\langle \cdot \rangle_0 \equiv \text{Tr}\{\cdot \rho_0\}$

Our ansatz for the trial density matrix is based on the non-interacting part of the Hamiltonian with an additional mean-field shift of all energies, such that the Hamiltonian of our system can be separated as

$$\hat{\mathcal{H}} = \hat{\mathcal{H}}_0 + \hat{\mathcal{H}}_1 \quad (1.41)$$

$$\hat{\mathcal{H}}_0 = \sum_{\vec{k}, \sigma=\pm} \left( \frac{(k_{\perp} + \kappa)^2 + k_z^2}{2m} - \mu + \xi \right) \hat{\Phi}_{\vec{k}, \sigma}^{\dagger} \hat{\Phi}_{\vec{k}, \sigma} \quad (1.42)$$

$$\hat{\mathcal{H}}_1 = \frac{g_{\uparrow\uparrow}}{2V} \sum_{\mathbf{p}, \vec{k}, \vec{q}} \hat{\Phi}_{\vec{k}+\vec{q}}^{\dagger} \hat{\Phi}_{\mathbf{p}-\vec{q}}^{\dagger} \hat{\Phi}_{\vec{k}} \hat{\Phi}_{\mathbf{p}} - \xi \sum_{\vec{k}, \sigma=\pm} \hat{\Phi}_{\vec{k}, \sigma}^{\dagger} \hat{\Phi}_{\vec{k}, \sigma} \quad (1.43)$$

We obtain

$$F \leq \frac{1}{\beta} \langle \log \rho_0 \rangle_0 + \langle \hat{\mathcal{H}}_0 \rangle_0 + \langle \hat{\mathcal{H}}_1 \rangle_0 = F_0 + \langle \hat{\mathcal{H}}_1 \rangle_0 \quad (1.44)$$

where  $F_0(T, \mu, \xi) = -T \log Z_0$  is the free energy of our reference system. Using Wick's theorem we get

$$\langle \hat{\mathcal{H}}_1 \rangle_0 = \frac{g_{\uparrow\uparrow}}{V} \sum_{\vec{k}} \langle \hat{\Phi}_{\vec{k}}^{\dagger} \hat{\Phi}_{\vec{k}} \rangle_0 \sum_{\mathbf{p}} \langle \hat{\Phi}_{\mathbf{p}}^{\dagger} \hat{\Phi}_{\mathbf{p}} \rangle_0 - \xi \sum_{\vec{k}, \sigma=\pm} \langle \hat{\Phi}_{\vec{k}, \sigma}^{\dagger} \hat{\Phi}_{\vec{k}, \sigma} \rangle_0 \quad (1.45)$$

Introducing the density of our mean-field approximation

$$n(\xi) = \frac{1}{V} \sum_k \langle \hat{\Phi}_k^\dagger \hat{\Phi}_k \rangle_0 = -\frac{T}{V} \frac{d}{d\xi} F_0 \quad (1.46)$$

the variational expression for the free energy writes

$$F \leq F_0(\xi) + V g_{\uparrow\uparrow} [n(\xi)]^2 - \xi V n(\xi) \quad (1.47)$$

Since we have

$$-\frac{\partial F_0(\xi)}{\partial \xi} = \frac{\partial F_0(\xi)}{\partial \mu} = \beta V n(\xi) \quad (1.48)$$

the derivative of the variational free energy with respect to  $\xi$  leads to the following condition for its minimum

$$-V n(\xi) + 2V g_{\uparrow\uparrow} n(\xi) n'(\xi) - V n(\xi) - \xi V n'(\xi) = 0 \quad (1.49)$$

which determines the mean-field energy shift self-consistently

$$\xi = 2g_{\uparrow\uparrow} n(\xi) \quad (1.50)$$

Explicitly, we then obtain a set of equations for the quasi-particle energies and density

$$\epsilon_{\pm}^{MF}(\mathbf{k}) = \frac{(k_{\perp} \pm \kappa)^2 + k_z^2}{2m} + 2g_{\uparrow\uparrow} n^{MF} \quad (1.51)$$

$$n^{MF}(\mu) = \sum_{\sigma=\pm} \int \frac{d^3k}{(2\pi)^3} \frac{1}{e^{\beta(\epsilon_{\sigma}^{MF}(\mathbf{k})-\mu)} - 1} \quad (1.52)$$

which has to be solved self-consistently. For fixed chemical potential, the single particle energies are shifted by a constant  $2g_{\uparrow\uparrow} n^{MF}$ . We see that the mean field approach at high temperature leads to qualitatively similar conclusions as for the ideal gas.

We will need this leading order approximation at high temperature to match our classical field calculations in Chapter II.

### 1.3.2 Mean Field ground states: Plane-Wave & Stripe phase

Our ideal gas calculations have shown that isotropic SOC may suppress Bose condensation at finite temperatures, and our previous mean field calculation only introduces a rigid shift of all energy levels.

Still, approaching zero temperature, the occupation of the lowest energy modes dominate and the formation of a condensate at zero temperature is expected. Here, we study possible phases of the ground state within the mean field approximation.

Let us rewrite the interaction energy, Eq. (1.36),

$$\mathcal{E}_{\text{int}} = \frac{1}{2} \int d\mathbf{r} \sum_{\sigma, \sigma'=\uparrow, \downarrow} g_{\sigma'\sigma} \langle n_{\sigma'}(\mathbf{r}) n_{\sigma}(\mathbf{r}) \rangle \quad (1.53)$$

using the density operator  $n_{\sigma}(\mathbf{r})$ . In a homogeneous (translationally invariant) system the tendency of the interaction is to flattened the coupled densities in real space. Neglecting density fluctuations, we expect two different situations to minimize the interaction energy:

**Case**  $g_{\uparrow\uparrow}, g_{\downarrow\downarrow} > g_{\uparrow\downarrow}$  Each densities  $n_{\uparrow}$  and  $n_{\downarrow}$  should be constant in space.

**Case**  $g_{\uparrow\downarrow} > g_{\uparrow\uparrow}, g_{\downarrow\downarrow}$  The sum of the two densities is constant but densities of opposite spin,  $n_{\uparrow}$  and  $n_{\downarrow}$ , avoid each other spatially.

Based on this heuristic considerations, we will now write down a mean field ansatz for the different ground states of isotropic and anisotropic SOCed Bosons.

#### Variational calculation

In Fourier space, using Eq. (1.11), the interaction Hamiltonian, Eq. (1.36), writes

$$\hat{\mathcal{H}}_{\text{int}} = \sum_{\mathbf{k}_1 + \mathbf{k}_2 = \mathbf{k}_3 + \mathbf{k}_4} \left[ \frac{g_{\uparrow\uparrow}}{2V} \hat{u}_{\mathbf{k}_1}^{\dagger} \hat{u}_{\mathbf{k}_2}^{\dagger} \hat{u}_{\mathbf{k}_3} \hat{u}_{\mathbf{k}_4} + \frac{g_{\downarrow\downarrow}}{2V} \hat{d}_{\mathbf{k}_1}^{\dagger} \hat{d}_{\mathbf{k}_2}^{\dagger} \hat{d}_{\mathbf{k}_3} \hat{d}_{\mathbf{k}_4} + \frac{g_{\uparrow\downarrow}}{V} \hat{u}_{\mathbf{k}_1}^{\dagger} \hat{d}_{\mathbf{k}_2}^{\dagger} \hat{u}_{\mathbf{k}_3} \hat{d}_{\mathbf{k}_4} \right] \quad (1.54)$$

where we have explicitly written out all three couplings. For our variational calculations of the ground state energy, we start with the simplest, less symmetric case of bosons with anisotropic SOC.

**Anisotropic SOC**,  $\eta_{soc} < 1$  In this case the single particle spectrum has two degenerate minima in  $\mathbf{k} = \boldsymbol{\kappa} = (\pm\boldsymbol{\kappa}, 0, 0)$  corresponding to the single particle states

$$\hat{\Phi}_{\pm\boldsymbol{\kappa}}^{-\dagger} |0\rangle = \frac{1}{\sqrt{2}} \left( \hat{u}_{\pm\boldsymbol{\kappa}}^{\dagger} \mp \hat{d}_{\pm\boldsymbol{\kappa}}^{\dagger} \right) |0\rangle \quad (1.55)$$

Introducing the angle  $\phi$  that described the linear superposition of the two minimal states (in a single particle), our mean field ansatz for the ground state then writes

$$|\Phi^{-}(\phi)\rangle = \frac{\left( \cos(\phi)\hat{\Phi}_{\boldsymbol{\kappa}}^{-\dagger} + \sin(\phi)\hat{\Phi}_{-\boldsymbol{\kappa}}^{-\dagger} \right)^N}{\sqrt{N!}} |0\rangle \quad (1.56)$$

with  $N$  the number of particles in the system. We then evaluate the interacting energy, Eq.(1.54),

$$\langle \Phi^{-}(\phi) | \hat{\mathcal{H}}_{\text{int}} | \Phi^{-}(\phi) \rangle \quad (1.57)$$

The non zero components of this expression can be decomposed into three different situations : (1) all the particles carry a  $\boldsymbol{\kappa}$  momentum, (2) all the particle carry a  $-\boldsymbol{\kappa}$  momentum, (3) the two particles carry different momenta  $\pm\boldsymbol{\kappa}$  and exchange a momentum  $2\boldsymbol{\kappa}$ . In this last case, four different arrangement of momenta  $\pm\boldsymbol{\kappa}$  are possible. When the two interacting particle carry a different spin, the negative sign in Eq. (1.55) has to be taken and it introduces a term proportional to  $-g_{\uparrow\downarrow} |\cos(\phi)|^2 |\sin(\phi)|^2$ . By explicitly calculating each non zero configuration and using the normalization condition we obtain,

$$\langle \Phi^{-} | \hat{\mathcal{H}}_{\text{int}} | \Phi^{-} \rangle = \frac{N(N-1)}{8V} \left( g_{\uparrow\uparrow} + g_{\downarrow\downarrow} + 2g_{\uparrow\downarrow} + |\sin(2\phi)|^2 (g_{\uparrow\uparrow} + g_{\downarrow\downarrow} - 2g_{\uparrow\downarrow}) \right) \quad (1.58)$$

Minimizing the interaction energy, Eq. (1.58), we distinguish three cases depending on the sign of the anisotropy of the interaction,  $g$ .

**Case  $g_{\uparrow\uparrow} + g_{\downarrow\downarrow} > 2g_{\uparrow\downarrow}$  i.e.  $g < 0$ :** The minimum of the energy corresponds to  $\phi = \{0, \pi/2\}$ . In this case the particle populate a single momentum  $\pm\boldsymbol{\kappa}$  and the state is called Plane Wave state.

**Case  $2g_{\uparrow\downarrow} > g_{\uparrow\uparrow} + g_{\downarrow\downarrow}$  i.e.  $g > 0$ :** The minimum of the energy corresponds to  $\phi = \pi/4$ . The particles are in a superposition of two opposite momenta  $\pm\boldsymbol{\kappa}$  e.g. in a superposition of two Plane Wave states. This standing wave forms stripes in the real space and is called Stripe Phase.

**Case  $g_{\uparrow\uparrow} + g_{\downarrow\downarrow} = 2g_{\uparrow\downarrow}$  i.e.  $g = 0$ :** The Plane Wave state and Stripe Phase are degenerate. This degeneracy is present within the mean field approximation and it is not expected to be robust beyond mean field.

**Isotropic SOC,  $\eta_{soc} = 1$**  As we have seen in the non-interacting section, when the spin-orbit coupling is isotropic in the  $x - y$  plane the single-particle ground state is infinitely degenerate along a momentum ring of radius  $\kappa$ . In order to minimize the energy, we can choose a mean-field ansatz where we choose to populate only one direction, so that we essentially recover the scenario above. Allowing for a combination of more momenta in the ansatz, the calculation also involves the angles  $\mathbf{k}_1, \mathbf{k}_2$  and  $\mathbf{k}_3, \mathbf{k}_4$  in Eq. (1.54). This approach was studied in reference [7] and numerical calculation done by reference [11] produced consistent with the results based on a single direction shown in figure 1.5.

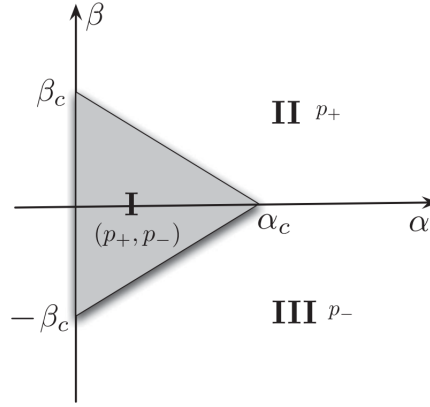


Figure 1.5: Mean field phase diagram from ref [11]  $\alpha = g_{\uparrow\downarrow}/g$ ,  $\beta = (g_{\uparrow\uparrow} - g_{\downarrow\downarrow})/\bar{g}$  and  $\bar{g} = (g_{\uparrow\uparrow} + g_{\downarrow\downarrow})/2$ . Using the formalism of this thesis, the critical value of  $\alpha$  is predicted for  $\alpha_c = 1$  and the indices  $p_+$  and  $p_-$  correspond to the directions  $k_x = \pm\kappa$ . Region I is a superposition of  $p_+$  and  $p_-$  e.g. the stripe phase. Region II and III are states in which only  $p_+$  and  $p_-$  are populated respectively.

### Mean field phase diagram and ground state wave function

We have seen that in the presence of interactions the mean field ground state breaks the symmetry of the degenerate single particle energy levels selecting one direction  $|\boldsymbol{\kappa}| = \kappa$ . The wave function of the mean field ground state, Eq. (1.56), writes

$$\psi_{\boldsymbol{\kappa}}^{MF}(\mathbf{r}) = \begin{pmatrix} \psi_{\uparrow, \boldsymbol{\kappa}}^{MF}(\mathbf{r}) \\ \psi_{\downarrow, \boldsymbol{\kappa}}^{MF}(\mathbf{r}) \end{pmatrix} = \frac{1}{\sqrt{2}} \left[ \cos(\phi) e^{i\boldsymbol{\kappa} \cdot \mathbf{r}} \begin{pmatrix} 1 \\ -e^{i\theta_{\boldsymbol{\kappa}}} \end{pmatrix} + \sin(\phi) e^{-i\boldsymbol{\kappa} \cdot \mathbf{r}} \begin{pmatrix} 1 \\ e^{i\theta_{\boldsymbol{\kappa}}} \end{pmatrix} \right] \quad (1.59)$$

up to total phase  $e^{i\theta}$ . Without loss of generality, we can choose  $\boldsymbol{\kappa} = \kappa(1, 0, 0)$ . For  $\phi = 0$  we have a pure plane-wave state :  $\psi_{\boldsymbol{\kappa}}^{MF}(\mathbf{r}) = \frac{1}{\sqrt{2}} (e^{i\kappa x}, -e^{i\kappa x})$ . The wave-function is described by a single plane-wave and the density of each spin component is therefore flat in space. For  $\phi = \pi/4$  we describe the stripe phase:  $\psi_{\boldsymbol{\kappa}}^{MF}(\mathbf{r}) = \frac{1}{\sqrt{2}} (\cos(\kappa x), i \sin(\kappa x))$ . The total density is also flat but the density of each component fluctuates spatially with a defined wavelength  $\kappa$  e.g. appearance of stripes.

However, since mean field usually overestimates ordering, it is questionable if these exotic mean field ground states are really stable at zero temperature, since the large degeneracy of the single particle spectrum may significantly enhance fluctuation effects.

*What are the main theories/results beyond the mean approach?*

## 1.4 Fluctuations & Open questions

**Fluctuations beyond mean-field** We propose in this section to review different approaches that have been applied to address questions beyond mean field.

- **Variational wave function** Fragmentation is a main example of a ground state not captured by the mean field approach. Despite being particularly fragile, references [31, 32] propose fragmented states as possible ground states. Based on very dilute limit arguments, reference [33] propose a fermionized many-body state by composite fermion construction as a ground state of interacting bosons.
- **Effective theory** At extremely low temperature, only low energy excitations are populated and the degrees of freedom of the system are therefore expected to be reduced. A more simple, effective theory based on minimal fluctuations around the mean field solution has been used to describe the system. Following this approach we can, for instance, consider only the lower branch of the energy spectrum  $\Phi^-(\mathbf{k})$  in Eq. (1.19). One standard approximation is for instance, by defining the wave-function as a phase and a density component, to integrate out density fluctuations and to consider only phase fluctuations. The Plane Wave state energy is then described by only one phase. On the other hand the Stripe Phase breaks the translational symmetry and is therefore described by two phases [9].

Within these approaches, references [9] and [10] propose a qualitative phase diagram at finite temperature of a SOCed Bose gas in two dimension. In the third chapter of this thesis, we will draw a significantly different phase diagram based on a classical field theory which is expected to be valid at finite temperature around the phase transition.

- **Renormalized T-matrix approach** In the pure Rashba case  $\eta_{soc} = 1$  the interacting term Eq. (1.54) couples any momentum relying on the ring minimum  $\mathbf{k} = \kappa$ . As we showed in the previous section, in the case of an fully isotropic interaction  $g = 0$  the ground state is degenerate. In order to lift this degeneracy, reference [34] consider renormalized interactions to determine the absolute ground state. Using the T-matrix formalism they consider a renormalized contact interaction that depends on the angle between the two momenta  $g_{\mathbf{k},\mathbf{k}',\sigma,\sigma'}$ . The effective interaction is stronger when  $\mathbf{k}$  and  $\mathbf{k}'$  are in the same direction, therefore indicating a stripe phase as an absolute ground state.

- **Bogoliubov approach** The Bogoliubov approach is suited for studying fluctuations on top of the mean field prediction. In our case, this study is particularly interesting in the case of isotropic contact interaction  $g = 0$  when no single ground state is selected within the mean field approximation. By an order by disorder mechanism, reference [35] finds that the absolute ground state corresponds to a Plane Wave state and results from a competition of the thermal and quantum fluctuations. By studying the depletion of the condensate and the impact of the finite temperature excitations, both references [35] and [7] draw a finite temperature phase diagram based on the Bogoliubov approximation, in particular in three dimensions (since the thermal fluctuations diverges in two dimensions).
- **Experimental challenge** The Stripe Phase is predicted to have supersolid properties by breaking both the gauge and the translational symmetries. Very fragile in experiments, many propositions were made to increase the stability of the stripe phase [36, 37, 38]. The predicted density modulation of the stripes were observed in 2017 by reference [39]. The role of an harmonic trap was also considered [40, 41] and the breaking of the stripe phase because of vortices was also carefully studied [15]. Because of the SOC term, the wave-function can change sign by either rotating the relative phase or by flipping spin. Half-quantum vortices are therefore naturally present in the system as non standard topological defects [42, 9, 43].
- **Superfluidity** Because of the breaking of Galilean invariance in SOCed system, the superfluidity is expected to be strongly affected by the presence of the SOC. In particular Landau's criterion for the critical velocity cannot be defined independently of the reference frame [44]. Reference [45] suggests that the normal density does not vanish at zero temperature, a strong reminder of the distinction between superfluidity and BEC.

Despite these efforts, the nature of the quantum ground state of interacting bosons with Rashba SO coupling remains an open issue. It is also a strong motivation for the experimental realization of such a SO coupling in cold atom systems, where a strongly correlated quantum state can be expected.

## 1.5 Outline of the thesis

**In the following, we wish to establish the phase diagram of a two-dimensional homogeneous gas of Rashba-Dresselhaus spin-orbit-coupled bosons.** This work has been inspired by both fundamental investigation and experimental progress, we will especially insist on a quantitative prediction of the phase diagram and on experimental implications of our results.

**Chapter II : The method** In order to focus on the finite temperature description of the bosonic gas, we selected a completely different approach from the methods presented in the previous section : the classical field approximation. This approximation is based on the field character description of the bosons that essentially occupy only the very low energy modes which become very highly populated. We then perform classical field Monte Carlo calculations which are expected to correctly describe the finite-temperature behavior close to a possible phase transition.

**Chapter III : BKT phase transition** After discussing the best numerical tools to correctly evaluate observables of interest like the condensed fraction and the density, we first show that the system undergoes a Kosterlitz-Thouless phase transition from a normal to superfluid state in presence of the SOC term. The thermodynamic limit behavior strongly depends on the anisotropy  $\eta_{soc}$  and in particular, we show that for  $\eta_{soc} = 1$  a crossover occurs for finite systems at similar phase-space densities, but no superfluid transition is expected for infinite sizes.

**Chapter IV : SP/PW orders** We then characterize the low temperature phases and we show that the spin order of the quasicondensate is driven by the anisotropy of the interparticle interaction. In particular in the superfluid state, we study the single-particle density matrix that decays algebraically and directly reflects the PW or SP character of the mean-field ground state. We show that in the case of an anisotropy  $g \neq 0$  spins exhibit a quasi-long-range order corresponding to the KT transition. In the case of a fully isotropic interparticle interaction, we show that the PW or SP degeneracy is unaffected by the transition. Our calculations then indicate a fractionalized quasicondensate where the mean-field degeneracy of the two states remains robust against critical fluctuations. We conclude on new prospects and motivations beyond the classical field approximation.

## 1.6 Résumé

Au cours du premier chapitre de cette thèse nous avons introduit le concept de champ de jauge artificiel. Afin de simuler des effets magnétiques dans les systèmes d'atomes neutres et ultra-froids, des techniques basées sur les transitions Raman entre deux états hyperfins des atomes ont été développées ces dernières années [1, 2, 3]. A l'aide de faisceaux lasers, ces différents champs peuvent être manipulés et contrôlés pour donner naissance en particulier à des vecteurs potentiels effectifs dont les composants ne commutent pas.

Un célèbre exemple, inclus dans ce dernier cas, est le couplage spin-orbite (SOC) dont nous avons sélectionné l'écriture en tant que interaction Rashba-Dresselhaus [17, 18] : les amplitudes du couplage selon les deux directions spatiales  $x$  et  $y$  peuvent être différentes et nous avons donc défini le nombre  $0 \leq \eta_{soc} \leq 1$  décrivant cette anisotropie.

Nous considérons ensuite le cas d'une particule isolée pour obtenir son spectre d'énergie en présence du terme SOC. Après avoir correctement transformé la base décrivant les deux états couplés de l'atome, nous avons mis en évidence la nouvelle dégénérescence de l'état fondamental induite par le couplage SOC. En effet dans le cas d'une anisotropie  $\eta_{soc} < 1$  le spectre d'énergie présente deux minima. Dans le cas d'un couplage SOC isotrope, le minimum de l'énergie correspond à un anneau dans l'espace des impulsions.

Dans ce dernier cas et pour un système de bosons non interagissants, nous avons également montré l'absence de transition de phase telle que la condensation de Bose-Einstein (BEC).

Nous avons alors introduit une première approche pour décrire les effets des interactions interparticules dans les gaz de bosons avec couplage SOC : l'approximation champ moyen. Deux régimes peuvent en principe être correctement décrits par cette méthode, celui d'une température infinie et celui d'une température nulle.

A très haute température l'effet des interactions correspond à un décalage effectif du potentiel chimique [30] égal à  $2g_{\uparrow\uparrow}n^{MF}$  avec  $g_{\uparrow\uparrow}$  l'interaction moyenne entre deux particules et  $n^{MF}$  la densité champ moyen déterminée de façon auto-cohérente. Celui-ci correspond au terme connu de Hartree.

A très basse température nous avons procédé par méthode variationnelle en écrivant un Ansatz de la fonction d'onde minimisant l'énergie d'une particule simple. Nous

avons alors déterminé les paramètres libres en minimisant l'énergie d'interaction.

Deux phases distinctes [11] sont alors apparues en fonction de l'intensité des interactions entre particules de même ( $g_{\uparrow\uparrow}$  et  $g_{\downarrow\downarrow}$ ) et différent spin ( $g_{\uparrow\downarrow}$ ). Pour  $g_{\uparrow\uparrow} + g_{\downarrow\downarrow} > 2g_{\uparrow\downarrow}$ , l'état fondamental correspond à une onde plane avec impulsion non nulle (PW). Dans le cas opposé,  $2g_{\uparrow\downarrow} > g_{\uparrow\uparrow} + g_{\downarrow\downarrow}$ , chaque particule est décrite comme une superposition de deux ondes planes avec impulsions opposées. Ce dernier état est appelé état de bande (SP) car des bandes apparaissent dans la densité en espace réel.

Enfin nous avons étudié les enjeux et avancées actuelles autour de ce type de système en insistant sur le rôle prépondérant des fluctuations [7, 35] qui dépassent les prédictions souvent trop schématiques des théories type champ moyen.



# Chapter 2

## Methods

### Contents

---

<b>2.1 Introduction</b> . . . . .	<b>35</b>
<b>2.2 Classical field approximation</b> . . . . .	<b>38</b>
<b>2.3 Markov Chain Monte Carlo</b> . . . . .	<b>41</b>
2.3.1 Effective action $S$ . . . . .	41
2.3.2 Monte Carlo algorithms: Metropolis, Heat bath and Fourier moves . . . . .	43
2.3.3 Partition function . . . . .	49
<b>2.4 Density matching</b> . . . . .	<b>50</b>
2.4.1 Procedure . . . . .	50
2.4.2 Lattice expressions for ideal and mean-field classical fields .	50
2.4.3 Convergence and scale of energy . . . . .	55
<b>2.5 <i>Résumé</i></b> . . . . .	<b>56</b>

---

### 2.1 Introduction

In this chapter we present the main methods we used to establish the finite-temperature phase diagram of two dimensional Bose gases in presence of SOC and inter particle interactions. We will concentrate on weakly interacting systems at low temperature region. From the absence of BEC in an ideal (or mean-field) gas at any finite temperature, invoking continuity, we can expect the critical temperature of any possible phase transition to approach zero temperature in the limit of vanishing

interaction. Approaching zero temperature, bosons essentially occupy only the very low energy modes which become very highly populated. In this regime the field character of the quantum particles dominates and the description in terms of a classical field theory becomes quantitatively accurate [46, 47, 48, 49, 50]. Beyond the weakly interacting region, classical field theory is still capable to describe the universal behavior around a continuous phase transition, a well known result from the theory of critical phenomena [51]. In this thesis, we have established for the first time the phase diagram of interacting SOCed bosons, based on classical field Monte Carlo calculations.

Roughly speaking, the classical field description emerges by replacing the occupation of a "quantum mode" of energy  $\varepsilon$ , given by the Bose distribution  $(\exp[\varepsilon/k_B T] - 1)$ , with that of the classical field  $k_B T/\varepsilon$ , and, further, neglecting the non-vanishing commutators of the quantum fields. Both approximations becomes exact for the low energy modes in the limit of  $T \rightarrow 0$  and provide the starting point to a quantitative description of weakly interacting Bose gases.

Still, due to interactions, we cannot explicitly diagonalize the Hamiltonian even within the classical field approximation. However, the calculation of static observables directly maps to the calculation of classical probability distributions, well known in classical statistical mechanics. In our work, we have used Monte Carlo methods to numerically sample the classical field distribution.

The weight of each classical field configuration is given by a Boltzmann distribution according to its energy. However, two technical issues arise. First, in order to well define the energy of a classical field theory, we have to regularize its behavior at high energies ("ultraviolet divergencies"). Within numerical Monte Carlo calculations, this is naturally taken into account by discretizing the fields on a lattice. Second, SOC formally introduces imaginary terms in the action of the two complex fields representing the two spin states. So we first have to show that we really obtain a probability distribution, i.e the discretized action stays real for any configuration of the fields. Then, we can correctly sample classical field configurations by proposing efficient Monte Carlo algorithms ensuring the ergodicity of the system.

Eventually, we have to correct the raw densities of our classical field calculations which depends on the lattice discretization and to take into account the correct behavior of high energy modes which are Bose distributed. However, since these low occupied modes are only weakly affected by the interaction, the mean field approximation provides an accurate description for them. Using this correction, we can in principle match any observable from classical field calculations to provide quantitative predictions for our systems which can be directly compared to experiment [46].

## 2.2 Classical field approximation

As discussed in Chapter I, in this thesis we are interested into establishing the phase diagram in the limit of small interaction strength,  $mg_{\uparrow\uparrow} \ll 1$  and small spin-orbit coupling,  $\kappa\lambda_T \ll 1$  where  $\lambda_T = \sqrt{2\pi\hbar^2/mk_B T}$  is the thermal wave length at temperature  $T$ .

In this limit, the leading order corrections to mean-field are captured within classical field theory where the occupation of low energy modes is high such that commutators like  $[\hat{\Psi}^\dagger(\mathbf{r}), \hat{\Psi}(\mathbf{r}')] can be neglected. In this approximation, the field operator,  $\hat{\Psi}(\mathbf{r})$ , can be replaced by two complex fields,  $\Psi(\mathbf{r}) \equiv (\Psi_\uparrow(\mathbf{r}), \Psi_\downarrow(\mathbf{r}))$ , one for each spin.$

Starting from the ideal gas results of two dimensional systems presented in chapter I, we first introduce the classical field approximation in the absence of a SOC. Calculating the phase-space density for particles in the low-energy modes with  $\epsilon_k < k_B T$ ,

$$n_{<} \lambda^2 \equiv \lambda^2 \int_{\beta\epsilon_k < 1} \frac{d^2 k}{(2\pi)^2} N_k = \log \left[ \frac{1 - e^{\beta\mu-1}}{1 - e^{\beta\mu}} \right] = n\lambda^2 + \log[1 - e^{\beta\mu-1}] \approx n\lambda^2 - \log \left[ \frac{e}{e-1} \right] \quad (2.1)$$

we notice that at high degeneracy,  $n\lambda^2$ , the occupation of higher energy modes becomes negligible. At the same level of accuracy, we may also replace the Bose occupation  $N_k$  by the occupation of classical field,

$$N_k \approx N_k^{cf} \equiv \frac{1}{\beta(\epsilon_k - \mu)} \quad (2.2)$$

which gives,

$$\lambda^2 \int_{\beta\epsilon_k < 1} \frac{d^2 k}{(2\pi)^2} N_k^{cf} = \log \left[ \frac{1 + |\beta\mu|}{|\beta\mu|} \right] \approx n\lambda^2 + |\beta\mu| \quad (2.3)$$

The classical field distribution with a simple cut-off  $\Lambda = \sqrt{2mk_B T/\hbar^2}$  therefore quantitatively describes the leading order behavior of the density up to corrections of order  $(n\lambda^2)^{-1}$ . The corresponding energy distribution of the classical fields writes

$$\mathcal{H}_{cf}^0 - \mu N = \sum_{k < \Lambda} (\epsilon_k - \mu) \alpha_k^* \alpha_k \approx \sum_{\mathbf{r}} \left[ -\frac{\hbar^2}{2m} |\nabla \psi(\mathbf{r})|^2 - \mu |\psi(\mathbf{r})|^2 \right] \quad (2.4)$$

where  $\alpha_k$  are complex numbers which describe the classical field. Their Fourier transform,  $\psi(r)$ , defines their real space distribution on a lattice with minimum distance

$\sim \Lambda^{-1}$ . The theory is therefore naturally regularized by discretizing space on a lattice of linear extension  $L$ . The probability distribution for a given field configuration,  $\psi(r)$ , is then

$$p[\psi(r)] = Z_{cf}^{-1} e^{-\beta(\mathcal{H}_{cf} - \mu N)} \quad (2.5)$$

where  $Z_{cf} = \int D\psi(r) e^{-\beta\mathcal{H}_{cf}}$  is the partition function, where  $\int D$  indicates the summation over all discrete field configurations. For our non-interacting system,  $\mathcal{H}_{cf} = \mathcal{H}_{cf}^0$  and we can explicitly perform the Gaussian integral to obtain  $Z_{cf}^0$ . The classical field description of the ideal Bose gas with SOC does not pose additional difficulties using the eigenmode basis.

For interacting fields, we simply add their interaction energy to the non-interacting system

$$\mathcal{H}_{cf} = \mathcal{H}_{cf}^0 - \mu N + \sum_{\mathbf{r}} \sum_{\sigma\sigma'} \frac{g_{\sigma\sigma'}}{2} |\psi_{\sigma}(\mathbf{r})|^2 |\psi_{\sigma'}(\mathbf{r})|^2 \quad (2.6)$$

where we have explicitly written out possible spin dependence of the interaction.

**Validity range** In order to study the validity range of the classical field distribution we Taylor expand the nominator of the Bose distribution for small energies,

$$N_k = \frac{1}{\exp(\beta(\epsilon_k - \mu)) - 1} = \left( \sum_{n=1}^{\infty} \frac{\beta^n (\epsilon_k - \mu)^n}{n!} \right)^{-1} \quad (2.7)$$

The leading order term is precisely the classical field distribution,  $N_k \rightarrow \frac{k_B T}{\epsilon_k - \mu}$  under the condition

$$\epsilon_k - \mu \leq k_B T \quad (2.8)$$

Outside this energy range, classical field theory cannot be taken literally. However, interaction corrections to high energy modes  $\epsilon_k - \mu \geq k_B T$  can usually be treated perturbatively in the limit of weak interactions. We can then match the classical field results with accurate high energy behavior obtained perturbatively.

At very low temperatures, the classical field distribution approaches the configuration which minimizes the energy. From the variation of the fields, we obtain the time independent Gross-Pitaevskii equation in the limit of vanishing temperature. Therefore, the classical field approximation merges continuously the Gross-Pitaevskii

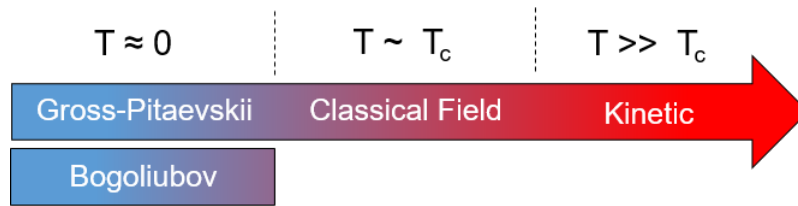


Figure 2.1: Qualitative scheme of the validity range of the theories in function of the temperature.

theory. However, quantum corrections, as contained for example in the Bogoliubov approximation, are not included. At high temperatures and weak interactions, the classical field as well as the full quantum field theory are both accurately described by their corresponding mean-field approximation, so that the difference between quantum and classical theory can be worked out analytically.

Between these two regimes, the classical field approximation captures the leading order thermal corrections to mean-field for the strongly degenerate, low energy states. In particular, it is capable to detect and correctly describe any possible finite temperature continuous phase transitions. For systems without SOC classical field theory correctly describes the BEC transition in three dimensions as well as the Kosterlitz-Thouless phase transition in two dimensions (e.g. the XY-model).

## 2.3 Markov Chain Monte Carlo

Even after applying the classical field approximation, we cannot explicitly integrate over the distribution  $p[\Psi(\mathbf{r})]$  Eq. (2.5) because of the interaction term from Eq. (1.36) that needs to be included. Indeed, the interaction term and the single-particle terms are both diagonal in different basis : real space and Fourier space, respectively.

We will therefore calculate the observables as numerical integrals. Multi-dimensional integrals like Eq. (2.5) can be evaluated using Monte Carlo methods. For numerical efficiency of the algorithm we aim to use a local form of the Hamiltonian. Since the Laplacian and derivative operators remain local around a point  $\mathbf{r}$  in the real space, we write down the effective total action for a given field configuration in real space.

### 2.3.1 Effective action S

We can write the probability  $p[\Psi(\mathbf{r})]$  of a given classical field configuration as proportional to  $\exp(-S[\Psi(\mathbf{r})])$ . Summing the kinetic energy, the SOC term and the contact interaction, the total local action  $S$  writes

$$\begin{aligned}
 S[\Psi(\mathbf{r})] = & \frac{a^2}{k_B T} \sum_{\mathbf{r}} \left\{ \sum_{\sigma=\uparrow,\downarrow} \left[ -\Psi_{\sigma}^*(\mathbf{r}) \frac{\hbar^2 \nabla_D^2}{2m} \Psi_{\sigma}(\mathbf{r}) - \mu |\Psi_{\sigma}(\mathbf{r})|^2 \right] \right. \\
 & + \frac{\hbar^2 \kappa}{m} \left[ \Psi_{\uparrow}^*(\mathbf{r}) \left( -i \partial_x^D - \eta_{soc} \partial_y^D \right) \Psi_{\downarrow}(\mathbf{r}) \right] \\
 & + \frac{\hbar^2 \kappa}{m} \left[ \Psi_{\downarrow}^*(\mathbf{r}) \left( -i \partial_x^D + \eta_{soc} \partial_y^D \right) \Psi_{\uparrow}(\mathbf{r}) \right] \\
 & \left. + \frac{1}{2} \sum_{\sigma, \sigma'=\uparrow,\downarrow} g_{\sigma\sigma'} |\Psi_{\sigma}(\mathbf{r})|^2 |\Psi_{\sigma'}(\mathbf{r})|^2 \right\} \quad (2.9)
 \end{aligned}$$

where  $a$  is the lattice spacing,  $\mu$  is the chemical potential, and  $\nabla_D$  and  $\partial_{\alpha}^D$  are finite difference expressions approximating the derivatives and we sum over all positions  $\mathbf{r}$  of the lattice. Provided that the expression of  $S[\Psi(\mathbf{r})]$  is real for any configuration of the field we can sample the distribution by Monte Carlo methods. Below we show explicitly that this discrete action is real.

**Kinetic term**

$$\sum_{\mathbf{r}} \Psi_{\sigma}^*(\mathbf{r}) \nabla_D^2 \Psi_{\sigma}(\mathbf{r}) = \sum_{\mathbf{r}} (\Psi_{\sigma}^R(\mathbf{r}) - i\Psi_{\sigma}^I(\mathbf{r})) \nabla_D^2 (\Psi_{\sigma}^R(\mathbf{r}) + i\Psi_{\sigma}^I(\mathbf{r})) \quad (2.10)$$

$$= \sum_{\mathbf{r}} \Psi_{\sigma}^R(\mathbf{r}) \nabla_D^2 \Psi_{\sigma}^R(\mathbf{r}) + \sum_{\mathbf{r}} \Psi_{\sigma}^I(\mathbf{r}) \nabla_D^2 \Psi_{\sigma}^I(\mathbf{r}) \quad (2.11)$$

$$+ i \left( \sum_{\mathbf{r}} \Psi_{\sigma}^R(\mathbf{r}) \nabla_D^2 \Psi_{\sigma}^I(\mathbf{r}) - \sum_{\mathbf{r}} \Psi_{\sigma}^I(\mathbf{r}) \nabla_D^2 \Psi_{\sigma}^R(\mathbf{r}) \right) \quad (2.12)$$

with  $\Psi_{\sigma}^R$  and  $\Psi_{\sigma}^I$  the real and imaginary part of the two component complex field  $\Psi$  having spin  $\sigma$ . Using the following finite difference expression of the Laplacian,

$$\nabla_D^2 \Psi_{\uparrow}(\mathbf{r}) = a^{-2} \sum_{\mathbf{i}}^d [\Psi_{\uparrow}(\mathbf{r} + \mathbf{ai}) + \Psi_{\uparrow}(\mathbf{r} - \mathbf{ai}) - 2\Psi_{\uparrow}(\mathbf{r})] \quad (2.13)$$

where  $\mathbf{i}$  denotes the unit vector pointing to the nearest neighbors on the lattice and  $a$  the lattice spacing. For simplicity we consider in this section the case  $a = 1$ . Together with periodic boundary conditions, we write

$$\sum_{\mathbf{r}} \Psi_{\sigma}^R(\mathbf{r}) \nabla_D^2 \Psi_{\sigma}^I(\mathbf{r}) \equiv \sum_{\mathbf{r}} [\Psi_{\sigma}^R(\mathbf{r}) \Psi_{\sigma}^I(\mathbf{r}-1) + \Psi_{\sigma}^R(\mathbf{r}) \Psi_{\sigma}^I(\mathbf{r}+1) - 2\Psi_{\sigma}^R(\mathbf{r}) \Psi_{\sigma}^I(\mathbf{r})] \quad (2.14)$$

$$\equiv \sum_{\mathbf{r}} [\Psi_{\sigma}^R(\mathbf{r}+1) \Psi_{\sigma}^I(\mathbf{r}) + \Psi_{\sigma}^R(\mathbf{r}-1) \Psi_{\sigma}^I(\mathbf{r}) - 2\Psi_{\sigma}^R(\mathbf{r}) \Psi_{\sigma}^I(\mathbf{r})] \quad (2.15)$$

$$\equiv \sum_{\mathbf{r}} \Psi_{\sigma}^I(\mathbf{r}) \nabla_D^2 \Psi_{\sigma}^R(\mathbf{r}) \quad (2.16)$$

Therefore the imaginary part of the kinetic energy identically vanishes and the corresponding action is real for any configuration of the fields.

**SOC term** Writing out the Pauli matrices in the SOC part of the action, we have

$$S_{\text{SOC}} = \sum_{\mathbf{x}} \left[ \Psi_{\uparrow}^*(\mathbf{r}) \left( i\partial_x^D + \eta\partial_y^D \right) \Psi_{\downarrow}(\mathbf{r}) + \Psi_{\downarrow}^*(\mathbf{r}) \left( i\partial_x^D - \eta\partial_y^D \right) \Psi_{\uparrow}(\mathbf{r}) \right] \quad (2.17)$$

Let us concentrate on the terms involving  $\partial_x^D$  first

$$\begin{aligned} \Psi_{\uparrow}^*(\mathbf{r}) \partial_x^D \Psi_{\downarrow}(\mathbf{r}) + \Psi_{\downarrow}^*(\mathbf{r}) \partial_x^D \Psi_{\uparrow}(\mathbf{r}) &= \Psi_{\uparrow}^R(\mathbf{r}) \partial_x^D \Psi_{\downarrow}^R(\mathbf{r}) + i\Psi_{\uparrow}^R(\mathbf{r}) \partial_x^D \Psi_{\downarrow}^I(\mathbf{r}) - i\Psi_{\uparrow}^I(\mathbf{r}) \partial_x^D \Psi_{\downarrow}^R(\mathbf{r}) \\ &+ \Psi_{\uparrow}^I(\mathbf{r}) \partial_x^D \Psi_{\downarrow}^I(\mathbf{r}) + \Psi_{\downarrow}^R(\mathbf{r}) \partial_x^D \Psi_{\uparrow}^R(\mathbf{r}) + i\Psi_{\downarrow}^R(\mathbf{r}) \partial_x^D \Psi_{\uparrow}^I(\mathbf{r}) \\ &- i\Psi_{\downarrow}^I(\mathbf{r}) \partial_x^D \Psi_{\uparrow}^R(\mathbf{r}) + \Psi_{\downarrow}^I(\mathbf{r}) \partial_x^D \Psi_{\uparrow}^I(\mathbf{r}) \end{aligned} \quad (2.18)$$

Again, using the finite difference expression together with periodic boundary condi-

tions

$$\sum_{\mathbf{r}} \Psi_{\uparrow}^R(\mathbf{r}) \partial_x^D \Psi_{\downarrow}^R(\mathbf{r}) + \Psi_{\downarrow}^R(\mathbf{r}) \partial_x^D \Psi_{\uparrow}^R(\mathbf{r}) = \sum_{\mathbf{r}} \partial_x^D \left( \Psi_{\uparrow}^R(\mathbf{r}) \Psi_{\downarrow}^R(\mathbf{r}) \right) = 0 \quad (2.19)$$

$$\sum_{\mathbf{r}} \Psi_{\downarrow}^I(\mathbf{r}) \partial_x^D \Psi_{\uparrow}^I(\mathbf{r}) + \Psi_{\uparrow}^I(\mathbf{r}) \partial_x^D \Psi_{\downarrow}^I(\mathbf{r}) = \sum_{\mathbf{r}} \partial_x^D \left( \Psi_{\downarrow}^I(\mathbf{r}) \Psi_{\uparrow}^I(\mathbf{r}) \right) = 0 \quad (2.20)$$

and we obtain

$$\sum_{\mathbf{r}} \Psi_{\uparrow}^*(\mathbf{r}) \partial_x^D \Psi_{\downarrow}(\mathbf{r}) + \sum_{\mathbf{r}} \Psi_{\downarrow}^*(\mathbf{r}) \partial_x^D \Psi_{\uparrow}(\mathbf{r}) \equiv 2i \sum_{\mathbf{r}} \left[ \Psi_{\downarrow}^I \partial_x^D \Psi_{\uparrow}^R + \Psi_{\uparrow}^I \partial_x^D \Psi_{\downarrow}^R \right] \quad (2.21)$$

After similar manipulations of the terms involving  $\partial_y^D$ , we obtain

$$\begin{aligned} S_{\text{SOC}} &= 2 \sum_{\mathbf{r}} \left[ \Psi_{\downarrow}^I(\mathbf{r}) \partial_x^D \Psi_{\uparrow}^R(\mathbf{r}) + \Psi_{\uparrow}^I(\mathbf{r}) \partial_x^D \Psi_{\downarrow}^R(\mathbf{r}) \right] \\ &+ 2\eta_{\text{soc}} \sum_{\mathbf{r}} \left[ \Psi_{\downarrow}^R(\mathbf{r}) \partial_y^D \Psi_{\uparrow}^R(\mathbf{r}) + \Psi_{\uparrow}^I(\mathbf{r}) \partial_y^D \Psi_{\downarrow}^I(\mathbf{r}) \right] \end{aligned} \quad (2.22)$$

Again, the SOC action is real for any field configurations, as well as the interaction energy.

$$S(\Psi(\mathbf{r})) \in \mathbb{R} \quad \forall \Psi(\mathbf{r}) \quad \text{in a periodic system} \quad (2.23)$$

Therefore,  $\exp(-S[\Psi(\mathbf{r})])$  is non negative and we can interpretate weight as a probability of a given field configuration suitable for Monte Carlo sampling.

### 2.3.2 Monte Carlo algorithms: Metropolis, Heat bath and Fourier moves

In this section, we briefly present few numerical algorithms that we have found essential to correctly sample the distribution of the fields using Monte Carlo methods based on a Markov process. Standard algorithms are typically based on Metropolis' rule for acceptance or rejection of changes in the field configuration.

The Markov chain is constructed by a random walk in configuration space, where the transition probability from one configuration  $\mathbf{R}$  (note that  $\mathbf{R}$  in our context labels the values of all fields at each lattice site) to another one  $\mathbf{R}'$  satisfies

$$\sum_{\mathbf{R}'} T(\mathbf{R} \rightarrow \mathbf{R}') = 1 \quad (2.24)$$

$$\sum_{\mathbf{R}} T(\mathbf{R} \rightarrow \mathbf{R}') = 1 \quad (2.25)$$

together with so called detailed balance condition

$$\pi(\mathbf{R})T(\mathbf{R} \rightarrow \mathbf{R}') = \pi(\mathbf{R}')T(\mathbf{R}' \rightarrow \mathbf{R}) \quad (2.26)$$

where  $\pi(\mathbf{R}) \propto \exp[-S(\mathbf{R})]$  is the probability distribution which we aim to sample.

Metropolis algorithm is a particularly simple solution for the transition where one proposes an arbitrary change of the configuration  $\mathbf{R}$  which is accepted with probability

$$T(\mathbf{R} \rightarrow \mathbf{R}') = \min \left[ 1, \frac{e^{-S(\mathbf{R}')}}{e^{-S(\mathbf{R})}} \right] \quad (2.27)$$

Whenever rejected, we remain at the same configuration. One can explicitly verify that Metropolis rule satisfies the detailed balance condition.

Since our action, Eq. (2.9) is local, we can efficiently compute  $S(\mathbf{R}') - S(\mathbf{R})$  for local changes avoiding the calculating of total action at each step.

However, standard Metropolis algorithm leads to a slow convergence for our purposes. Two main problems appear when decreasing the temperature. First, the acceptance of the moves decreases since Metropolis steps are completely random and most of the moves at low temperature lead to high energy changes which are highly unlikely. Secondly, different degenerate ground states of the ideal (or mean-field) system are separated from each other in the sense that they are not connected by local moves. In practice, local moves in real space do not ensure the ergodicity of the sampling for large systems where the probability to tunnel from one ground state to another gets exponentially small.

During the next sections, we propose few ways to tackle these problems. First, we will study the action itself and propose efficient changes instead of total random ones leading eventually to the Heat Bath, Gaussian, and Fourier space algorithms.

**A priori probabilities** To increase the acceptance probability of the simple Metropolis algorithm, we decompose the transition probability

$$T(\mathbf{R} \rightarrow \mathbf{R}') = \mathcal{A}(\mathbf{R} \rightarrow \mathbf{R}') p(\mathbf{R} \rightarrow \mathbf{R}') \quad (2.28)$$

into the a-priori probability  $\mathcal{A}(\mathbf{R} \rightarrow \mathbf{R}')$  and the final acceptance rate  $p(\mathbf{R} \rightarrow \mathbf{R}')$ . Our strategy will be to choose an a-priori probability which is easy to compute, typically

a Gaussian, and which increases the final acceptance rate given by

$$p(\mathbf{R} \rightarrow \mathbf{R}') = \min \left[ 1, \frac{e^{-S(\mathbf{R}')} \mathcal{A}(\mathbf{R}' \rightarrow \mathbf{R})}{e^{-S(\mathbf{R})} \mathcal{A}(\mathbf{R} \rightarrow \mathbf{R}')} \right] \quad (2.29)$$

Instead of proposing completely random moves, we therefore try to orientate changes. In order to propose the most efficient local move, let us consider the action keeping all the fields fixed except one component  $\Psi_\alpha(\mathbf{r})$ . We will then propose an optimized change of  $\Psi_\alpha(\mathbf{r})$ , the value of the  $\alpha$  field at  $\mathbf{r}$ . The part of the action without spin-orbit coupling involving  $\Psi_\alpha(\mathbf{r})$  writes

$$-\frac{1}{2} \left( \sum_i^d [\Psi_\alpha(\mathbf{r} + a\mathbf{i}) + \Psi_\alpha(\mathbf{r} - a\mathbf{i})] \right) \Psi_\alpha(\mathbf{r}) + \left( -\mu + \frac{\kappa^2}{2} + d \right) \Psi_\alpha(\mathbf{r})^2 + \frac{g_{\uparrow\uparrow}}{2} \left( \sum_{\beta=1}^N \Psi_\beta(\mathbf{r})^2 \right)^2 \quad (2.30)$$

where we have assumed symmetric interactions for simplicity. Note that the change of the action is diagonal in the different field components  $\Psi_\alpha(\mathbf{r}) = \{\Psi_\uparrow^R(\mathbf{r}), \Psi_\uparrow^I(\mathbf{r}), \Psi_\downarrow^R(\mathbf{r}), \Psi_\downarrow^I(\mathbf{r})\}$ , whereas the spin-orbit interaction couples different component of the fields.

$$\Delta S_{\text{SOC}}(\Psi_\uparrow^R(\mathbf{r})) \propto \text{const} \quad (2.31)$$

$$\Delta S_{\text{SOC}}(\Psi_\uparrow^I(\mathbf{r})) \propto \kappa \partial_x^D \Psi_\uparrow^R(\mathbf{r}) \quad (2.32)$$

$$\Delta S_{\text{SOC}}(\Psi_\downarrow^R(\mathbf{r})) \propto \kappa \left( \partial_x^D \Psi_\uparrow^R(\mathbf{r}) + \partial_y^D \Psi_\uparrow^I(\mathbf{r}) \right) \quad (2.33)$$

$$\Delta S_{\text{SOC}}(\Psi_\downarrow^I(\mathbf{r})) \propto \kappa \partial_y^D \Psi_\uparrow^R(\mathbf{r}) \quad (2.34)$$

Thus, changes in the total action involving  $\Psi_\alpha(\mathbf{r})$  can be written in the general form

$$\Delta S(\Psi_\alpha(\mathbf{r})) \propto b \Psi_\alpha(\mathbf{r}) - a \Psi_\alpha(\mathbf{r})^2 - \frac{g_{\uparrow\uparrow}}{2} \Psi_\alpha(\mathbf{r})^4 \quad (2.35)$$

with

$$b = \frac{1}{2} \sum_i^d [\Psi_\alpha(\mathbf{r} + \mathbf{i}) + \Psi_\alpha(\mathbf{r} - \mathbf{i})] + \Delta S_{\text{SOC}}(\Psi_\alpha(\mathbf{r})) \quad (2.36)$$

$$a = -\mu + \frac{\kappa^2}{2} + d + g_{\uparrow\uparrow} \sum_{\beta \neq \alpha} \Psi_\beta(\mathbf{r})^2 \quad (2.37)$$

where  $\Delta S_{\text{SOC}}(\mathbf{r})$  is linear in the field components  $\Psi_\beta(\mathbf{r})$  with  $\beta \neq \alpha$  containing the contributions from the SOC.

### Heat bath algorithm

The heat bath algorithm provides an exact sampling at high temperatures where interaction effects are small. Neglecting the anharmonic term,  $\propto g_0 \Psi_\alpha(\mathbf{r})^4$ , the change of the action, Eq. (2.35), becomes a quadratic form. The distribution  $\exp(-\Delta S[\Psi(\mathbf{r})])$  is therefore Gaussian centered around the minimum given by

$$2a\overline{\Psi_\alpha(\mathbf{r})} = b \quad (2.38)$$

or

$$\overline{\Psi_\alpha(\mathbf{r})} = \frac{b}{2a} = \frac{\sum_i^d [\Psi_\alpha(\mathbf{r})(\mathbf{r}+\mathbf{i}) + \Psi_\alpha(\mathbf{r}-\mathbf{i})] + 2\Delta S_{SOC}(\mathbf{r})}{2(-2\mu + \kappa^2 + 2d)} \quad (2.39)$$

for  $g_{\uparrow\uparrow} = 0$ . Explicitly, we have

$$\Delta S \propto -(-\mu + \kappa^2/2 + d) \left( \Psi_\alpha(\mathbf{r}) - \overline{\Psi_\alpha(\mathbf{r})} \right)^2 \quad (2.40)$$

We can sample exactly the distribution using

$$\Psi_\alpha(\mathbf{r}) \rightarrow \Psi_\alpha(\mathbf{r}') = \overline{\Psi_\alpha(\mathbf{r})} + \delta\Psi \quad (2.41)$$

where  $\delta\Psi$  is sampled from a normal distribution of variance

$$\sigma^2 = \frac{1}{-2\mu + \kappa^2 + 2d} \quad (2.42)$$

The corrections needed for the acceptance rate then writes

$$\log \left[ \frac{\mathcal{A}(\mathbf{R}' \rightarrow \mathbf{R})}{\mathcal{A}(\mathbf{R} \rightarrow \mathbf{R}')} \right] = \frac{-\left( \Psi_\alpha(\mathbf{r}) - \overline{\Psi_\alpha(\mathbf{r})} \right)^2 - \delta\Psi^2}{2\sigma^2} \quad (2.43)$$

We can further improve the acceptance using Eq. (2.37) for  $g_0 \neq 0$  which takes into account the local interactions with the other field components.

### Gaussian algorithm

The Heat Bath algorithm is based on an essentially exact sampling of the non-interacting system. However, for interacting systems with  $g_{\uparrow\uparrow} > 0$ , we have shown in Chapter I section 1.3.1 that the effective chemical potential is shifted by the mean field interactions. The chemical potential  $\mu$  can become positive, and the variance of the Gaussian sampling is not any more guaranteed to be positive.

In order to adapt to this situation, we make a general Gaussian ansatz for the a-priori probability

$$\mathcal{A}(\mathbf{R}' \rightarrow \mathbf{R}) = \exp\left(-\frac{(\Psi(\mathbf{R}) - \Psi(\mathbf{R}') + f(\Psi(\mathbf{R}')))^2}{2\sigma^2}\right) \quad (2.44)$$

We determine the mean  $f$  and variance  $\sigma^2$  of this Gaussians such that the acceptance rate gets close to one. We have

$$\begin{aligned} \log\left[\frac{e^{-S(\mathbf{R}')}\mathcal{A}(\mathbf{R}' \rightarrow \mathbf{R})}{e^{-S(\mathbf{R})}\mathcal{A}(\mathbf{R} \rightarrow \mathbf{R}')}\right] &= -S(\Psi') + S(\Psi) - \frac{(\Psi - \Psi' + f')^2}{2\sigma^2} + \frac{(\Psi' - \Psi + f)^2}{2\sigma^2} \\ &= -S(\Psi') + S(\Psi) \\ &\quad - \frac{f'(\Psi - \Psi')}{\sigma^2} + \frac{f(\Psi' - \Psi)}{\sigma^2} + \frac{f'^2}{2\sigma^2} - \frac{f^2}{2\sigma^2} \end{aligned} \quad (2.45)$$

Assuming small changes in the field, we can expand the action  $S(\Psi) = S(\Psi') + \frac{\partial S}{\partial \Psi'}(\Psi - \Psi') + \Theta(\Psi - \Psi')^2$  and approximate the acceptance rate

$$\begin{aligned} \log\left[\frac{e^{-S(\mathbf{R}')}\mathcal{A}(\mathbf{R}' \rightarrow \mathbf{R})}{e^{-S(\mathbf{R})}\mathcal{A}(\mathbf{R} \rightarrow \mathbf{R}')}\right] &= \frac{(\partial_{\Psi} S + \partial_{\Psi'} S)(\Psi - \Psi')}{2} \\ &\quad - \frac{(f + f')(\Psi - \Psi')}{\sigma^2} + \frac{f'^2 - f^2}{2\sigma^2} + \Theta(\Psi - \Psi')^2 \end{aligned} \quad (2.46)$$

Up to first order, the acceptance of the moves  $p(\mathbf{R} \rightarrow \mathbf{R}') \rightarrow 1$  is maximized by  $f(\Psi) = \frac{\sigma^2}{2}\partial_{\Psi} S$ , and we have

$$\log\left[\frac{e^{-S(\mathbf{R}')}\mathcal{A}(\mathbf{R}' \rightarrow \mathbf{R})}{e^{-S(\mathbf{R})}\mathcal{A}(\mathbf{R} \rightarrow \mathbf{R}')}\right] = \frac{\sigma^2}{8} \left( (\partial_{\Psi'} S)^2 - (\partial_{\Psi} S)^2 \right) + \Theta(\Psi - \Psi')^2 \quad (2.47)$$

From the second order terms, we can determine the variance  $\sigma^2$ . However, a simpler solution is to consider  $\sigma^2$  as an external parameter of our Monte Carlo algorithm, which we adapt for different temperatures to maximize the efficiency of the moves.

### Fourier algorithm

Still, at low energy, ergodic sampling of the configurations is challenging. Local moves in the real space can easily change the high momenta  $k$  of the energy spectrum. However, it is very difficult at low temperature to equally sample the degenerate energy minima of SOCed bosons.

In order to sample efficiently these minima, we have implemented Metropolis moves in the Fourier space around the minima of the non-interacting energy spectrum. The calculation of the action for this moves scales worse in the system size,  $N \log(N)$  where  $N$  the number of discretized points, using fast Fourier transform. Below we present the main steps of our Fourier space Metropolis algorithm.

- Calculate the Fourier transforms  $\Phi_{\mathbf{k}}^+$  and  $\Phi_{\mathbf{k}}^-$  as defined in Chapter I or later in Eq. 2.62.
- Propose a change of mainly  $\Phi_{\mathbf{k}}^-$  around the minima of the energy i.e the most populated momenta

$$\Phi_{\mathbf{k}}^- \rightarrow \Phi_{\mathbf{k}}^{-'} = \Phi_{\mathbf{k}}^- + z \quad z \in \mathbb{C} \quad (2.48)$$

where  $z$  is a random, Gaussian distributed, complex variable. To gain efficiency, we simultaneously compute

$$u_{\mathbf{k}}' = u_{\mathbf{k}} + e^{-i\theta_{k_{\perp}}} z \quad d_{\mathbf{k}}' = d_{\mathbf{k}} - z \quad (2.49)$$

We then choose a momentum  $\mathbf{k}$  around the minimum of the energy selecting it from the distribution,

$$f(\mathbf{k}) \propto \left( e^{-\frac{k^2}{2} + \kappa \sqrt{k_x^2 + \eta_{soc}^2 k_y^2}} \right)^{\alpha} \quad \alpha \in \mathbb{R} \quad (2.50)$$

where  $\alpha$  is arbitrarily chosen to fit the density of state in function of the temperature.

- If the change is accepted, we calculate the inverse Fourier transform and update the fields.

**Algorithms interplay** In order to optimize the efficiency and reduce the time consumption of the computation, we switch between different algorithms during a single simulation run. At each Monte Carlo step, we randomly select, according to a externally selected probability, one of the different algorithms.

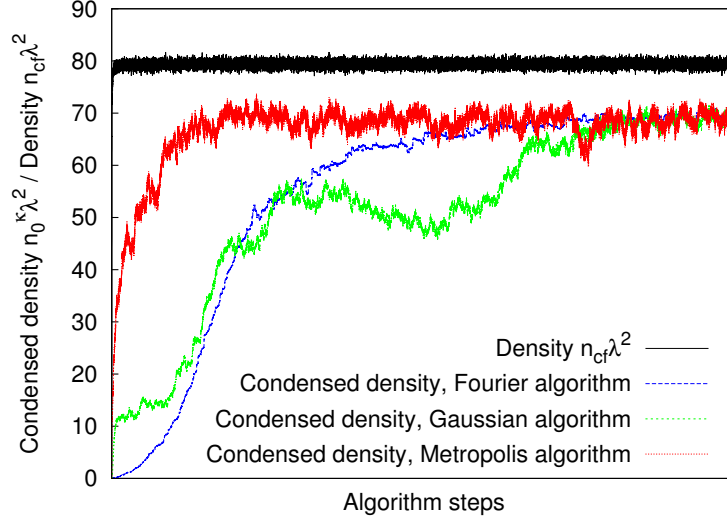


Figure 2.2: Example of convergence of different algorithms. The plot represents the condensed fraction starting from a random set in function of the steps of the different algorithms. Using Metropolis algorithm we obtain a much larger variance and incertitude on the observable than using the Heat Bath and Gaussian algorithm.

### 2.3.3 Partition function

We have presented different algorithms to correctly sample the distribution  $p[\psi(r)]$ ,

$$p[\psi(r)] = Z_{cf}^{-1} e^{-\beta(\mathcal{H}_{cf} - \mu N)} \quad (2.51)$$

where  $Z_{cf} = \int D\psi(r) e^{-\beta\mathcal{H}_{cf}}$  is the partition function. One of our central observables in the following is total density as a function of the chemical potential. Discretizing the system size  $L$  on  $N$  sites, it is given by

$$n_{cf} = \frac{\prod_{\alpha} \prod_{i=1}^N [\int D\psi_{\alpha}(i) |\psi_{\alpha}(i)|^2] e^{-\beta\mathcal{H}_{cf}(\psi_{\alpha}(1), \psi_{\alpha}(2), \dots, \psi_{\alpha}(N))}}{Z_{cf}} \quad (2.52)$$

Together with the density of particles in the energy minimum state, we will be able to draw the phase diagram of the interacting SOCed bosons in Chapter III. However, as we have seen above, predictions of the classical field theory may systematically differ from those of interacting bosons, in particular in the high temperature limit. In the next section, we will show how to reduce this differences in order to make quantitative predictions for dilute Bose gases.

## 2.4 Density matching

### 2.4.1 Procedure

Within classical field theory, the occupation of eigenmodes of energy is given by the equipartition theorem instead of the full Bose distribution. For weakly interacting systems at high energy, mean-field theory correctly describes the leading order interaction corrections [29] and the occupation of energy eigenstates asymptotically approaches their mean-field values at high energy. Therefore, we can correct the densities of our classical field calculations to account for the correct ultraviolet behavior adding the difference

$$\Delta n = \frac{1}{L^2} \sum_{\mathbf{k}, \alpha=\pm} \left[ n_B(\varepsilon_{\mathbf{k}\alpha}^{mf,B} - \mu) - n_{cf}(\varepsilon_{\mathbf{k}\alpha}^{mf,cf} - \mu) \right] \quad (2.53)$$

where the single particle mean-field energies are given by  $\varepsilon_{\mathbf{k}\alpha}^{mf,B/cf} = \varepsilon_{\mathbf{k}\alpha}^{B,cf} + 2 \sum_{\alpha'} g_{\alpha\alpha'} n_{\alpha'}^{mf,B/cf}$ , where  $\varepsilon_{\mathbf{k}\alpha}^{B,cf}$  are the eigen energies of the ideal SOC gas (see below). The corresponding mean-field densities,  $n_{\alpha}^{mf,B/cf} = L^{-2} \sum_{\mathbf{k}} n_{cf/B}(\varepsilon_{\mathbf{k}\alpha}^{mf} - \mu)$ , have to be determined self-consistently as presented in figure 2.3.

Note that the Bose distribution of the occupation numbers merges the classical field occupation for low energies, as we have shown before. Therefore, the low energy modes do not contribute to the density difference, Eq. (2.53), the difference only arises from the different ultraviolet behavior.

### 2.4.2 Lattice expressions for ideal and mean-field classical fields

In the notation above we have indicated one further subtlety arising from the regularization of our classical field theory. The eigenmodes of our classical field theory on the lattice in general differ from those of the Bose gas for high momenta already for an ideal gas.

Let us therefore calculate explicitly the eigenmodes,  $\varepsilon_{\mathbf{k}\alpha}^{cf}$  and the occupation numbers,  $n_{cf}(\varepsilon_{\mathbf{k}\alpha}^{cf} - \mu)$ , of the non interacting classical field system as presented in figure 2.4. The action of the ideal system is diagonal in the Fourier space

$$\Psi_{\uparrow}(\mathbf{r}) = \frac{1}{L^2} \sum_{i,j=1}^L u_{\mathbf{k}_{i,j}} e^{i\mathbf{k}_{i,j} \cdot \mathbf{r}} \quad \Psi_{\downarrow}(\mathbf{r}) = \frac{1}{L^2} \sum_{i,j=1}^L d_{\mathbf{k}_{i,j}} e^{i\mathbf{k}_{i,j} \cdot \mathbf{r}} \quad (2.54)$$

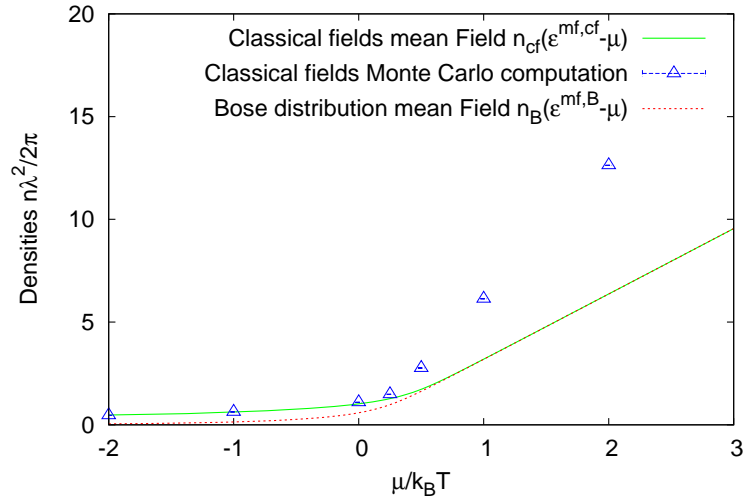


Figure 2.3: Density as a function of the chemical potential. We have corrected the densities of our classical field calculations to account for the correct ultraviolet behavior. We see especially at low density that the Hartree mean field approach developed in Chapter I recovers the numerical integration. At low temperature the density is proportional to the chemical potential as expected c.f Chapter I section 1.3.

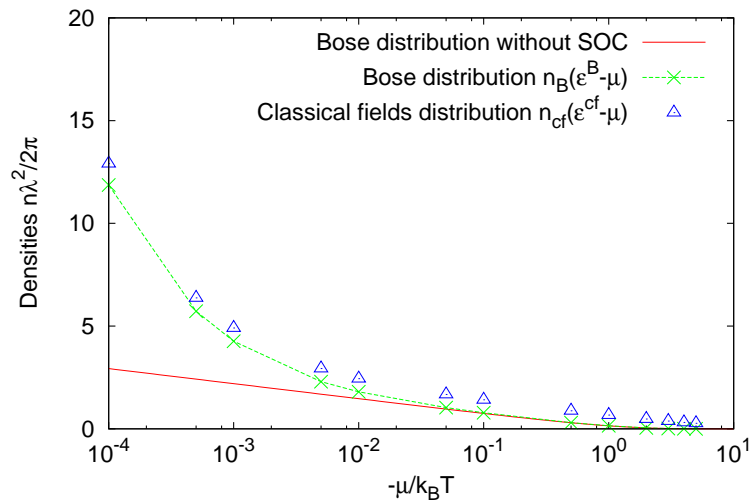


Figure 2.4: Density as a function of the chemical potential for non interacting SOCed bosons. It is interesting to notice that  $n_{Id,MC}$  as a constant deviation from the exact solution  $n_{Id,SOC}$ . As expected from the non interacting results in Chapter I the SOC term increases the density at a fixed chemical potential.

with  $\mathbf{k}_{i,j} = \frac{2\pi}{L}(i, j)$ . The action can then be written

$$\begin{aligned}
S_U &= \frac{1}{L^2} \sum_{i,j} \left[ \frac{k_{ij,U}^2}{2} - \mu + \frac{\kappa^2}{2} \right] \left( u_{-\mathbf{k}_{i,j}} u_{\mathbf{k}_{i,j}} + d_{-\mathbf{k}_{i,j}} d_{\mathbf{k}_{i,j}} \right) \\
&+ \frac{\kappa}{L^2} \sum_{i,j} [k_{x,U} - i\eta_{soc} k_{y,U}] u_{-\mathbf{k}_{i,j}} d_{\mathbf{k}_{i,j}} + \frac{\kappa}{L^2} \sum_{i,j} [k_{x,U} + i\eta_{soc} k_{y,U}] d_{-\mathbf{k}_{i,j}} u_{\mathbf{k}_{i,j}}
\end{aligned} \tag{2.55}$$

where  $k_{x,U}$  and  $k_U^2$  are the Fourier transform of the finite difference expressions approximating the derivatives. Using the lowest order finite difference expressions of the Laplacian, we have

$$\nabla_U^2 \Psi_{\uparrow}(\mathbf{r}) = a^{-2} \sum_i^d [\Psi_{\uparrow}(\mathbf{r} + a\mathbf{i}) + \Psi_{\uparrow}(\mathbf{r} - a\mathbf{i}) - 2\Psi_{\uparrow}(\mathbf{r})] \tag{2.56}$$

$$k_U^2 \equiv a^{-2} \sum_i^d [2 - 2\cos(k(i)a)] = k^2 + \mathcal{O}(a^2 k^4) \tag{2.57}$$

The derivatives and the corresponding wave vectors in Fourier space write

$$\partial_{x,U} \Psi_{\uparrow}(\mathbf{r}) = \frac{1}{2a} [\Psi_{\uparrow}(\mathbf{r} + a\mathbf{i}_x) - \Psi_{\uparrow}(\mathbf{r} - a\mathbf{i}_x)] \tag{2.58}$$

$$k_{x,U} \equiv \frac{1}{a} \sin(k_x a) = k_x + \mathcal{O}(a^6 k_x^3) \tag{2.59}$$

Diagonalizing the action similar to the continuous system studied in section I.1.2, we obtain the corresponding lattice expressions

$$\begin{aligned}
S_U &= \frac{1}{L^2} \sum_{i,j} \left[ \frac{k_{ij,U}^2 + \kappa^2}{2} - \mu + \kappa \sqrt{k_{x_i,U}^2 + \eta_{soc}^2 k_{y_j,U}^2} \right] \Phi_{-\mathbf{k}}^+ \Phi_{\mathbf{k}}^+ \\
&+ \frac{1}{L^2} \sum_{i,j} \left[ \frac{k_{ij,U}^2 + \kappa^2}{2} - \mu - \kappa \sqrt{k_{x_i,U}^2 + \eta_{soc}^2 k_{y_j,U}^2} \right] \Phi_{-\mathbf{k}}^- \Phi_{\mathbf{k}}^-
\end{aligned} \tag{2.60}$$

With the new basis vectors

$$\Phi^+(\mathbf{r}) = \frac{e^{i\theta_k} \Psi_{\uparrow}(\mathbf{r}) + \Psi_{\downarrow}(\mathbf{r})}{\sqrt{2}} \quad \Phi^-(\mathbf{r}) = \frac{e^{i\theta_k} \Psi_{\uparrow}(\mathbf{r}) - \Psi_{\downarrow}(\mathbf{r})}{\sqrt{2}} \tag{2.61}$$

$$\Phi_{\mathbf{k}}^+ = \frac{1}{L^2} \sum_{\mathbf{r}} \Phi_+(\mathbf{r}) e^{-i\mathbf{k}\cdot\mathbf{r}} \quad \Phi_{\mathbf{k}}^- = \frac{1}{L^2} \sum_{\mathbf{r}} \Phi_-(\mathbf{r}) e^{-i\mathbf{k}\cdot\mathbf{r}} \tag{2.62}$$

where  $e^{i\theta_k} = (k_{x,U} + i\eta_{soc} k_{y,U}) / \sqrt{k_{x,U}^2 + \eta_{soc}^2 k_{y,U}^2}$

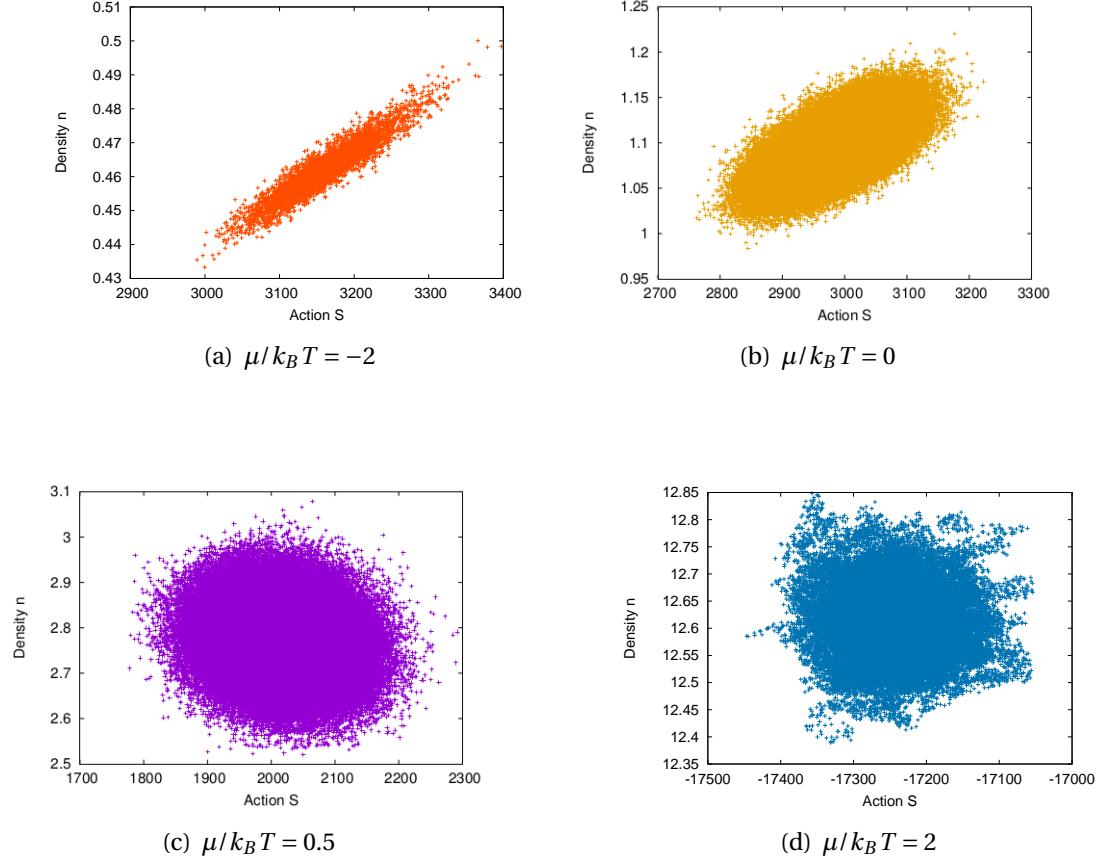


Figure 2.5: Density  $n$  as a function of the action  $S$  for a finite system length  $L/a = 40$  with small anisotropy  $g = \pi/100$ , spin-orbit coupling  $\kappa = \pi/20$  and anisotropy  $\eta_{soc} = 0$ . Each point corresponds to one Monte Carlo iteration step. We observe that at high temperature  $\mu = -2$  the density is small, the fluctuations are strong and its value is strongly correlated to the value of the action  $S$ . Indeed, in this regime every point of  $\Psi(\mathbf{r})$  is almost independent and the action is determined by the chemical potential  $\mu$ . For increasing chemical potential, i.e decreasing temperature, we observe a decorrelation of the density and the action. As presented in the Appendix, at low temperature, fluctuations of the density are strongly suppressed and the value of the action is determined by the many body state i.e interactions and density of state.

Since these fields are non interacting, we can then explicitly calculate the density Eq. (2.52) as a Gaussian integral

$$\begin{aligned}
 n_{cf}(\varepsilon_{\mathbf{k}\alpha}^{cf} - \mu) &= \frac{1}{2L^2} \sum_{i,j} \left[ \frac{1}{\frac{k_{ij,U}^2}{2} - \mu + \frac{\kappa^2}{2} + \kappa \sqrt{k_{x_i,U}^2 + \eta_{soc}^2 k_{y_j,U}^2}} \right] \\
 &+ \frac{1}{2L^2} \sum_{i,j} \left[ \frac{1}{\frac{k_{ij,U}^2}{2} - \mu + \frac{\kappa^2}{2} - \kappa \sqrt{k_{x_i,U}^2 + \eta_{soc}^2 k_{y_j,U}^2}} \right] \quad (2.63)
 \end{aligned}$$

with  $k_x = \frac{2\pi i}{N}$  and  $k_y = \frac{2\pi j}{N}$ .

The analytical results of the non-interacting classical field on the lattice already presents an important benchmark of our numerical Monte Carlo calculation in the non-interacting limit. In order to include the mean field corrections, it is rather straightforward to use these results and solve the self-consistent mean-field equation for the density  $n_{cf}(\varepsilon_{\mathbf{k}\alpha}^{mf,cf} - \mu)$ .

### 2.4.3 Convergence and scale of energy

Figure 2.5 presents, at each step of an algorithm, the density as a function of the corresponding instantaneous value of the action. We see that at high temperature i.e low density, the action is only determined by the chemical potential and fluctuations of the density are strong. At low temperature, fluctuations around the mean density are highly suppressed. We comment in more detail of this feature in the Appendix. In this strongly degenerate regime the convergence of the algorithm towards the correct distribution can be rather slow and must be checked for each observable separately.

Studying the correlation of the observable with the value of the action can give important insight into its convergence properties.

- **I. Density  $n$**  In all regimes, the density usually converges fast since density changes are strongly correlated with the action. As shown in figure 2.2, the density converges rapidly towards its mean value determined by the chemical potential  $\mu$ .
- **II. Condensed fraction and momentum distribution  $n(\mathbf{k})$**  As shown in figure 2.2, the condensed fraction converges significantly slower than the density.
- **III. SP and PW states  $n_0^\kappa$**  The correct balance between the population of degenerate momenta is typically converging slower than the condensate fraction. Since in our later study we focus on the regime of very small anisotropy  $g$ , PW and SP states are always very close in energy. At low temperature, the local minima are ubiquitous and the distribution is converging too slowly for purely local moves. Global changes like the Fourier algorithm described in the previous section are needed to reach convergence.

## 2.5 Résumé

Au cours de ce chapitre nous avons présenté les principales méthodes utilisées au cours de cette thèse pour établir le diagramme de phase à température non nulle d'un gaz de bosons bidimensionnels en présence d'un couplage spin-orbite et d'interactions interparticules. Nous nous sommes intéressés à des systèmes avec de faibles interactions et à des températures basses. En se basant sur l'absence d'un condensat de Bose-Einstein dans un gaz idéal (ou dans le cas des théories champ moyen) des arguments de continuité tendraient vers une température critique d'une possible transition repoussée à zéro dans la limite d'une interaction également infiniment proche de zéro.

En approchant le zéro absolu, la vaste majorité des bosons occupent les états de très basse énergie qui sont donc fortement peuplés. Dans ce régime, le caractère ondulatoire des particules quantiques domine et la description en tant que champs classiques devient quantitativement correcte [46, 47, 48, 49, 50]. Au-delà du régime de faibles interactions, la théorie de champs classiques reste capable de décrire des comportements universels autour d'une transition continue, un phénomène très connu des théories critiques [51]. Au cours de cette thèse et en se basant sur des calculs de champs classiques, nous avons établi pour la première fois le diagramme de phase de bosons interagissant avec couplage spin-orbite.

De manière schématique, la description type champs classiques apparaît en remplaçant l'occupation d'un état quantique donnée par la distribution de Bose ( $\exp[\varepsilon/k_B T] - 1$ ) avec une énergie  $\varepsilon$ , par l'occupation d'un champ classique  $k_B T/\varepsilon$  tout en négligeant les commutateurs des champs quantiques. Ces deux approximations deviennent exactes pour les états de basse énergie dans la limite  $T \rightarrow 0$  et elles fournissent le point de départ d'une description quantitativement correcte d'un gaz de Bose faiblement interagissant.

Pourtant, à cause des interactions, il n'est pas possible de diagonaliser explicitement l'Hamiltonien même après avoir appliqué l'approximation type champs classiques. Toutefois, le calcul des observables statiques correspond directement à un calcul de distribution de probabilités, bien connu en physique statistique classique. Au cours de cette étude et en se basant sur ce constat, nous avons utilisé les méthodes Monte Carlo pour échantillonner numériquement la distribution des champs classiques.

Le poids de chaque configuration du champ classique est donné par la distribution de Boltzmann en fonction de son énergie. Cependant, deux problèmes techniques

---

apparaissent en préambule de notre calcul. Premièrement, afin de correctement définir l'énergie d'une théorie de champs classiques, il faut régulariser son comportement à hautes énergies ("divergences ultraviolettes"). Au travers du calcul numérique Monte Carlo, cet obstacle est naturellement résolu par la discrétisation des champs sur réseau. Deuxièmement, le couplage spin-orbite introduit des termes imaginaires dans l'action des deux champs complexes représentant les deux états de spin. Nous devons donc montrer que l'on obtient réellement une distribution de probabilité, c'est à dire que l'action discrétisée est maintenue réelle quelque soit la configuration des champs. Ensuite seulement, il est possible de correctement échantillonner les configurations des champs classiques en proposant des algorithmes Monte Carlo efficaces qui assurent l'ergodicité du système.

Enfin, nous avons corrigé les densités brutes provenant des calculs de champs classiques qui dépendent de la discrétisation sur réseau en tenant compte des comportements à haute énergie des modes distribués selon la statistique de Bose. Cependant, ces états étant peu peuplés, ils sont peu affectés par les interactions et l'approximation type champ moyen en fournit donc une description très pertinente. En utilisant cette correction, il est en principe possible de corriger chaque observable à partir des calculs de champs classiques et de fournir des prédictions quantitatives pour nos systèmes alors directement comparables aux expériences [46].



# Interacting Bosons with SOC in 2D: Phase Diagram

## Contents

---

<b>3.1 Introduction . . . . .</b>	<b>59</b>
<b>3.2 Bose gas without SOC: Berezinskii, Kosterlitz and Thouless phase transition . . . . .</b>	<b>61</b>
<b>3.3 Bose gas with SOC: condensate fraction . . . . .</b>	<b>62</b>
<b>3.4 Superfluidity . . . . .</b>	<b>69</b>
<b>3.5 Conclusion and phase diagram . . . . .</b>	<b>70</b>
<b>3.6 <i>Résumé</i> . . . . .</b>	<b>71</b>

---

## 3.1 Introduction

In this chapter, we explore the phase diagram of a two dimensional SOCed Bose gas based on the methods presented in the last chapter. Here, we will first establish the presence or absence of a finite temperature phase transition in the interacting system and provide quantitative predictions for the phase diagram. In the next chapter, we will study and characterize the (quasi-) ordering of the different phases at low temperature.

According the Mermin-Wagner theorem [52, 53, 54], no long range order can occur at finite temperatures. Still, in the absence of SOC, a Berezinskii-Kosterlitz-Thouless

phase (BKT) transition from the normal to a superfluid phase occurs for interacting Bose gases [50] where the low temperature superfluid phase is characterized by algebraic (quasi-long range) order.

Our numerical studies clearly establish that the weakly interacting Bose gas still undergoes a BKT phase transition for anisotropic SOC,  $\eta_{soc} < 1$ . In the low temperature phase, the condensate fraction decays algebraically with system size and the gas becomes superfluid. However, for isotropic SOC,  $\eta_{soc} = 1$ , our calculations show a cross-over behavior at finite systems, with strong evidence for the absence of a finite temperature phase transition in the thermodynamic limit.

## 3.2 Bose gas without SOC: Berezinskii, Kosterlitz and Thouless phase transition

Let us first briefly review the Berezinskii, Kostelitz and Thouless transition of the interacting two-dimensional Bose gas without SOC described by the Hamiltonian

$$\mathcal{H} = \int d^2r \Psi^\dagger(r) \left( -\frac{\hbar^2}{2m} \Delta + \frac{g_0}{2} \Psi^\dagger(r) \Psi(r) \right) \Psi(r) \quad (3.1)$$

where  $g_0$  is the interaction strength. At low temperatures, density fluctuations are strongly suppressed. Keeping only phase fluctuations,  $\Psi(r) = \sqrt{\rho} e^{i\theta(r)}$ , the Hamiltonian can be reduced to the so-called XY model [55].

In the XY-model, a Berezinskii-Kosterlitz-Thouless transition takes place [56, 57, 58] where the superfluid density,  $n_S$ , jumps from  $n_S = 0$  at high temperatures to  $n_S = 2mk_B T / \pi \hbar^2$  (or  $n_S \lambda^2 = 4$ ) at the transition temperature  $T_C$ . Below  $T_C$ , the first-order correlation function,  $g_1(r) = \langle \Psi^\dagger(r) \Psi(0) \rangle$ , algebraically decays,  $g_1(r) \sim r^{-\eta(T)}$  characterized by a temperature dependent exponent  $\eta(T) = 1/n_S \lambda^2$ . At  $T_C$ ,  $\eta(T_C) = 1/4$ , and the exponent decreases with decreasing temperature. Thus, the algebraic decay is quite slow, so that for any finite size system we can expect a significant condensate fraction

$$n_0 = \frac{N_0}{N} = \frac{1}{N} \int d^2r g_1(r) \sim \frac{L^{2-\eta}}{L^2} \sim N^{-\eta/2} \quad (3.2)$$

Although the condensate fraction vanishes in the thermodynamic limit, numerical simulations as well as many experimental systems will be affected by strong finite size effects. Experiments on ultra cold atomic gases typically involve mesoscopic system sizes, e.g.  $N \sim 10^4-8$ , where the condensate fraction at  $T_C$  still plays a dominating role,  $n_0 \sim 10^{-1}$ .

As presented in Chapter I, in a SOCed two dimensional system the dispersion relation of the single particle is very different from Eq. (3.1), and quasi-long range order may be destroyed in certain parameter regimes [59].

*What is the effect of the SOC on the BKT scenario ?*

In the following, we study the condensate and superfluid fraction for different SOC anisotropy,  $\eta_{soc} = 0, 0.5, 0.9$ , and 1, for signatures of a possible finite temperature phase transition.

### 3.3 Bose gas with SOC: condensate fraction

For a single component Bose gas without SOC, the single particle density matrix depends only on distance and decays algebraically in the low temperature superfluid phase [56, 57, 58]. The same algebraic decay propagates to the condensate fraction. In the case of a two-component Bose gas with SOC, the single particle density matrix further depends on the spin-projection,  $G_{\sigma,\sigma'}(\mathbf{r}, \mathbf{r}')$ . Quasi-long range order occurs in the distribution of the modes and the single particle density matrix gets dominated by one or few highly occupied modes. We therefore project  $G_{\sigma,\sigma'}(\mathbf{r}, \mathbf{r}')$  over all degenerate PW mean-field ground states, e.g. we sum over all the minima of the single particle spectrum

$$n_0^\kappa = \sum_{\mathbf{k}=(\pm\kappa,0)} \sum_{\sigma\sigma'} \int \frac{d\mathbf{r}d\mathbf{r}'}{L^2} \psi_{\mathbf{k}\sigma}^{MF}(\mathbf{r}) G_{\sigma,\sigma'}(\mathbf{r}, \mathbf{r}') \psi_{\mathbf{k}\sigma'}^{MF*}(\mathbf{r}') \quad (3.3)$$

to estimate the condensate fraction  $n_0^\kappa/n$  where  $n = \sum_{\sigma} G_{\sigma\sigma}(\mathbf{r}, \mathbf{r})$  is the total particle density. It is important to notice that  $n_0^\kappa$  is a direct indicator for a phase transition. However, it does not fully describe the character of the low temperature phase, in particular it does not distinguish between PW or SP order.

In figure 3.1 we show  $n_0^\kappa$  as a function of density for a finite system of extension  $L/a = 80$  where  $a = \hbar/\sqrt{mk_B T}$  is the minimal distance on our lattice. The condensate fraction grows rapidly around a cross-over density which decreases from  $\eta_{soc} = 0$  to  $\eta_{soc} = 1$ . However, no differences are visible changing the sign of our small anisotropic interaction from negative to positive  $g$ . We therefore expect that the cross-over/transition temperature is a smooth, continuous function of  $g$  around  $g = 0$ .

In two dimensional systems of infinite size, the condensate density is expected to vanish at any finite temperature. However, as explained in the previous section, huge finite size effects are expected. In order to determine a possible sharp phase transition in the thermodynamic limit, we have to determine the behavior of the condensate fraction increasing the system size. The occurrence of a BKT phase then shows up in the algebraic scaling of the condensate fraction with system size,  $n_0^\kappa/n \sim L^{-\eta(T)}$ .

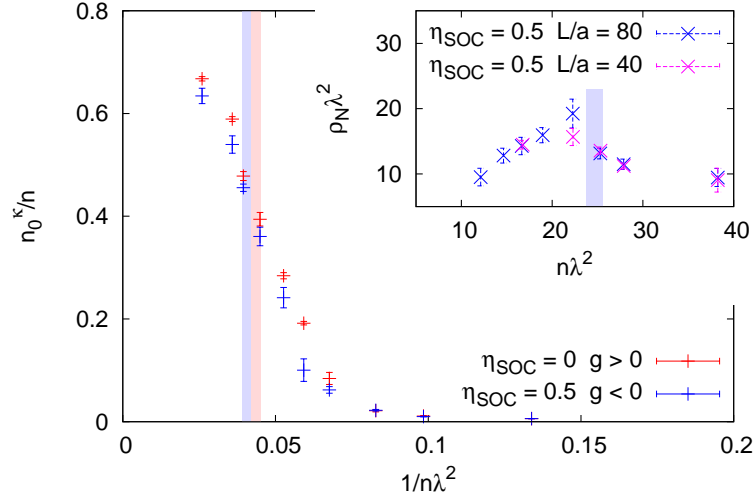


Figure 3.1: Condensate fraction  $n_0^\kappa/n$  as a function of inverse phase space density  $[n\lambda^2]^{-1}$  for a finite system of length  $L/a = 80$ . The cross-over from normal to condensed phase slightly lowers with increasing SOC anisotropy,  $\eta_{soc}$ . Although the PW/SOC character of the condensate depends essentially on the sign of the anisotropic interaction  $mg = \pm\pi/100$ , differences in  $n_0^\kappa$  between  $g \geq 0$  and  $g < 0$  for equal SOC are beyond our resolution. The colored zones indicate our estimates for the Kosterlitz-Thouless transition in the thermodynamic limit from finite-size-scaling of the condensate fraction described in the text.

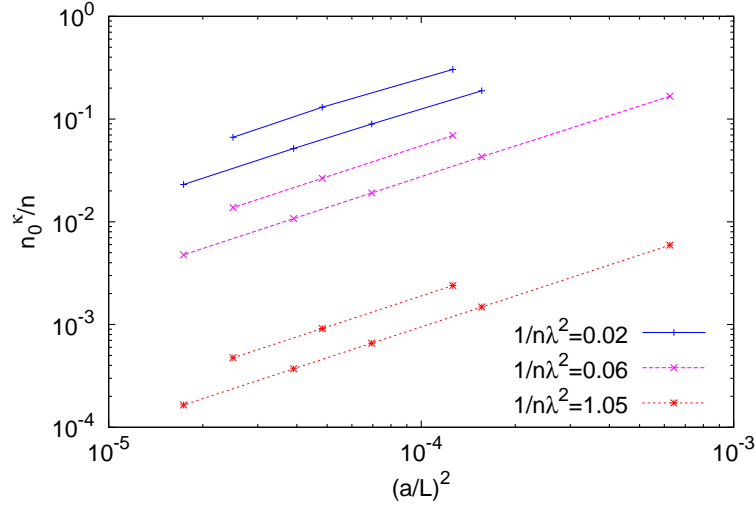


Figure 3.2: Condensate fraction,  $n_0^\kappa/n$ , as a function of inverse volume in presence of the SOC but in absence of interactions. As we will precisely detail in the paragraph dedicated to the isotropic SOC, we notice that the absolute value of the condensed density depends on the sum introduced in Eq. 3.4, describing the number of degenerate points corresponding to the fundamental state  $|\mathbf{k}| = \kappa$ . The condensate density decreases with the volume for any density, no transition occurs.

### Non-interacting system

Let us start discussing finite size effects for non-interacting bosons. In figure 3.2 we show the behavior of the condensate fraction in the non-interacting case. The exact expressions of this limiting case not only provide a benchmark for our simulation, but also serve to illustrate the finite size scaling of the condensate in the normal phase. We then obtain

$$\begin{aligned}
 n &= \frac{k_B T}{L^2} \sum_{i,j} \left[ \frac{1}{\frac{k_{ij,U}^2}{2} - \mu + \frac{\kappa^2}{2} + \kappa \sqrt{k_{x_i,U}^2 + \eta_{soc}^2 k_{y_j,U}^2}} \right] \\
 &+ \frac{k_B T}{L^2} \sum_{i,j} \left[ \frac{1}{\frac{k_{ij,U}^2}{2} - \mu + \frac{\kappa^2}{2} - \kappa \sqrt{k_{x_i,U}^2 + \eta_{soc}^2 k_{y_j,U}^2}} \right] \\
 n_0^\kappa &= \sum_{|\mathbf{k}|=\kappa} \frac{k_B T}{L^2 \mu} \tag{3.4}
 \end{aligned}$$

In the expression of the condensate density, we explicitly sum over all degenerate ground states with  $|\mathbf{k}| = \kappa$ . It is important to keep in mind that the number of degenerate minima depends on the isotropicity of the SOC. For  $\eta_{soc} < 1$ , we have two degenerate minima, whereas for isotropic SOC,  $\eta_{soc} = 1$ , we have an infinite degeneracy, a circle in momentum space in the thermodynamic limit. Finite size effects introduce qualitative changes for  $\eta_{soc} = 1$ , where the additional symmetry of the underlying lattice strongly reduces the degeneracy to a finite number. These effects are present in both figures 3.4 and 3.5.

Nevertheless, in both cases, we see that the condensate density decreases with the system size as  $\frac{n_0^\kappa}{n} \propto \frac{1}{L^2}$ . This exponent of this algebraic decay simply reflects that the condensate fraction decays as  $1/L^2$  for all densities and no phase transition occurs.

### Interacting system with anisotropic SOC

We now turn to the interacting systems, summarizing our results of the classical field Monte Carlo calculations. Whereas in the high temperature, normal phase the condensate density decreases with the volume,  $\eta = 2$ , the exponent changes rapidly around the temperature where condensation occurs in the finite system. At lower temperatures, the exponent almost vanishes. This behavior is consistent with a Berenzinskii-Kosterlitz-Thouless transition [56, 57, 58]. Assuming the transition to be within the Kosterlitz-Thouless class, the critical temperature can be estimated to

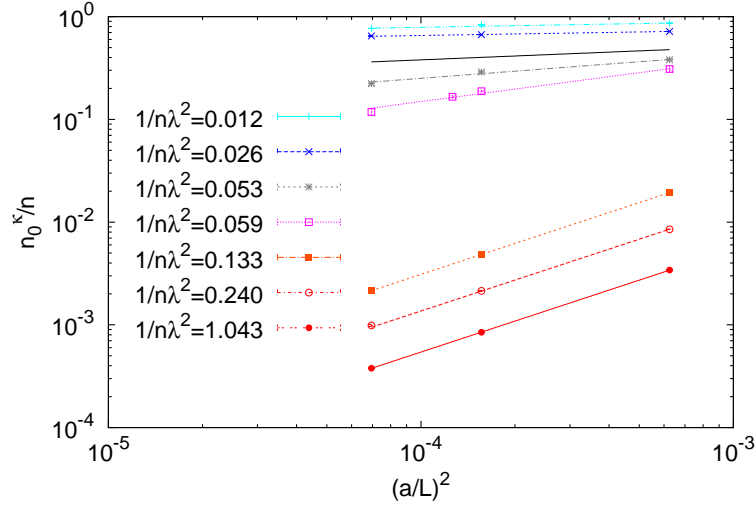


Figure 3.3: Condensate fraction,  $n_0^k/n$ , as a function of the inverse volume,  $L^{-2}$ , for anisotropic SOC bosons with  $\eta_{soc} = 0$  at different phase space densities and anisotropic interaction,  $g > 0$ . We observe a transition between the high temperature regime, where the condensate density decreases with the volume, and the low temperature regime where the exponent depends on the density and eventually vanishes. The solid black line indicates the critical exponent  $\eta = 1/4$ .

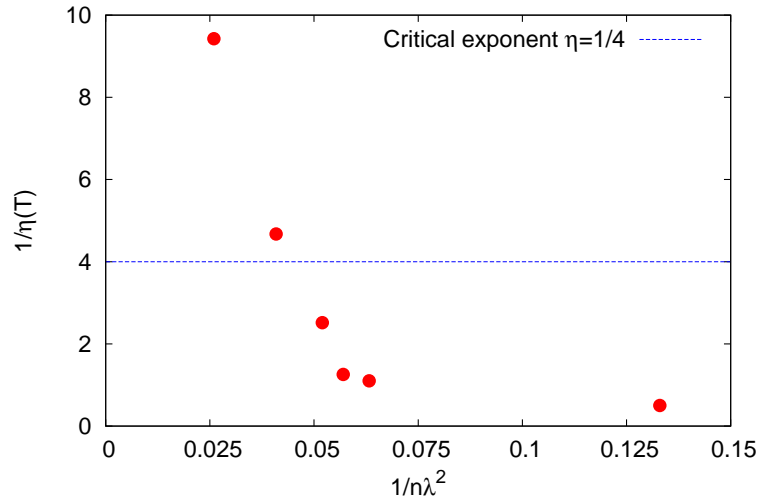


Figure 3.4: Exponent  $\eta(T)$  as a function of the density. The exponent is obtained by scaling the condensate fraction from figure 3.3, with the system size  $n_0^k/n \sim L^{-\eta(T)}$ . By scaling the condensed fraction for different SOC anisotropies  $\eta_{soc}$  we obtain the phase diagram showed in figure 3.7.

occur when  $\eta(T_{KT}) = 1/4$ . Our simulations indicate that for anisotropic SOC,  $\eta_{soc} < 1$ , the Berenzinskii-Kosterlitz-Thouless phase occurs at finite temperature, independent of the sign of the anisotropy  $g$  of the interaction (see figure 4.1 for  $\eta_{soc} = 0$ ). Further, the limit of isotropic interaction,  $g = 0$ , is approached smoothly from both sides,  $g > 0$  and  $g < 0$ , so that the critical temperature is continuous around  $g = 0$ . This latter behavior is in contradiction with the discontinuity predicted in reference [9].

### Interacting system with isotropic SOC

For isotropic SOC,  $\eta_{soc} = 1$ , the system behaves qualitatively different. As shown in figure 3.3 for  $g < 0$ , we do not observe the onset of quasi-long range order over the whole density regime and system sizes we considered.

For  $g > 0$ , we observe a cross-over similar to  $\eta_{soc} < 1$ , but this time the onset of algebraic order strongly depends on the number of degenerate mean-field ground states. For our finite simulation box, only 4 or 8 minima are strictly degenerate for the system sizes we considered. The circular degeneracy only occurs after performing the thermodynamic limit. As shown in figure 3.5, the behavior of the condensate fraction is qualitatively and quantitatively affected by the number of degenerate states. In particular, the onset of algebraic order is shifted towards considerable higher densities, i.e. lower temperatures, increasing the degeneracy from 4 to 8 degenerate modes. For  $\eta_{soc} = 1$  and infinity system sizes, the transition will therefore be shifted to zero temperature and no finite temperature transition with algebraic order in the single particle channel should occur.

It is important to point out that the BKT transition is absent within the classical field calculation. Therefore, the transition is suppressed by purely classical fluctuations in strong contrast to prediction of reference [10] i.e. quantum fluctuations do not play an essential role.

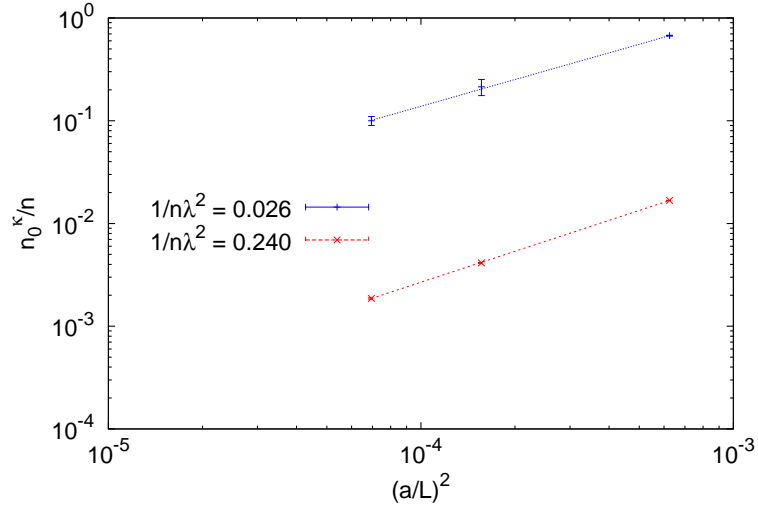


Figure 3.5: Condensate fraction,  $n_0^K/n$ , as a function of the inverse volume,  $L^{-2}$ , for isotropic SOC bosons with  $\eta_{soc} = 1$  at different phase space densities and anisotropic interaction,  $g < 0$ . We do not observe any quasi-long range order.

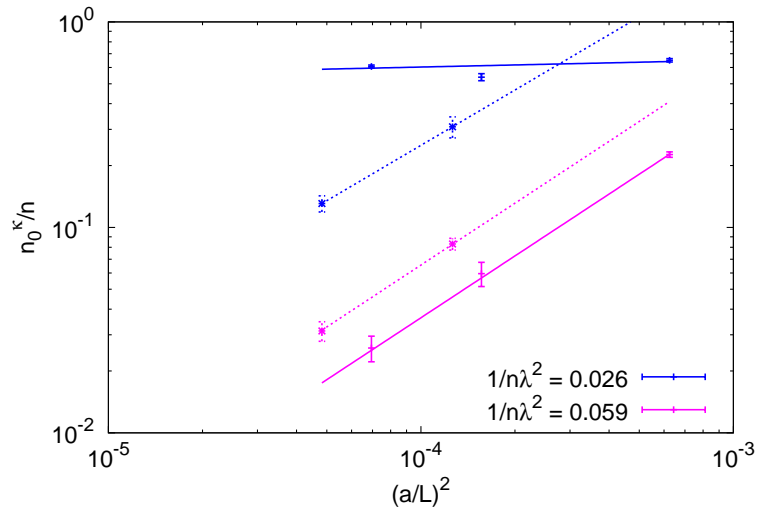
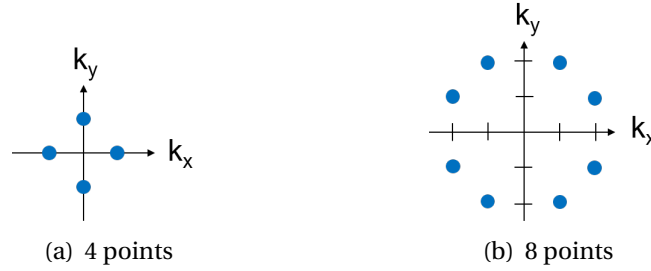


Figure 3.6: Solid lines: Condensate fraction,  $n_0^K/n$ , as a function of inverse volume for isotropic SOC,  $\eta_{soc} = 1$ , of finite systems with 4 degenerate minima and  $g > 0$ . Dashed lines corresponds to finite systems with 8 degenerate minima where the algebraic behavior,  $n_0^K \sim L^{-\eta}$  with  $\eta > 1/4$ , at high phase space density is suppressed.

Let us illustrate in more detail the degeneracy of the finite size simulation for isotropic SOC. In our simulations, we have chosen the value of the SOC strength  $\kappa = \frac{2\pi}{40}$ , commensurate with  $\kappa \equiv k = \frac{2\pi i}{L}$  for system sizes  $L = 40, 80, 120$  where we have four minima at  $k = (\pm\kappa, 0)$  and  $k = (0, \pm\kappa)$ . Instead, for  $L = 81, 144$ , we have eight minima as in the scheme shown below.



Notice, that for  $g < 0$ , where mean field predicts PW, we have four or eight possibilities for the direction. Instead, for  $g > 0$ , the mean field ground state is a superposition of two opposite PW phases, so that we only have half of the possibilities for the unsigned momentum direction, two or four possibilities in our case. This simple picture may already explain the main qualitative different behavior of the condensate fraction depending on the sign  $g$  of the interparticle interaction we have observed in our simulations.

### Intermezzo: XY vs Heisenberg model

In the thermodynamic limit, for  $\eta_{soc} = 0$  and isotropic interaction, we can eliminate the SOC via a gauge transformation, and we obtain a Bose gas with two internal spin component and isotropic interaction. This model is equivalent to a field theory with  $N = 4$  internal components. Only the model with  $N = 2$  maps to the XY model giving rise to a BKT transition. For  $N > 2$ , a Kosterlitz-Thouless phase transition is absent [60, 61], in accordance with the absence of a phase transition in the 2D Heisenberg model.

However, in the case of  $\eta_{soc} = 0$ , the thermodynamic limit is singular. For any finite system, the above argument only applies for situations where  $\kappa$  is commensurate with the boundary conditions. Here, we address the limit  $\eta_{soc} \rightarrow 0$  continuously connected to non vanishing  $\eta_{soc} > 0$ , which corresponds to situation with non-commensurate values of  $\kappa$  of any finite system, so that the BKT transition survives even in the limit of infinite system sizes. The situation  $\eta_{soc} = 0$  is therefore singular.

### 3.4 Superfluidity

In systems without SOC, the quasi-long range order in the low temperature phase also implies superfluidity, and one of the most striking prediction of the Kosterlitz-Thouless transition is the occurrence of a universal jump of the superfluid density at the critical temperature [62, 58, 63]. In SOC systems, Galilean invariance is broken with important consequences for the superfluid phase. In such systems peculiar features have been predicted like the appearance of spatial anisotropic superfluidity, BEC with zero superfluid fraction at zero temperature [45], and a critical velocity which is not uniquely defined [44].

In thermal equilibrium, the superfluid mass density  $\rho_S$  can be directly related to the phase stiffness  $\rho_S = \frac{\partial^2 F(\theta)}{\partial \theta^2}$  where  $F(\theta)$  is the free-energy density where the momentum operator  $\hat{p}$  is replaced by  $\hat{p} - \theta$  in the Hamiltonian [64, 65, 66, 67].

We have therefore further calculated the superfluid and normal mass density,  $\rho_n = mn - \rho_s$  from the phase stiffness. For  $\eta_{soc} = 0$  and isotropic interactions, we have

$$\rho_n = \frac{1}{k_B T L^2} \langle [P_x^{\text{tot}} + \hbar \kappa S_x^{\text{tot}}]^2 \rangle \quad (3.5)$$

where  $\mathbf{P}^{\text{tot}}$  is the total momentum and  $\mathbf{S}^{\text{tot}} = \int d\mathbf{r} \mathbf{S}(\mathbf{r})$  the total magnetization of the system. Deviations from a Boltzmann distribution of  $[P_x^{\text{tot}} + \hbar \kappa S_x^{\text{tot}}]^2 / (2mnL^2)$  are directly connected to the quantization of the center of mass motion in the  $x$  direction. For general  $\eta_{soc} > 0$  or anisotropic interactions  $g \neq 0$ , quantum effects may modify superfluid properties [68], but we can still use Eq. (3.5) to study the universal behavior of the normal density around a superfluid phase transition.

Our results for the normal/superfluid density (see inset of figure 3.1 for  $\eta_{soc} = 0.5$ ,  $g < 0$ ) confirm the conclusions drawn above from the finite-size analysis of the condensate fraction. Consistent with the prediction of Berenzinskii, Kosterlitz and Thouless, the low temperature, algebraically ordered phase is superfluid for  $\eta_{soc} < 1$ . The transition temperature is roughly independent of the sign of  $g$  and decreases with increasing  $\eta_{soc}$ . It vanishes for isotropic SOC with increasing degeneracy. This absence of a transition for isotropic SOC is consistent with recent hydrodynamical results predicting the appearance of rigid flow at zero temperature in three spatial dimensions [45].

### 3.5 Conclusion and phase diagram

In conclusion we have drawn the finite temperature phase diagram of a two dimensional SOCed Bose gas. We have shown the signature of a KT transition in the case of  $\eta_{soc} < 1$  with the presence of superfluidity in the low temperature phase. By scaling the condensed fraction with the system size we have predicted the critical densities corrected by the matching presented in Chapter II. In the particular case of a pure Rashba SOC  $\eta_{soc} = 1$ , we have shown that a crossover occurs for finite systems at similar phase-space densities, but no superfluid transition is expected in the thermodynamic limit.

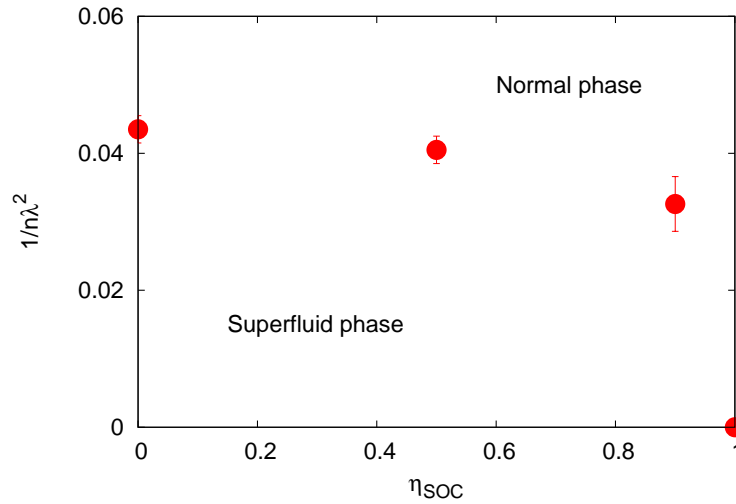


Figure 3.7: Critical densities as a function of the SOC anisotropy  $\eta_{soc}$ . The KT phase transition from normal to superfluid phase takes place at slightly higher densities with increasing SOC anisotropy,  $\eta_{soc}$ . No finite temperature phase transition occurs for isotropic SOC  $\eta_{soc} = 1$ .

### 3.6 Résumé

Au cours de ce chapitre, nous explorons le diagramme de phase d'un gaz de bosons bidimensionnel avec couplage spin-orbite en utilisant les différentes méthodes définies dans le chapitre précédent. Nous avons établi spécifiquement la présence ou l'absence d'une transition de phase à température finie dans le système avec interactions interparticules. Nous avons également proposé des prédictions quantitatives pour le diagramme de phase. Au cours du prochain chapitre nous proposons d'étudier et correctement caractériser le (quasi-) ordre des différentes phases à basse température.

Selon le théorème de Mermin-Wagner [52, 53, 54], aucun ordre à longue portée ne peut s'établir à température finie. Cependant, en absence de couplage spin-orbite, une transition de phase Berenzinskii-Kosterlitz-Thouless (BKT) est possible dans un gaz de bosons interagissant entre une phase normale et une phase superfluide. Cette dernière est caractérisée par un ordre algébrique de quasi-longue portée.

Nos études numériques établissent que une transition BKT a toujours lieu dans le gaz de bosons faiblement interagissant en présence d'un couplage spin-orbite anisotrope  $\eta_{soc} < 1$ . Dans la phase basse température, la fraction condensée décroît de manière algébrique en fonction de la dimension du système et le gaz devient alors superfluide. Au contraire, pour un couplage spin-orbite isotrope,  $\eta_{soc} = 1$ , nos calculs indiquent une absence de transition de phase à température finie et à la limite thermodynamique. Une transition lisse (cross-over) subsiste pour des systèmes à taille finie. La figure 3.7 présente le diagramme de phase de notre système, détaillant les densités critiques en fonction de l'anisotropie du couplage spin-orbite  $\eta_{soc}$ .



# Low temperature states: Plane Wave and Stripe Phase

## Contents

---

<b>4.1 Introduction and motivations</b> . . . . .	<b>73</b>
<b>4.2 Reduced single body density matrix</b> . . . . .	<b>75</b>
<b>4.3 Local Spin Density</b> . . . . .	<b>80</b>
<b>4.4 Spin density correlation functions</b> . . . . .	<b>84</b>
<b>4.5 Isotropic interaction: Fragmented condensate</b> . . . . .	<b>84</b>
<b>4.6 Low temperature wave-function</b> . . . . .	<b>86</b>
4.6.1 Bosons pairs . . . . .	88
<b>4.7 Résumé</b> . . . . .	<b>90</b>

---

## 4.1 Introduction and motivations

In Chapter III, we have studied the phase diagram of a two-dimensional SOCed Bose gas. For anisotropic SOC, we have identified a low and high temperature phases separated by a transition that we have shown to be within the Kosterlitz-Thouless class. As we have seen in Chapter I, mean field theory predicts exotic many body ground states, in particular, depending on the strength of interactions between same and different spins (defined in Eq. (1.38))

$$g = 2g_{\uparrow\downarrow} - g_{\uparrow\uparrow} - g_{\downarrow\downarrow}$$

the mean-field ground state is either given by a single Plane Wave State (PW), or by a linear superposition of two Plane Waves with opposite momenta, the Stripe Phase (SP).

Beyond mean field, the existence and appearance of such exotic phases are still unclear and open questions remain. As an example, reference [69] proposes a phase diagram based on qualitative argument in the very dilute limit, which does not depend on the sign of anisotropy  $g$ , in contrast to the mean field predictions. In the following, we will investigate in detail, the character of the low temperature phases observed in our classical field simulation.

In particular, we will study the magnetic ordering of the atoms/spins at low temperature and link it to the BKT phase transition studied in Chapter III. We show that in the case of an anisotropy  $g \neq 0$  the spin correlations exhibit quasi-long-range order induced by the KT transition in contrast to prediction of long range order from reference [70]. We therefore find a phase diagram in strong connexion to the Kosterlitz-Thouless transition. We also investigated predictions of zero momentum transition by [71, 72], or the appearance of bosons pairs by references [69, 9] but we did not find any indications of such exotic phases and behavior.

In the case of isotropic interactions,  $g = 0$ , mean field calculations do not select a unique ground state, SP and PW states remain degenerate. In this case, one may expect that thermal and quantum fluctuations break this degeneracy and select a unique ground state. The classical field approximation allows us to address the question of thermal fluctuations in a direct and explicit way. Here, we show that the system undergoes a KT transition without selecting a unique ground state. Instead, our calculations predict a fractionalization of the condensate where SP and PW remain degenerate.

**Parameter values in the simulations** In order to study the competition between SOC and interparticle interaction, we have fixed  $\sum_{\sigma\sigma'=\uparrow\downarrow} mg_{\sigma\sigma'}/4 = \kappa/\sqrt{mk_B T} = \pi/20$  with  $mg = 0$  to address isotropic interaction and  $mg = \pm\pi/100$  to slightly break the spin isotropy of scattering particles.

## 4.2 Reduced single body density matrix

In the previous chapter, we have observed a Kosterlitz-Thouless transition for  $\eta_{soc} < 1$ . The low temperature phase was characterized by the occurrence of a quasi-condensate, a large, though non extensive, occupation of the two degenerate single particle ground states. More precise information on the character of the quasi-condensate can be expected from the full calculation of the reduced single-particle density matrix given by

$$G_{\sigma,\sigma'}(\mathbf{r}, \mathbf{r}') = \langle \hat{\Psi}_{\sigma'}^\dagger(\mathbf{r}') \hat{\Psi}_\sigma(\mathbf{r}) \rangle \quad (4.1)$$

In the high temperature regime, the one-body density matrix decays to zero over a distance given by the thermal de Broglie length  $\lambda_T$ . At the transition, quasi-long range order appears, characterized by an algebraic decay. In momentum space, the reduced one-body density matrix writes

$$G_{\sigma,\sigma'}(\mathbf{k}, \mathbf{k}') = \langle \hat{\Phi}_{\mathbf{k}'}^{\sigma' \dagger} \hat{\Phi}_{\mathbf{k}}^\sigma \rangle \quad (4.2)$$

and the distinction between quasi and true long range order is directly connect to the occurrence of a quasi-condensate or full BEC in momentum space.

**BEC** The momentum distribution for a system revealing BEC exhibits a singular behavior at the minimum of the energy spectrum. In the case of a three dimensional ideal Bose gas without SOC, only the zero momentum state is macroscopically occupied. In real space, the one-body density matrix at large distances saturates to a finite value set by the condensate fraction of the gas. The system is then said to show off diagonal long-range order, i.e. finite values in  $G(\mathbf{r}, \mathbf{r}')$  for  $\mathbf{r} \neq \mathbf{r}'$ . The criterion for BEC of a macroscopic occupation given by Penrose and Onsager [73] is thus equivalent to the existence of a long range order.

In the case of ideal SOCed Bosons in three dimensions, the ground state is degenerate leading to a macroscopic occupation of all modes with  $|\mathbf{k}| = \kappa$ . The Fourier transform of these modes will lead to oscillations of the one-body density matrix in real space. Although possible, the observation of true-long range order gets more involved in the real space density matrix than in Fourier space. In general, BEC corresponds to a macroscopic occupation of one (or more) eigenmodes of the single-particle density matrix. In the case of SOC, these eigenmodes in general couple spin and momentum degrees of freedom.

**BKT phase** In the case of a quasi-condensate below the BKT transition in two dimensions, the single particle density matrix in real space is algebraically decaying, with additional oscillations for systems with SOC corresponding to peaks of the momentum distribution at non-vanishing momenta. The spin-structure of the quasi-condensate can be obtained from the dominating modes after diagonalization of the single particle density matrix.

Since the occupation number is strongly peaked for  $\mathbf{k} = \boldsymbol{\kappa}$  with

$$|\boldsymbol{\kappa}| = \kappa$$

we have calculated the reduced single particle density matrix only for momenta at the minimum of the single particle energy spectrum,  $G_{\sigma,\sigma'}(\boldsymbol{\kappa}, \boldsymbol{\kappa}')$ . For  $\eta_{soc} < 1$ , we only need to consider  $(\pm\kappa, 0)$ . The resulting  $4 \times 4$  matrix can be calculated using classical field Monte Carlo.

Explicitly, using the definition 1.11, this reduced density matrix writes  $\langle \mathcal{M}(\boldsymbol{\kappa}) \rangle$  with

$$\mathcal{M}(\boldsymbol{\kappa}) = \begin{pmatrix} u_{\boldsymbol{\kappa}}^* & d_{\boldsymbol{\kappa}}^* & u_{-\boldsymbol{\kappa}}^* & d_{-\boldsymbol{\kappa}}^* \end{pmatrix} \otimes \begin{pmatrix} u_{\boldsymbol{\kappa}} \\ d_{\boldsymbol{\kappa}} \\ u_{-\boldsymbol{\kappa}} \\ d_{-\boldsymbol{\kappa}} \end{pmatrix} \quad (4.3)$$

**Population of momenta  $\pm\boldsymbol{\kappa}$**  In the last Chapter we have shown that for  $\eta_{soc} < 1$  the system undergoes a BKT transition. There are only two minima in the single particle energy spectrum  $\pm\boldsymbol{\kappa} = (\pm\kappa, 0)$  and their population  $n(\pm\boldsymbol{\kappa})$  depends on the sign of the interaction  $g$ . In order to study the matrix  $\mathcal{M}(\mathbf{k})$  the two directions  $\pm\boldsymbol{\kappa}$  are of course equivalent.

For isotropic SOC,  $\eta_{soc} = 1$ , the minimum of the energy spectrum is a full ring of radius  $|\mathbf{k}| = \kappa$  in the thermodynamic limit. However, for our numerical calculation on a finite system, we have only a small number of degenerate single particle ground states, typically four or eight. However, we numerically observe that for finite simulation time, only one direction  $\boldsymbol{\kappa}$  is selected. The two corresponding momenta  $\pm\boldsymbol{\kappa}$  are almost macroscopically populated, whereas the other momenta on the ring have a negligible occupation at low temperature when the density is large  $n\lambda^2 > \sim 1$ . Averaging over different initial conditions reestablishes the symmetry between all directions  $\boldsymbol{\kappa}$ .

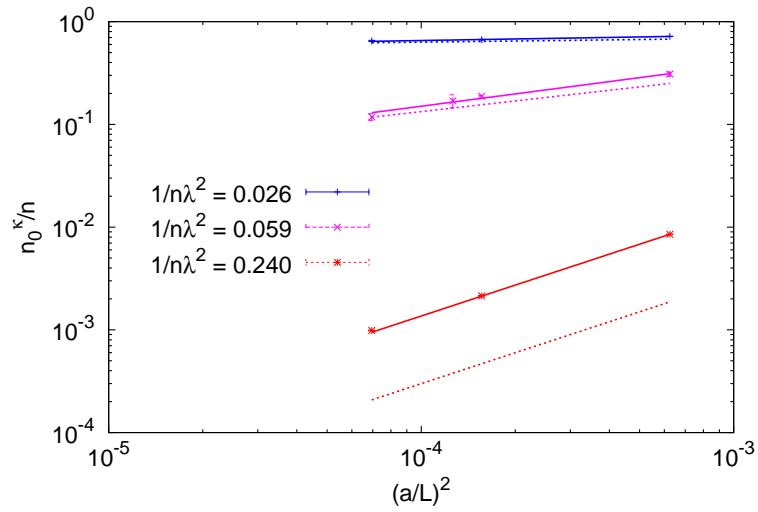


Figure 4.1: Solid lines: Condensate fraction,  $n_0^k/n$ , as a function of the inverse volume,  $L^{-2}$ , for anisotropic SOC bosons with  $\eta_{soc} = 0$  at different phase space densities and anisotropic interaction,  $g > 0$ . Dashed lines show the corresponding maximal occupation number after diagonalizing the single body density matrix (not ensemble averaged). In the normal phase at low phase space density, we have  $n_0^k \sim L^{-2}$  and two degenerate modes, whereas in the superfluid phase at high phase space density we have  $n_0^k \sim L^{-\eta}$  with  $\eta < 1/4$ , the degeneracy is broken, and only one mode contributes to the quasi-condensate.

**Link between low temperature order and the BKT transition for  $\eta_{soc} < 1$  and  $g \neq 0$**  In the last chapter, we have determined the BKT from the appearance of a quasi-condensate density, averaged over the two momentum states which minimize the single particle energy. From the diagonalization of the single particle density matrix, we obtain additional information.

Above the critical temperature, we obtain two degenerate modes within our numerical accuracy – both minima in momentum space are equally populated within a single Monte Carlo run. Below the critical temperature, the system spontaneously chooses one mode which dominates. The two minima are only equivalent after ensemble averaging different Monte Carlo calculations. As shown in figure 4.1, for  $g \neq 0$ , in the BKT phase, the single particle density matrix is dominated by a single, highly occupied mode.

**PW and SP phase** Since the low temperature phase of the system is dominated by a single mode of the reduced density matrix, the spin-structure of the corresponding eigenstate characterizes the spin-structure of the BKT phase, e.g. an algebraically decaying PW or SP quasi-condensate.

Diagonalizing the matrix  $\mathcal{M}(\mathbf{k})$ , we numerically obtain the eigenvectors that describe the appearing order. However, in order to interpret better these results, let us first analyze the structure of the matrix assuming PW or SP order.

Our mean-field ground state introduced in Chapter I Eq. (1.55), we based on the following

$$|\Phi^-(\phi)\rangle = \frac{\left(\cos(\phi)\hat{\Phi}_{\kappa}^{-\dagger} + \sin(\phi)\hat{\Phi}_{-\kappa}^{-\dagger}\right)^N}{\sqrt{N!}}|0\rangle \quad (4.4)$$

The resulting structure of the matrix  $\mathcal{M}$  for pure PW ( $\phi = 0$ ) or SP ( $\phi = \pi/4$ ) states is then

**Plane Wave :**  $\phi = 0$

$$\mathcal{M}(\boldsymbol{\kappa}) \propto (1 \ -1 \ 0 \ 0) \otimes \begin{pmatrix} 1 \\ -1 \\ 0 \\ 0 \end{pmatrix} \quad (4.5)$$

**Stripe phase :**  $\phi = \frac{\pi}{4}$

$$\mathcal{M}(\boldsymbol{\kappa}) \propto (1 \ -1 \ 1 \ 1) \otimes \begin{pmatrix} 1 \\ -1 \\ 1 \\ 1 \end{pmatrix} \quad (4.6)$$

We recover these features in our numerical calculation and we extracted numerically the angle  $\phi$ . At high temperature, where we have two degenerate modes, the angle  $\phi$  is not correctly defined. Approaching the transition point, when one mode starts to dominate, the value of angle becomes well defined. Its mean value depends on the anisotropy  $g > 0$  or  $g < 0$  (SP and PW respectively), fluctuations around it are strongly suppressed.

Our analysis of the eigenmodes and their occupations clearly connects the quasi-condensate structure with the spin-ordering in the BKT phase showing PW or SP depending on the sign of  $g$ . Although there is clearly one mode dominating, the occupation is slowly decaying with system size. Therefore, also in spin space, there is no true, but only quasi-long range order. In the next section, we will study the spin order in a more intuitive and experimentally better accessible way, calculating correlation functions of the local spin density.

### 4.3 Local Spin Density

The PW and SP character of the reduced one-body density matrix computation naturally propagates to various observables and higher order correlation function. In the following we will analyze the spin-order in terms of the local spin density.

**Spin Density** Since we labeled the two hyperfine states of the atoms as spin up and spin down we can use the formalism of magnetism to study the ordered phases. For instance, counting the difference of the number of atoms in the two hyperfine states is equivalent to compute the magnetic moment in the direction  $z$

$$\sigma_z(\mathbf{r}) \equiv \frac{\Psi^\dagger(\mathbf{r})\sigma_z\Psi(\mathbf{r})}{\Psi^\dagger(\mathbf{r})\Psi(\mathbf{r})} = \frac{|\psi_\uparrow(\mathbf{r})|^2 - |\psi_\downarrow(\mathbf{r})|^2}{(|\psi_\uparrow(\mathbf{r})|^2 + |\psi_\downarrow(\mathbf{r})|^2)} \quad (4.7)$$

The colors of figures 4.2, 4.3 and 4.4 represent the value of the local spin density  $\sigma_z(\mathbf{r})$  of the field at each point of space  $\mathbf{r}$ . These quantities are not averages but they are rather obtained at single step of the algorithm. For  $g > 0$  we can clearly identify stripes at low temperature whereas for  $g < 0$  the density is constant in space.

**Spin projections** We can then generalize the spin formalism to the other directions of the spin. Note that the gas is confined in two dimensions but the spin degree of freedom is three-dimensional. Then using the Pauli matrices,

$$\sigma_x = \begin{pmatrix} 0 & 1 \\ 1 & 0 \end{pmatrix} \quad \sigma_y = \begin{pmatrix} 0 & -i \\ i & 0 \end{pmatrix} \quad \sigma_z = \begin{pmatrix} 1 & 0 \\ 0 & -1 \end{pmatrix} \quad (4.8)$$

we can then compute the local spin density of the field in the three directions

$$\sigma_x(\mathbf{r}) = \frac{\Psi^\dagger(\mathbf{r})\sigma_x\Psi(\mathbf{r})}{\Psi^\dagger(\mathbf{r})\Psi(\mathbf{r})} = \frac{\Re[\psi_\uparrow^\dagger(\mathbf{r})\psi_\downarrow(\mathbf{r})]}{|\psi_\uparrow(\mathbf{r})|^2 + |\psi_\downarrow(\mathbf{r})|^2} \quad (4.9)$$

$$\sigma_y(\mathbf{r}) = \frac{\Psi^\dagger(\mathbf{r})\sigma_y\Psi(\mathbf{r})}{\Psi^\dagger(\mathbf{r})\Psi(\mathbf{r})} = \frac{\Im[\psi_\uparrow^\dagger(\mathbf{r})\psi_\downarrow(\mathbf{r})]}{|\psi_\uparrow(\mathbf{r})|^2 + |\psi_\downarrow(\mathbf{r})|^2} \quad (4.10)$$

$$\sigma_z(\mathbf{r}) = \frac{\Psi^\dagger(\mathbf{r})\sigma_z\Psi(\mathbf{r})}{\Psi^\dagger(\mathbf{r})\Psi(\mathbf{r})} = \frac{|\psi_\uparrow(\mathbf{r})|^2 - |\psi_\downarrow(\mathbf{r})|^2}{|\psi_\uparrow(\mathbf{r})|^2 + |\psi_\downarrow(\mathbf{r})|^2} \quad (4.11)$$

and by this way obtain all the information about the spin structure of the field.

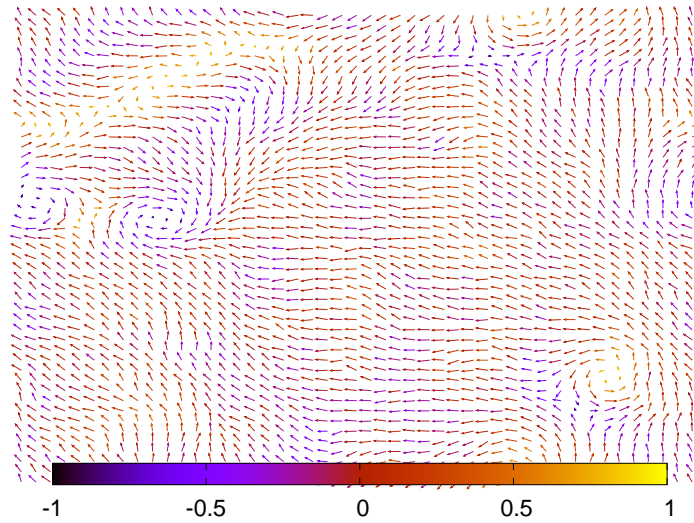


Figure 4.2: Spin local projection at extremely low temperature for anisotropic interaction  $g < 0$  i.e Plane Wave state. The arrows' directions represent the local spin  $\sigma_x$  and  $\sigma_y$  projection on the x-y plane. Colors represent the value of the local spin density  $\sigma_z$ . As expected for the Plane Wave state, spins' projections point in average in the same direction. We observe vortices typical of the KT physics.

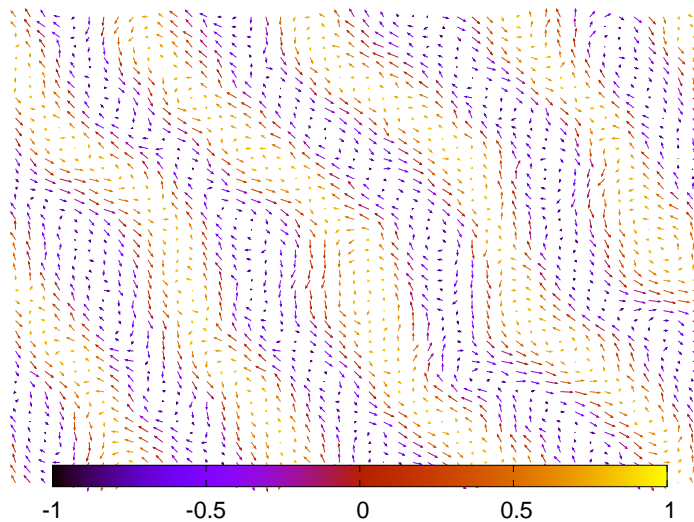


Figure 4.3: Spin local projection at extremely low temperature for anisotropic interaction  $g > 0$  i.e Stripe Phase state. The arrows' directions represent the local spin  $\sigma_x$  and  $\sigma_y$  projection on the x-y plane and colors represent the value of the local spin density  $\sigma_z$ . We observe the signature of a SP order : spins rotate with periodicity  $2\kappa$ . The direction of the rotation is determined by the direction of the two populated momenta  $\pm\kappa$ .

**Mean-field predictions** It is instructive to explicitly write down the mean-field spin density for PW and SP using the mean-field wave function

$$\psi_{\boldsymbol{\kappa}}^{MF}(\mathbf{r}) = \begin{pmatrix} \psi_{\uparrow, \boldsymbol{\kappa}}^{MF}(x, y) \\ \psi_{\downarrow, \boldsymbol{\kappa}}^{MF}(x, y) \end{pmatrix} = \frac{1}{\sqrt{2}} \left[ \cos(\phi) e^{i\kappa x} \begin{pmatrix} 1 \\ -1 \end{pmatrix} + \sin(\phi) e^{-i\kappa x} \begin{pmatrix} 1 \\ 1 \end{pmatrix} \right]$$

For  $g < 0$  the mean-field ground state corresponds to  $\phi = 0$ , a Plane Wave state, with

$$\sigma_x(\mathbf{r}) = 1 \quad \sigma_y(\mathbf{r}) = 0 \quad \sigma_z(\mathbf{r}) = 0 \quad (4.12)$$

All the spins are aligned and point in the direction  $\boldsymbol{\kappa} = (\kappa, 0)$  of the minimum.

For  $g < 0$ , the minimum of the energy corresponds to  $\phi = \frac{\pi}{4}$ , the Stripe Phase state, where we have

$$\sigma_x(\mathbf{r}) = 0 \quad \sigma_y(\mathbf{r}) = \sin(2\kappa x) \quad \sigma_z(\mathbf{r}) = \cos(2\kappa x) \quad (4.13)$$

Now the spins direction rotates around the x-axis with periodicity  $2\kappa$ .

**Numerical simulation** From figures 4.2 and 4.3 we observe that the spin density of our classical field simulation reflects the mean-field ground state at very low temperature. However, at slightly higher temperature, thermal excitations mask the state. Further, we also observe vortices due to thermal excitations, typical for BKT physics.

Figure 4.4 also shows that few thermal excitations are enough to significantly modify the stripe order of the local spin density. In the following, we will use spin density correlations for a more quantitative study to characterize spin ordering.

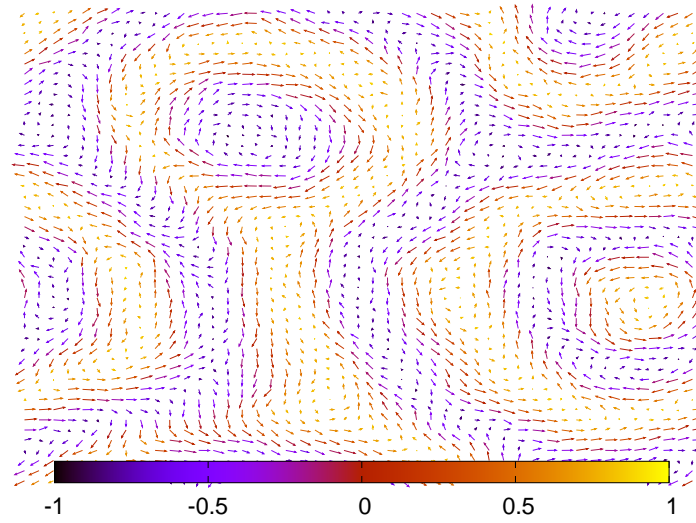


Figure 4.4: Spin local projection at low extremely temperature for anisotropic interaction  $g > 0$  i.e Stripe Phase state. The arrows' directions represent the local spin  $\sigma_x$  and  $\sigma_y$  projection on the x-y plane and colors represent the value of the local spin density  $\sigma_z$ . Due to thermal excitations, vortices interact with the Stripe Phase ordering. In particular in the superfluid phase at intermediate temperature, we cannot observe directly stripes in the density due to these excitations. The SP signature is however observable in the correlation function as showed in figure 4.5.

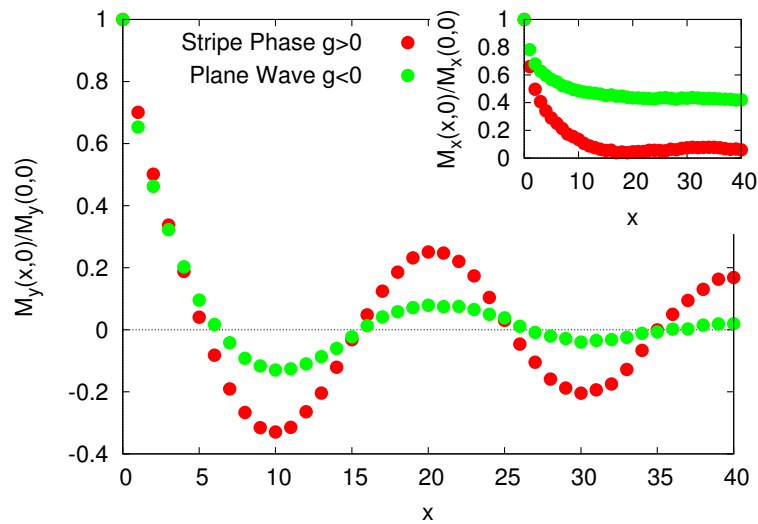


Figure 4.5: Spins density correlation function,  $M_\alpha(x, 0)$ , at phase space density  $1/n\lambda^2 \simeq 0.026$  for  $\eta_{soc} = 0.9$  where  $n_0^k/n \sim 40\%$ . For  $g < 0$ ,  $M_x(x, 0)$  shows quasi-long range order indicating PW, whereas  $M_y(x, 0)$  is short ranged. For  $g > 0$  we obtain SP where the amplitude of the oscillations of  $M_y(x, 0)$  decays algebraically and no order is present in  $M_x(x, 0)$ .

## 4.4 Spin density correlation functions

In the last section, we have shown the local spin density of an instantaneous field configuration. For a more quantitative study, we calculated the spin-density correlation function averaged over many field configurations

$$M_\alpha(\mathbf{r}) = \langle \hat{S}_\alpha(\mathbf{r}) \hat{S}_\alpha(0) \rangle \quad \text{with} \quad \hat{S}_\alpha(\mathbf{r}) = \hat{\Psi}^\dagger(\mathbf{r}) \sigma_\alpha \hat{\Psi}(\mathbf{r}) \quad (4.14)$$

As shown in figure 4.5, the spin structure of this condensate mode is directly reflected in the spin correlation function  $M_\alpha(\mathbf{r})$ .

**Quasi-long range order** Quasi-long range stripe order is reflected in slowly decaying oscillations of period  $2\kappa$  in  $M_y(x, 0)$ . For  $g < 0$ ,  $M_x(x, 0)$  develops quasi-long range order. In both cases, the exponent of the algebraic decay is given by the scaling exponent of  $n_0^\kappa$  and compatible with  $\eta(T)$  obtained from the superfluid density. Therefore, the quasi-long range spin order results from the spin structure of the underlying quasi-condensate.

**Anisotropy** We also notice that the correlation functions,  $M_x(x, 0)$  and  $M_y(x, 0)$ , remain short ranged in the SP and PW state, respectively. The system therefore exhibits a strong anisotropy between the direction  $\kappa$  and the one orthogonal to it. Reference [45] addresses this feature, focusing in particular on the possibility of anisotropic superfluidity.

## 4.5 Isotropic interaction: Fragmented condensate

Let us now study the case of isotropic interparticle interaction  $g = 0$ . As shown in Chapter I, mean field calculations do not select an unique ground state between SP and PW states.

Since SP and PW degeneracy may only reflect the insensitivity of the mean field ansatz for the ground state, many studies focused on looking for the true absolute ground state [72, 35, 34, 6]. In these approaches the symmetry between the SP and PW phases is broken by different physical mechanisms, for example by introducing quantum fluctuations [35] or by renormalization procedures [34].

However, as shown in figure 4.6 for two fundamentally distinct cases  $\eta_{soc} = 0$  and  $\eta_{soc} = 1$ , in the limit of isotropic interaction,  $g = 0$ , we always obtain two highly occupied modes of the single particle density matrix, degenerate within our

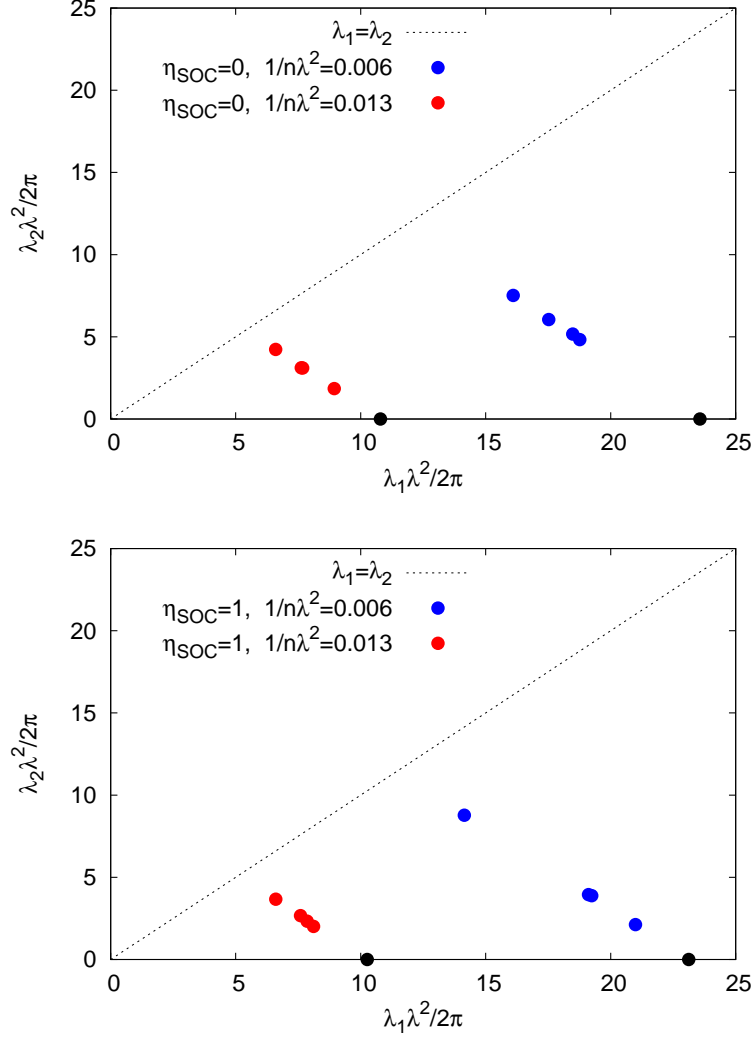


Figure 4.6: Second largest eigenvalue  $\lambda_2$  of the reduced density matrix  $\mathcal{M}(\boldsymbol{\kappa})$  as a function of the largest eigenvalue  $\lambda_1$  for isotropic interactions  $g = 0$ . The top and bottom plots correspond to two opposite SOC anisotropies  $\eta_{\text{SOC}}$ , respectively  $\eta_{\text{SOC}} = 0$  and  $\eta_{\text{SOC}} = 1$ . Each point represents a single long run of a computation at extremely low temperature in a regime numerically challenging within our approximation. In the superfluid regime and for any density, we observe a strong signature of fractionalization. Black points show the corresponding eigenvalues in the case of an anisotropic interaction  $g \neq 0$  when only one eigenvalue  $\lambda_1$  is non zero ( $\lambda_2 \sim 10^{-2} \lambda_1$ ).

numerical precision. By analyzing the spin correlation functions as in the previous sections, we find that both  $M_x(x, 0)$  and  $M_y(x, 0)$  become quasi-long ranged and indicate simultaneous PW and SP characters.

Therefore, for our great surprise, PW and SP remain degenerate and robust against thermal, critical fluctuations. In case of macroscopically occupied modes, this phenomena corresponds to a fractionalized condensate [74]. Since we do not have true long range order, we observe for the first time a fractionalized quasi-condensate.

This unusual behavior indicates that although two modes are extremely populated, the phase  $\phi$  between them is not locked and the spin does not prefer any particular direction. However, classical field description takes only into account thermal fluctuations. From the Bogoliubov approximation around the  $T = 0$  mean-field ground states, we expect that quantum fluctuations lift the degeneracy and favor the PW character decreasing the temperature without further phase transition [35].

## 4.6 Low temperature wave-function

References [69, 9] predicted the occurrence of a paired condensate. Our classical field Monte Carlo have not shown any evidence for the occurrence of this phase. However, it is not clear which observable would best show up such a phase. Here, we present some of our analysis done on the whole field distribution.

Figure 4.8 shows the distribution of the field along the real (x-axis) and imaginary axis (y-axis) at high and low temperature. At a single single Monte Carlo step, we plot the field  $\Psi_\sigma(\mathbf{r})$  at every point in space  $\mathbf{r}$  for both  $\sigma = \uparrow$  and  $\sigma = \downarrow$ .

At high temperature we recognize the Gaussian regime centered on  $\langle \Psi_\sigma(\mathbf{r}) \rangle = 0$ . At low temperature, we recover the mean-field predictions in addition to a broadening due to thermal fluctuations .

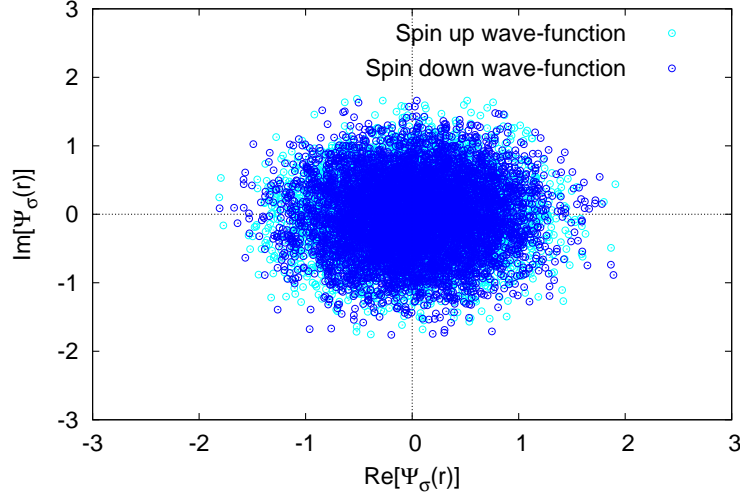


Figure 4.7: Imaginary part of the wave-function as a function of its real part at every point in space  $\mathbf{r}$ . The system size is  $L/a = 80$ , the SOC anisotropy  $\eta_{soc} = 0$  and the space density  $1/n\lambda^2 = 0.240$ . As expected, at high temperature the density is Gaussian distributed.

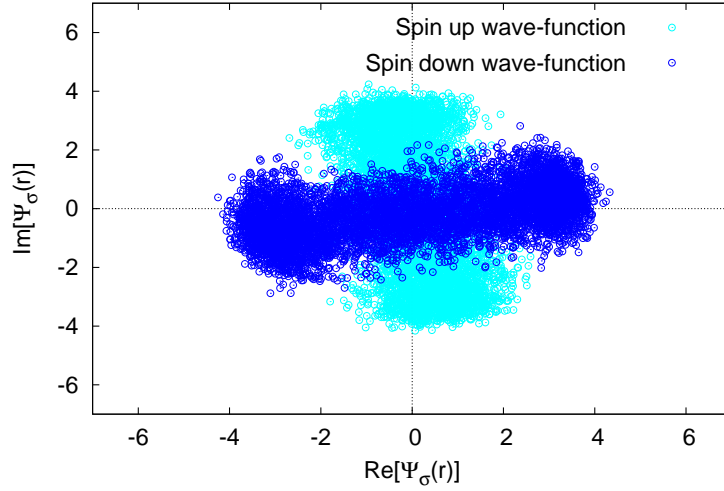


Figure 4.8: Imaginary part of the wave-function as a function of its real part at every point in space  $\mathbf{r}$ . The system size is  $L/a = 80$ , the SOC anisotropy  $\eta_{soc} = 0$ , the space density  $1/n\lambda^2 = 0.0126$  and the contact interaction anisotropy is set to  $g > 0$  i.e. Stripe Phase state. At low temperature, in addition to a broadening due to thermal fluctuations, we recover the mean-field prediction of  $\psi_{\kappa}^{MF}(\mathbf{r}) \equiv \begin{pmatrix} \cos(\kappa x) \\ -i \sin(\kappa x) \end{pmatrix}$ .

### 4.6.1 Bosons pairs

In this distribution, we can notice a great difference between the SP and the other phases. Indeed the average  $\langle \Psi^2 \rangle$  is non zero in the case of a SP wave-function and zero otherwise.

**High temperature Gaussian regime** The average of a squared Gaussian distributed function is zero.

**Plane Wave** The average of a squared Plane Wave is also zero.

$$\langle (e^{ikx})^2 \rangle = \langle e^{i2kx} \rangle = 0 \quad (4.15)$$

**Stripe Phase** The square of a Stripe Phase wave-function is not zero

$$\langle \sin(2\kappa x)^2 \rangle = 0.5 \quad (4.16)$$

The results discussed in last chapter, indicated that for isotropic SOC,  $\eta_{soc} = 1$ , no standard BKT transition occurs. In this particular region of the phase diagram and for  $g > 0$ , in the Stripe Phase, condensation of pairs of bosons were predicted by references [69, 9].

We analyzed how this observable for pairing scales with the system size. Figure 4.10 shows that it decreases with the system size  $L^2$  depending on the discrete number of degenerate minima as the condensate fraction observable studied before. Therefore we do not find any indications of a phase transition to a pairing phase as proposed in reference [9]. However, we cannot exclude the possibility of pair superfluidity at considerably lower densities or much larger system sizes.

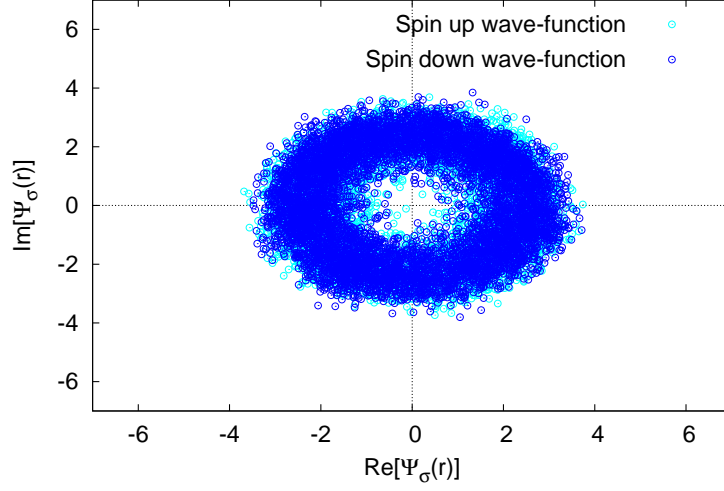


Figure 4.9: Imaginary part of the wave-function as a function of its real part at every point in space  $\mathbf{r}$ . The system size is  $L/a = 80$ , the SOC anisotropy  $\eta_{soc} = 0$ , the space density  $1/n\lambda^2 = 0.0126$  and the contact interaction anisotropy is set to  $g < 0$  i.e Plane Wave state. At low temperature, in addition to a broadening due to thermal fluctuations, we recover the mean-field prediction of  $\psi_{\mathbf{\kappa}}^{MF}(\mathbf{r}) \equiv e^{i\mathbf{\kappa}x} \begin{pmatrix} 1 \\ -1 \end{pmatrix}$ .

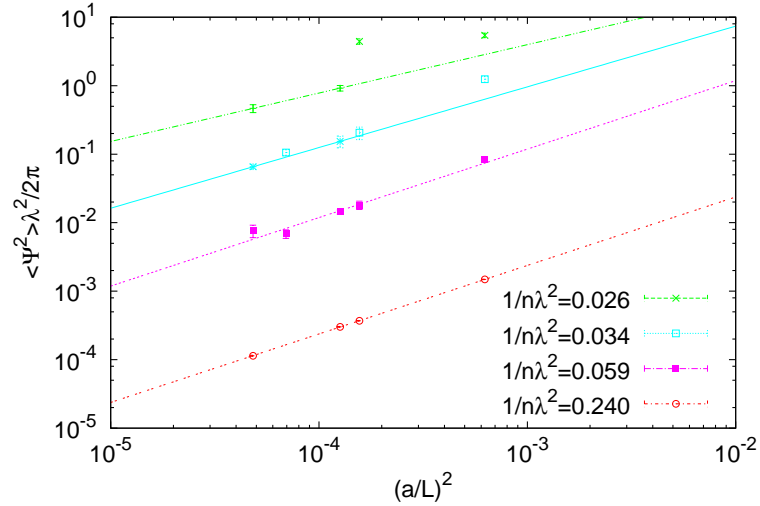


Figure 4.10: Pairs of bosons  $\langle \Psi^2 \rangle$  as a function of the inverse volume,  $L^{-2}$ , for isotropic SOC with  $\eta_{soc} = 1$  at different phase space densities and anisotropic interaction,  $g > 0$  i.e Stripe Phase. We recognize the dependency of this observable on the discrete number of degenerate minima as the condensate fraction studied before. We do not find any indication of a finite temperature phase transition.

## 4.7 Résumé

Au cours du Chapitre III, nous avons étudié le diagramme de phase d'un gaz de Bose bidimensionnel en présence d'un couplage spin-orbite. Dans le cas d'un couplage spin-orbite anisotrope, nous avons identifié deux phases distinctes à basse et haute température séparées par une transition de phase dont nous avons montré l'appartenance à la classe Kosterlitz-Thouless. Présentée en Chapitre I, la théorie champ moyen prédit l'existence de phases exotiques comme états fondamentaux à plusieurs corps. En particulier, ces dernières dépendent fortement des amplitudes d'interactions entre mêmes et différents spins (comme défini Eq. (1.38))

$$g = 2g_{\uparrow\downarrow} - g_{\uparrow\uparrow} - g_{\downarrow\downarrow}$$

l'état fondamental par champ moyen est alors décrit soit comme une onde plane (PW) soit comme une superposition de deux ondes planes avec impulsions opposées appelée état de bande (SP) [69].

Au-delà de l'approximation type champ moyen, l'existence et l'apparition de ces phases exotiques n'est pas établi et beaucoup de questions restent ouvertes. Par exemple, la référence [69] propose un diagramme de phase basé sur des arguments qualitatifs dans la limite du régime fortement dilué. Les différentes phases ne dépendraient plus alors du signe de l'anisotropie  $g$ , en fort contraste avec les prédictions en champ moyen. Nous avons, à notre tour, caractérisé les différentes phases à basse température observées au sein de nos simulations de champs classiques.

En particulier, nous avons étudié l'ordre magnétique des atomes/spins à basse température que nous avons relié à la transition BKT étudiée au cours du chapitre précédent. Nous avons également montré que dans le cas d'une anisotropie  $g \neq 0$  les corrélations de spin présentent un ordre de quasi-longue portée induit par la transition KT en opposition avec les prédictions de ordre longue portée de la part de la référence [70]. Nous observons donc un diagramme de phase fortement déterminé par la transition Kosterlitz-Thouless. Nous avons également sondé différentes prédictions, en particulier celle d'une transition à impulsion nulle [71, 72] ainsi que l'apparition de paires de bosons [69, 9]. Toutefois, nous n'avons pas trouvé de trace de ces comportements et phases très exotiques.

Dans le cas d'interactions isotropes,  $g = 0$ , l'approximation type champ moyen ne sélectionne pas d'état fondamental unique, les états SP et PW restent alors

dégénérés. Dans ce cas spécifique, il serait attendu que les fluctuations thermiques et quantiques lèvent cette dégénérescence et qu'un unique état fondamental soit sélectionné. L'approximation type champs classiques nous permet d'aborder la question des fluctuations thermiques de façon directe et explicite. Nous avons montré que le système subit une transition de phase sans sélectionner d'état fondamental unique. Nos calculs prédisent dans ce cas une fractionalisation du condensat, les états PW et SP se maintenant dégénérés.

Dans le cadre de notre étude et pour étudier la compétition entre couplage spin-orbite et interactions interparticules, nous avons fixé  $\sum_{\sigma\sigma'=\uparrow\downarrow} mg_{\sigma\sigma'}/4 = \kappa/\sqrt{mk_B T} = \pi/20$  avec  $mg = 0$  pour étudier le cas d'une interaction isotrope et  $mg = \pm\pi/100$  pour étudier le cas d'une fine brisure de symétrie entre les diffusions des différents spins.



## Conclusion and Perspectives

**I**N THIS THESIS we have determined the finite-temperature phase diagram of a two-dimensional interacting Bose gas with two hyperfine (pseudospin) states coupled via Rashba-Dresselhaus spin-orbit interaction using classical field Monte Carlo calculations.

Our numerical studies clearly establish that the weakly interacting Bose gas undergoes a BKT phase transition for anisotropic SOC,  $\eta_{soc} < 1$ . In the low temperature phase, the condensate fraction decays algebraically with system size and the gas becomes superfluid. However, for isotropic SOC,  $\eta_{soc} = 1$ , our calculations shows a cross-over behavior at finite systems, with strong evidence for the absence of a finite temperature phase transition in the thermodynamic limit.

We have further characterized superfluid many body states for  $\eta_{soc} < 1$  as a function of a vanishing or small spin-anisotropy of the interparticle interaction,  $g = 2g_{\uparrow\downarrow} - g_{\uparrow\uparrow} - g_{\downarrow\downarrow}$ , of positive or negative sign. In particular, we have shown that in the case of an anisotropy  $g \neq 0$  the spin correlations exhibit quasi-long-range order and that the magnetic ordering of the atoms/spins at low temperature is linked to the BKT phase transition. Our calculations confirm mean field predictions for the character of the quasi-condensate in the superfluid state, i.e. PW or SP order depending on the sign of  $g$ .

For isotropic interactions,  $g = 0$ , we obtained a fractionalized quasi-condensate with two degenerate modes at the transition showing both, PW and SP character.

Originally motivated by the mean field prediction of the degeneracy between the SP/PW states, the system of isotropically interacting bosons,  $g = 0$ , with Rashba spin-orbit coupling,  $\eta_{soc} = 1$ , has attracted considerable attention [7, 35]. Fluctuations and correlations beyond mean field were expected to break this degeneracy. Using classical field Monte Carlo calculations, we directly addressed the role of thermal fluctuations. The stability of the SP/PW degeneracy leading to a fractionalized quasi-condensate in our calculations came out unexpectedly. However, within classical field theory, quantum effects due to non-vanishing commutators of the quantum fields are neglected.

Close to zero temperature, the Bogoliubov approach is suited for studying quantum fluctuations around the mean field state. Reference [35] shows that, within the Bogoliubov approximation, the three dimensional isotropic SOCed Bose gas condenses into a single-momentum state of the Rashba spectrum, thus resulting in order by disorder.

In two dimensions, thermal fluctuations destabilize the system at any finite temperature. Nevertheless, decreasing temperature, the analogous calculation of reference [35] predicts quantum fluctuations to lift the degeneracy and favor the PW character for  $\eta_{soc} < 1$  and  $g = 0$ . However, the exact transition from a fractionalized quasi-condensate at the critical temperature to the broken degeneracy at zero temperature is unclear and still an open question.

Addressing numerically the full quantum system is extremely challenging due to the presence of the SOC which introduces a sign problem into all known quantum Monte Carlo algorithms. Similar to the fermionic sign problem, the error of such a calculation increases exponentially with system size, inverse proportional to temperature. Similar, already for classical field calculations, SOC prevents the use of the Worm algorithm [75] to speed up our computation.

As an outlook, we want to include quantum fluctuations, as described in the Bogoliubov theory, within our classical field approach, with the hope to quantitatively describe both thermal and quantum fluctuations for a weakly interacting SOCed Bose gas.

## *Conclusion et Perspectives*

AU COURS de cette thèse nous avons déterminé le diagramme de phase à température finie d'un gaz de Bose bidimensionnel avec deux états hyperfins (pseudospin) couplés au travers d'une interaction spin-orbite Rashba-Dresselhaus en utilisant des calculs Monte-Carlo basés sur champs classiques.

Nos études numériques établissent clairement qu'un gaz de Bose interagissant subit une transition de phase de type BKT en présence d'un couplage spin-orbite anisotrope  $\eta_{soc} < 1$ . La phase à basse température présente une fraction condensée qui décroît algébriquement avec la taille du système et le gaz devient alors superfluide. Au contraire, dans le cas d'un couplage spin-orbite isotrope,  $\eta_{soc} = 1$ , nos calculs pointent l'absence d'une transition de phase à température finie et à la limite thermodynamique. Une transition lisse (cross-over) subsiste pour des systèmes à taille finie.

Nous avons ensuite étudié plus en détail les différents états fondamentaux à plusieurs corps pour  $\eta_{soc} < 1$  en fonction d'une anisotropie des interactions interparticules  $g = 2g_{\uparrow\downarrow} - g_{\uparrow\uparrow} - g_{\downarrow\downarrow}$  nulle, positive ou négative. En particulier, nous avons montré que dans le cas d'une fine anisotropie  $g \neq 0$  les corrélations de spins présentent un ordre quasi-longue portée et que l'ordre magnétique des atomes/spins à basse température est lié à la transition de phase BKT. Nos calculs confirment les prédictions de type champ moyen à propos de la nature du quasi-condensat dans la phase superfluide c'est à dire la sélection des ordres SP et PW en fonction du signe de  $g$ . Dans le cas d'interactions isotropes,  $g = 0$ , nous obtenons un quasi-condensat fractionnalisé avec deux modes dégénérés à la transition et qui présente deux ordres simultanément PW et SP.

Une attention toute particulière de la part de la communauté [7, 35] est portée sur le système composé de bosons interagissant de manière isotrope,  $g = 0$ , avec un couplage spin-orbite également isotrope,  $\eta_{soc} = 1$  provoquée à l'origine par la prédiction d'une dégénérescence entre les états SP et PW dans le cadre des théories de type champ moyen. Il serait attendu que cette dégénérescence soit levée par les fluctuations au-delà du champ moyen. En utilisant les calculs de champs classiques par Monte Carlo, nous avons pour notre part abordé directement le rôle des fluctuations thermiques. C'est alors que la stabilité de la dégénérescence entre les ordres SP et PW entraînant une fractionalisation du quasi-condensat est apparue dans nos calculs de façon inattendue. Toutefois, au sein d'une théorie de champs classiques, les effets quantiques dûs aux commutateurs des champs quantiques

sont négligés.

Au contraire, en se rapprochant de la limite à température nulle, l'approche Bogoliubov est particulièrement adaptée pour l'étude des fluctuations quantiques autour de l'état fondamental provenant du champ moyen. En particulier la référence [35] montre que, au sein de l'approximation Bogoliubov, le gaz de Bose tridimensionnel avec couplage spin-orbite isotrope condense dans un état du spectre Rashba avec une unique impulsion, ceci se traduisant alors dans un processus de ordre par le désordre.

En deux dimensions, les fluctuations thermiques déstabilisent le système pour n'importe quelle température non nulle. Néanmoins, en diminuant la température, des calculs analogues à ceux de la référence [35] prédisent que les fluctuations quantiques lèvent la dégénérescence et favorise la nature PW du système pour  $\eta_{soc} < 1$  et  $g = 0$ . Pourtant, la transition exacte entre un quasi-condensat fractionnalisé autour de la température critique vers une dégénérescence brisée à température nulle, est incertaine et plusieurs questions restent ouvertes.

Résoudre numériquement le système quantique complet est extrêmement difficile à cause de la présence du couplage spin-orbite qui introduit un problème de signe abondamment connu dans tous les algorithmes de Monte Carlo quantique. De façon semblable au problème du signe fermionique, l'erreur provenant de ce type de calcul croît de façon exponentielle avec la taille du système et de manière inversement proportionnelle à la température. De manière analogue dans le cadre des calculs de champs classiques que nous avons développés, le terme traduisant le couplage spin-orbite empêche l'utilisation des algorithmes type Worm [75] pour accélérer nos calculs.

Comme projet futur et comme proposition d'ouverture, nous souhaitons inclure les fluctuations quantiques, telles celles décrites dans la théorie de Bogoliubov, au sein de notre approche se basant sur des champs classiques avec l'espoir de décrire de manière quantitativement correcte simultanément les fluctuations quantiques et les fluctuations thermiques dans un gaz de Bose faiblement interagissant.





## Appendix

### 6.1 Fluctuations of the density at low temperature

As shown in figure 2.5, at low temperature, the interaction energy,  $gn^2/2$ , dominates over the kinetic energy,  $\propto n\lambda^2$ . For simplicity, let us consider the system in absence of SOC,  $\kappa = 0$ , where the density distribution at low temperature is approximately given by

$$p[\psi(r)] \sim \exp[-\beta(\mathcal{H}_{cf} - \mu N)] \sim \exp[-\beta \int d^2r \frac{g}{2} (|\psi(r)|^2 - \mu/g)^2] \quad (6.1)$$

Therefore, fluctuations of the density around its mean value,  $n = \langle n \rangle \equiv \mu/g$ , are Gaussian distributed, with mean-square fluctuations

$$\Delta n^2 \equiv \langle n^2(r) \rangle - n^2 \sim \frac{nk_B T}{g}, \quad n\lambda^2 \gg \pi/g \quad (6.2)$$

and highly suppressed for large phase space density,  $\Delta n^2/n^2 \sim [gn\lambda^2]^{-1} \simeq 0$ , in contrast to the non interacting case. Approaching zero temperature, density fluctuations smoothly vanish. At high temperature, fluctuations around the density are much larger, since the kinetic energy can never be neglected. In this regime, the Fourier modes of the fields are Gaussian distributed leading to qualitatively different density fluctuations,  $\langle n^2 \rangle = 2n^2$ .



# Bibliography

- [1] Jean Dalibard, Fabrice Gerbier, Gediminas Juzeliūnas, and Patrik Öhberg. Colloquium. *Rev. Mod. Phys.*, 83:1523–1543, Nov 2011.
- [2] Y.-J. Lin, K. Jimenez-Garcia, and I. B. Spielman. Spin-orbit-coupled bose-einstein condensates. *Nature*, 471(7336):83–86, Mar 2011.
- [3] K. Jiménez-García, L. J. LeBlanc, R. A. Williams, M. C. Beeler, C. Qu, M. Gong, C. Zhang, and I. B. Spielman. Tunable spin-orbit coupling via strong driving in ultracold-atom systems. *Phys. Rev. Lett.*, 114:125301, Mar 2015.
- [4] Victor Galitski and Ian B. Spielman. Spin-orbit coupling in quantum gases. *Nature*, 494(7435):49–54, Feb 2013.
- [5] Zhan Wu, Long Zhang, Wei Sun, Xiao-Tian Xu, Bao-Zong Wang, Si-Cong Ji, Youjin Deng, Shuai Chen, Xiong-Jun Liu, and Jian-Wei Pan. Realization of two-dimensional spin-orbit coupling for bose-einstein condensates. *Science*, 354(6308):83–88, 2016.
- [6] Tomoki Ozawa and Gordon Baym. Stability of ultracold atomic bose condensates with rashba spin-orbit coupling against quantum and thermal fluctuations. *Phys. Rev. Lett.*, 109:025301, Jul 2012.
- [7] Tomoki Ozawa and Gordon Baym. Condensation transition of ultracold bose gases with rashba spin-orbit coupling. *Phys. Rev. Lett.*, 110:085304, Feb 2013.
- [8] Hui Zhai. Degenerate quantum gases with spin-orbit coupling: a review. *Reports on Progress in Physics*, 78(2):026001, 2015.
- [9] Chao-Ming Jian and Hui Zhai. Paired superfluidity and fractionalized vortices in systems of spin-orbit coupled bosons. *Phys. Rev. B*, 84:060508, Aug 2011.

- [10] Renyuan Liao, Zhi-Gao Huang, Xiu-Min Lin, and Oleksandr Fialko. Spin-orbit-coupled bose gases at finite temperatures. *Phys. Rev. A*, 89:063614, Jun 2014.
- [11] Tin-Lun Ho and Shizhong Zhang. Bose-einstein condensates with spin-orbit interaction. *Phys. Rev. Lett.*, 107:150403, Oct 2011.
- [12] Chunji Wang, Chao Gao, Chao-Ming Jian, and Hui Zhai. Spin-orbit coupled spinor bose-einstein condensates. *Phys. Rev. Lett.*, 105:160403, Oct 2010.
- [13] Eiji Kawasaki and Markus Holzmann. Finite-temperature phases of two-dimensional spin-orbit-coupled bosons. *Phys. Rev. A*, 95:051601, May 2017.
- [14] Immanuel Bloch, Jean Dalibard, and Wilhelm Zwerger. Many-body physics with ultracold gases. *Rev. Mod. Phys.*, 80:885–964, Jul 2008.
- [15] Masaya Kato, Xiao-Fei Zhang, and Hiroki Saito. Vortex pairs in a spin-orbit-coupled bose-einstein condensate. *Phys. Rev. A*, 95:043605, Apr 2017.
- [16] Markus König, Steffen Wiedmann, Christoph Brüne, Andreas Roth, Hartmut Buhmann, Laurens W. Molenkamp, Xiao-Liang Qi, and Shou-Cheng Zhang. Quantum spin hall insulator state in hgte quantum wells. *Science*, 318(5851):766–770, 2007.
- [17] Yu A Bychkov and E I Rashba. Oscillatory effects and the magnetic susceptibility of carriers in inversion layers. *Journal of Physics C: Solid State Physics*, 17(33):6039, 1984.
- [18] G. Dresselhaus. Spin-orbit coupling effects in zinc blende structures. *Phys. Rev.*, 100:580–586, Oct 1955.
- [19] C. L. Kane and E. J. Mele.  $Z_2$ . *Phys. Rev. Lett.*, 95:146802, Sep 2005.
- [20] B. Andrei Bernevig, Taylor L. Hughes, and Shou-Cheng Zhang. Quantum spin hall effect and topological phase transition in hgte quantum wells. *Science*, 314(5806):1757–1761, 2006.
- [21] D. Hsieh, D. Qian, L. Wray, Y. Xia, Y. S. Hor, R. J. Cava, and M. Z. Hasan. A topological dirac insulator in a quantum spin hall phase. *Nature*, 452(7190):970–974, Apr 2008.
- [22] Y.-J. Lin, R. L. Compton, K. Jimenez-Garcia, J. V. Porto, and I. B. Spielman. Synthetic magnetic fields for ultracold neutral atoms. *Nature*, 462(7273):628–632, Dec 2009.

- [23] Tin-Lun Ho and V. B. Shenoy. Local spin-gauge symmetry of the bose-einstein condensates in atomic gases. *Phys. Rev. Lett.*, 77:2595–2599, Sep 1996.
- [24] J. Higbie and D. M. Stamper-Kurn. Periodically dressed bose-einstein condensate: A superfluid with an anisotropic and variable critical velocity. *Phys. Rev. Lett.*, 88:090401, Feb 2002.
- [25] Y.-J. Lin, R. L. Compton, A. R. Perry, W. D. Phillips, J. V. Porto, and I. B. Spielman. Bose-einstein condensate in a uniform light-induced vector potential. *Phys. Rev. Lett.*, 102:130401, Mar 2009.
- [26] D. L. Campbell, G. Juzeliūnas, and I. B. Spielman. Realistic rashba and dresselhaus spin-orbit coupling for neutral atoms. *Phys. Rev. A*, 84:025602, Aug 2011.
- [27] Gordon Baym and Tomoki Ozawa. Condensation of bosons with rashba-dresselhaus spin-orbit coupling. *Journal of Physics: Conference Series*, 529(1):012006, 2014.
- [28] Xiaoling Cui and Qi Zhou. Enhancement of condensate depletion due to spin-orbit coupling. *Phys. Rev. A*, 87:031604, Mar 2013.
- [29] L.P. Pitaevskii and S. Stringari. *Bose-Einstein Condensation*. International Series of Monographs on Physics. Clarendon Press, 2003.
- [30] J. P. Blaizot and G. Ripka. *Quantum Theory of Finite Systems*. The MIT Press, Cambridge, Massachusetts, 1986.
- [31] Tudor D. Stanescu, Brandon Anderson, and Victor Galitski. Spin-orbit coupled bose-einstein condensates. *Phys. Rev. A*, 78:023616, Aug 2008.
- [32] Qi Zhou and Xiaoling Cui. Fate of a bose-einstein condensate in the presence of spin-orbit coupling. *Phys. Rev. Lett.*, 110:140407, Apr 2013.
- [33] Tigran A. Sedrakyan, Alex Kamenev, and Leonid I. Glazman. Composite fermion state of spin-orbit-coupled bosons. *Phys. Rev. A*, 86:063639, Dec 2012.
- [34] Tomoki Ozawa and Gordon Baym. Ground-state phases of ultracold bosons with rashba-dresselhaus spin-orbit coupling. *Phys. Rev. A*, 85:013612, Jan 2012.
- [35] Ryan Barnett, Stephen Powell, Tobias Grass, Maciej Lewenstein, and S. Das Sarma. Order by disorder in spin-orbit-coupled bose-einstein condensates. *Phys. Rev. A*, 85:023615, Feb 2012.

- [36] G. I. Martone. Visibility and stability of superstripes in a spin-orbit-coupled bose-einstein condensate. *The European Physical Journal Special Topics*, 224(3):553–563, 2015.
- [37] Giovanni I. Martone, Yun Li, and Sandro Stringari. Approach for making visible and stable stripes in a spin-orbit-coupled bose-einstein superfluid. *Phys. Rev. A*, 90:041604, Oct 2014.
- [38] Tomoki Ozawa and Gordon Baym. Striped states in weakly trapped ultracold bose gases with rashba spin-orbit coupling. *Phys. Rev. A*, 85:063623, Jun 2012.
- [39] Jun-Ru Li, Jeongwon Lee, Wujie Huang, Sean Burchesky, Boris Shteynas, Furkan Çağrı Top, Alan O. Jamison, and Wolfgang Ketterle. A stripe phase with supersolid properties in spin-orbit-coupled bose-einstein condensates. *Nature*, 543(7643):91–94, March 2017.
- [40] Subhasis Sinha, Rejish Nath, and Luis Santos. Trapped two-dimensional condensates with synthetic spin-orbit coupling. *Phys. Rev. Lett.*, 107:270401, Dec 2011.
- [41] B. Ramachandhran, Bogdan Opanchuk, Xia-Ji Liu, Han Pu, Peter D. Drummond, and Hui Hu. Half-quantum vortex state in a spin-orbit-coupled bose-einstein condensate. *Phys. Rev. A*, 85:023606, Feb 2012.
- [42] Predrag Nikolić. Vortices and vortex states in rashba spin-orbit-coupled condensates. *Phys. Rev. A*, 90:023623, Aug 2014.
- [43] Alexander L. Fetter. Vortex dynamics in a spin-orbit-coupled bose-einstein condensate. *Journal of Low Temperature Physics*, 180(1):37–52, 2015.
- [44] Qizhong Zhu, Chuanwei Zhang, and Biao Wu. Exotic superfluidity in spin-orbit coupled bose-einstein condensates. *EPL (Europhysics Letters)*, 100(5):50003, 2012.
- [45] Sandro Stringari. Diffused vorticity and moment of inertia of a spin-orbit coupled bose-einstein condensate. *Phys. Rev. Lett.*, 118:145302, Apr 2017.
- [46] Gordon Baym, Jean-Paul Blaizot, Markus Holzmann, Franck Laloë, and Dominique Vautherin. The transition temperature of the dilute interacting bose gas. *Phys. Rev. Lett.*, 83:1703–1706, Aug 1999.
- [47] Markus Holzmann and Gordon Baym. Condensate density and superfluid mass density of a dilute bose-einstein condensate near the condensation transition. *Phys. Rev. Lett.*, 90:040402, Jan 2003.

- [48] Luca Giorgetti, Iacopo Carusotto, and Yvan Castin. Semiclassical field method for the equilibrium bose gas and application to thermal vortices in two dimensions. *Phys. Rev. A*, 76:013613, Jul 2007.
- [49] Nikolay Prokof'ev and Boris Svistunov. Two-dimensional weakly interacting bose gas in the fluctuation region. *Phys. Rev. A*, 66:043608, Oct 2002.
- [50] Markus Holzmann, Gordon Baym, Jean-Paul Blaizot, and Franck Laloë. Superfluid transition of homogeneous and trapped two-dimensional bose gases. *Proceedings of the National Academy of Sciences*, 104(5):1476–1481, 2007.
- [51] J. Zinn-Justin. *Quantum Field Theory and Critical Phenomena*. International series of monographs on physics. Clarendon Press, 2002.
- [52] P. C. Hohenberg. Existence of long-range order in one and two dimensions. *Phys. Rev.*, 158:383–386, Jun 1967.
- [53] N. D. Mermin and H. Wagner. Absence of ferromagnetism or antiferromagnetism in one- or two-dimensional isotropic heisenberg models. *Phys. Rev. Lett.*, 17:1133–1136, Nov 1966.
- [54] Sidney Coleman. There are no goldstone bosons in two dimensions. *Communications in Mathematical Physics*, 31(4):259–264, Dec 1973.
- [55] Jürg Fröhlich and Thomas Spencer. The kosterlitz-thouless transition in two-dimensional abelian spin systems and the coulomb gas. *Communications in Mathematical Physics*, 81(4):527–602, Dec 1981.
- [56] V. L. Berezinskiĭ. Destruction of Long-range Order in One-dimensional and Two-dimensional Systems Possessing a Continuous Symmetry Group. II. Quantum Systems. *Soviet Journal of Experimental and Theoretical Physics*, 34:610, 1972.
- [57] J M Kosterlitz and D J Thouless. Ordering, metastability and phase transitions in two-dimensional systems. *Journal of Physics C: Solid State Physics*, 6(7):1181, 1973.
- [58] J M Kosterlitz. The critical properties of the two-dimensional xy model. *Journal of Physics C: Solid State Physics*, 7(6):1046, 1974.
- [59] Pei-Song He, Jia Zhao, Ai-Cong Geng, Deng-Hui Xu, and Rong Hu. Instability of a two-dimensional bose–einstein condensate with rashba spin–orbit coupling at finite temperature. *Physics Letters A*, 377(34–36):2207 – 2209, 2013.

- [60] A.M. Polyakov. Interaction of goldstone particles in two dimensions. applications to ferromagnets and massive yang-mills fields. *Physics Letters B*, 59(1):79, 1975.
- [61] E. Brézin and J. Zinn-Justin. Spontaneous breakdown of continuous symmetries near two dimensions. *Phys. Rev. B*, 14:3110–3120, Oct 1976.
- [62] David R. Nelson and J. M. Kosterlitz. Universal jump in the superfluid density of two-dimensional superfluids. *Phys. Rev. Lett.*, 39:1201–1205, Nov 1977.
- [63] G. Agnolet, D. F. McQueeney, and J. D. Reppy. Kosterlitz-thouless transition in helium films. *Phys. Rev. B*, 39:8934–8958, May 1989.
- [64] G. Baym. The microscopic description of superfluidity. In R.C. Clark and G.H. Derrick, editors, *Mathematical Methods in Solid State and Superfluid Theory*, page 121. Oliver and Boyd, Edinburgh, 1969.
- [65] Markus Holzmann and Gordon Baym. Condensate superfluidity and infrared structure of the single-particle green's function: The josephson relation. *Phys. Rev. B*, 76:092502, Sep 2007.
- [66] B. D. Josephson. Relation between the superfluid density and order parameter for superfluid he near  $T_c$ . *Phys. Lett.*, 21:608, July 1966.
- [67] E. L. Pollock and D. M. Ceperley. Path-integral computation of superfluid densities. *Phys. Rev. B*, 36:8343–8352, Dec 1987.
- [68] Yi-Cai Zhang, Zeng-Qiang Yu, Tai Kai Ng, Shizhong Zhang, Lev Pitaevskii, and Sandro Stringari. Superfluid density of a spin-orbit-coupled bose gas. *Phys. Rev. A*, 94:033635, Sep 2016.
- [69] Sarang Gopalakrishnan, Austen Lamacraft, and Paul M. Goldbart. Universal phase structure of dilute bose gases with rashba spin-orbit coupling. *Phys. Rev. A*, 84:061604, Dec 2011.
- [70] Shih-Wei Su, I-Kang Liu, Shih-Chuan Gou, Renyuan Liao, Oleksandr Fialko, and Joachim Brand. Hidden long-range order in a spin-orbit-coupled two-dimensional bose gas. *Phys. Rev. A*, 95:053629, May 2017.
- [71] Xiao-Long Chen, Xia-Ji Liu, and Hui Hu. Quantum and thermal fluctuations in a raman spin-orbit-coupled bose gas. *Phys. Rev. A*, 96:013625, Jul 2017.

- [72] Zeng-Qiang Yu. Ground-state phase diagram and critical temperature of two-component bose gases with rashba spin-orbit coupling. *Phys. Rev. A*, 87:051606, May 2013.
- [73] Oliver Penrose and Lars Onsager. Bose-einstein condensation and liquid helium. *Phys. Rev.*, 104:576–584, Nov 1956.
- [74] Erich J. Mueller, Tin-Lun Ho, Masahito Ueda, and Gordon Baym. Fragmentation of bose-einstein condensates. *Phys. Rev. A*, 74:033612, Sep 2006.
- [75] Nikolay Prokof'ev and Boris Svistunov. Worm algorithms for classical statistical models. *Phys. Rev. Lett.*, 87:160601, Sep 2001.





---

## Abstract

---

In this thesis, we theoretically study the occurrence of exotic phases in a dilute two component (spin) Bose gas with artificial spin-orbit coupling (SOC) between the two internal states. Including spin-orbit coupling in classical field Monte Carlo calculations, we show that this method can be used for reliable, quantitative predictions of the finite temperature phase diagram. In particular, we have focused on SOCed bosons in two spatial dimensions and established the phase diagram for isotropic and anisotropic SOC and interparticle interactions. In the case of anisotropic SOC, the system undergoes a Berenzinskii-Kosterlitz-Thouless transition from a normal to a superfluid state at low temperature. The spin order of the quasicondensate in the low temperature superfluid phase is driven by the spin dependence of the interparticle interaction, favoring either the occurrence of a single plane wave state at non-vanishing momentum (PW) or a linear superposition of two plane waves with opposite momenta, called stripe phase (SP). For spin-independent interparticle interaction, our simulations indicate a fractionalized quasicondensate where PW and SP remain degenerate. For isotropic SOC, our calculations indicate that no true phase transition at finite temperature occurs in the thermodynamic limit, but a cross-over behavior remains visible for large, but finite number of atoms.

---

## Résumé

---

Cette thèse est dédiée à l'étude théorique de phases exotiques dans un gaz dilué de bosons avec deux composantes (spins) en présence d'un couplage spin-orbite (SOC) entre ces deux états internes. En ajoutant ce dernier couplage à une description de type champs classiques de notre système, nous montrons que cette méthode permet de prédire le diagramme de phase à température finie de manière quantitative, efficace et fiable. Notre étude porte en particulier sur un système de bosons bidimensionnels avec SOC dont nous dessinons le diagramme de phase en fonction de l'anisotropie du SOC ainsi que des interactions. Dans le cas d'un SOC anisotrope, une transition de phase de type Berenzinskii-Kosterlitz-Thouless sépare une phase dite normale d'une phase superfluide à plus basse température. L'ordre des spins du quasi-condensat dans la phase superfluide est alors guidé par les interactions de contact dépendantes du spin. Elles favorisent l'apparition soit d'un état onde plane avec moment non-nul (PW) soit d'une superposition linéaire de deux ondes planes appelée état de bande (SP). Pour des interactions indépendantes du spin des particules, nos simulations indiquent une fractionalisation du quasi-condensat. Les états PW et SP restent alors dégénérés. Dans le cas d'un SOC isotrope, nos calculs n'indiquent aucune transition de phase à la limite thermodynamique et à température finie. Un changement de comportement non critique (transition lisse ou cross-over) subsiste pour un nombre important mais fini d'atomes.